FORM AND FUNCTION OF THE SECONDARY HEMILINEAGES IN THE ADULT DROSOPHILA THORACIC NERVOUS SYSTEM

Robin Harris

A dissertation

submitted in partial fulfillment of the

requirements for the degree of

Doctor of Philosophy

University of Washington

2012

Reading committee:

James Truman, Chair

Thomas Daniel, Chair

Horacio de la Iglesia

Leo Pallanck

Program Authorized to Offer Degree:

Neurobiology and Behavior

University of Washington

Abstract

Form and Function of the Secondary Hemilineages in the Adult Drosophila Thoracic Nervous System

Robin Harris

Chair of the Supervisory Committee:

Professor Emeritus James W. Truman, Chair

Biology

Professor Thomas L. Daniel, Chair

Biology

The majority of the neurons in the adult *Drosophila* thoracic nervous system are produced by one unpaired and twenty-four bilaterally paired, segmentally reiterated neuroblasts (NBs). Each neuroblast divides repeatedly, producing a series of ganglion mother cells. Each ganglion mother cell, in turn, divides to form 2 daughter neurons, one that is Notch-on and the other Notch-off. Collectively, the Notch-on neurons are called the "A" hemilineage, and their Notch-off siblings are the "B" hemilineage. Neurons within a hemilineage extend initial neurites to the same stereotyped location, then arrest development until the onset of metamorphosis. It seems reasonable, based on their

common developmental origin and very similar larval morphology, to hypothesize that neurons within a hemilineage could share functional properties in the adult. In this thesis, I describe a set of genetic reagents to direct gene expression to these hemilineages in the adult (Chapter 2), characterize their adult morphology (Chapter 3), and document the behaviors induced by activating them using the conditional transgenic neural activator TRPA1 (Chapter 4). I find that the neurons within a secondary hemilineage occupy a unique space in the thoracic neuropil, and cause a characteristic combination of behaviors when activated. This supports the hypothesis that these neurons are functionally related and paves the way for future investigation.

TABLE OF CONTENTS

Page

LIST OF FIGURES

LIST OF TABLES

Table Number Page

ACKNOWLEDGEMENTS

This thesis is but the humble offering of a grad student, but it means a lot to me, and I am supremely grateful to the wonderful people who have made this endeavor possible.

First on the list is, of course, Jim Truman. In addition to nurturing and mentoring and paying me for the last six years, he very generously provided me with an incredible opportunity to work at the then-brand-new Janelia Farm Research Campus. Shortly after I started, he announced that after thirty-four years in Seattle, he was closing down the lab and moving to Virginia. It would have been simple for him to tell me to find another lab, since it was still my first year in grad school. Instead, he took me with him. As grateful as I was then, I could never have imagined the scientific and educational benefits I gained from that gift.

I also owe a huge debt to Tom Daniel, who adopted me and gave me a home for the year between when Jim moved to Janelia and when I did. I learned a lot from Tom and his lab in a short amount of time, both technical advice and what it means to have a career in science. My deepest gratitude goes out to Tom and the Daniel lab, especially Dave Williams, Zane Aldworth, Armin Hinterwirth, Andrew Mountcastle, Bert Tanner, and Alexandre Dieudonne, and extra-specially Jess Fox.

I am grateful to my committee members, who have been very patient and understanding during the long-distance grad student process. Horacio de la Iglesia, Leo Pallanck, and Celeste Berg periodically provided invaluable insights to keep me in line. In addition, Lucia Wisdom and Ann Wilkinson of the UW NeuBeh program, Judy

Farrow of UW Biology, and Sarah Moorehead and Alison Howard at Janelia, were tremendously helpful in keeping the details straight and making this happen.

All glory to the Janelia Fly Core, especially Karen Hibbard, Monti Mercer, and Don Hall.

Barret Pfeiffer and Gerry Rubin deserve special mention: without our close collaboration, capitalizing on Gerry's support and Barret's molecular biology brilliance, these experiments would have failed. Johannes Seelig provided vital advice on statistics and data analysis, and also German lessons.

Along with the Truman lab, I thank Lynn Riddiford and her lab for being close and valuable colleagues. Many thanks to Triddifords past and present, in Seattle and Virginia. I am grateful to Wanda Moats, Heather Brown, Sue McNabb, Margrit Schubiger, Janet Altman, Sara Lennox, and Lisa Marin for introducing me to fly husbandry and the art of confocal microscopy (also Wai Pang Chan!); Christen Mirth, Michael Texada, Troy Shirangi, Shannon Ballard, Wayne Pereanu, Feng Li, Julide Bilen, and Lee Henry for much-appreciated discussions, support, and fun; and special thanks to Hans Kelstrup and Dave Mellert for solidarity and motivation, particularly towards the end. And Snup Dog.

Unfortunately, I don't have room to name all of the other friends, family and colleagues who helped me through this process; but I love them all, and I thank them for making these some of the best years of my life.

DEDICATION

To my grandparents, educators all

Chapter 1

INTRODUCTION

Rationale

Nervous systems enable animals to translate sensory inputs into appropriate motor outputs, but the nature and mechanisms of these transforms remain almost entirely unknown. One of the primary obstacles is the brain's staggering complexity: the relatively simple nervous system of *Drosophila* has on the order of 100,000 neurons (Cuccati 1888, Power 1943), while the human brain has over 100 billion (Herculano-Houzel 2009), and each of these neurons is capable of making connections with hundreds of synaptic partners.

A huge advance in neuroscience has come from the advent and prolific development of transgenic organisms and genetic tools. The ability to introduce transgenes into specific groups of neurons and monitor or manipulate them *in vivo* is extremely powerful, and there is no organism as genetically accessible as *Drosophila melanogaster*. Indeed, thousands of reagents exist for the genetic manipulation of the *Drosophila* central nervous system (see below).

Drosophila made its mark on neuroscience long before transgenic reagents became widely used. Benzer's identification of mutations affecting *Drosophila* phototaxis (Benzer 1967) was the first inroad into the genetic mechanisms underlying innate behaviors, launching the field of neurogenetics. Over the next forty years, the Benzer lab

and many others characterized genes affecting all kinds of *Drosophila* behaviors, from locomotion to learning and memory. However, satisfying as these genetic insights were, it was still difficult to envision a mechanism by which a gene could affect a specific behavior. Hotta and Benzer's work on sex mosaics revealed that the behavioral effects of genes could sometimes be mapped to specific regions of the nervous system (1976). This was arguably the first foothold connecting behavioral genetics to neural substrates. The concept that genes shape behaviors by specifying the connectivity or activity of specific groups of neurons became a central principle in our understanding of nervous system development and function.

It is in the quest to assign behaviors to specific neurons that the genetic accessibility of *Drosophila* becomes truly indispensible. Efforts to tie the actions of genes regulating behavior to specific neurons have met with mixed success. As an alternative approach, there are thousands of *Drosophila* enhancer-trap lines that can direct transgene expression repeatably to specific groups of neurons, allowing forward screens for neurons that affect a given behavior. This approach has been used with admirable success to identify "command neurons" that are necessary and sufficient for aspects of different behaviors, such as courtship (e.g., von Philipsborn et al. 2011, Pan et al. 2012), feeding (e.g., Marella et al. 2012), and aggression (e.g., Certel et al. 2010, Wang and Anderson 2010).

The trouble with such screens is that it is difficult to then trace the behavior to the next relay upstream or downstream. A neuron or group of neurons may elicit a behavior when

stimulated, but which inputs drive that specific pathway, and through which outputs? Even once you have an interesting neuron in hand, it is a formidable task to locate another single neuron appropriately situated to be a presynaptic or postsynaptic partner among the tens or hundreds of neurons projecting to and from a given region, much less determine the role that next relay may play in the circuit. Moreover, although there are instances of single neurons that are both necessary and sufficient for a behavior (such as the examples above), it seems likely that in other cases groups of neurons must act in concert to produce behavior, as is usually the case in the vertebrate brain. Under this assumption, it would seem reasonable to try to target neural classes, rather than single cells, in order to untangle circuits and behavioral phenotypes. Of course, one then faces the surprisingly difficult question of defining a "neural class." Karel Svoboda summarized the problem thusly: "A logical definition [for a neural class] would be functional: neurons that perform the same function within the circuit belong to the same cell type. But this definition is useless, since the function of most neurons in the brain remains to be discovered" (2011). Rather, one must choose a group of cells based on morphology, gene expression patterns, electrophysiological properties, or some other characteristic or characteristics and ask whether they are functionally related in an informative way.

One appealing idea is to assign neural classes developmentally, by their lineage of origin. The neurons of the *Drosophila* ventral nerve system (VNS), analogous to the vertebrate spinal cord, are produced by a segmental set of 30 paired and one unpaired neuroblasts (NBs). These generate an initial set of neurons that are used in the larval VNS. Six of the

paired NBs then die, but the remaining 24 pairs plus one reactivate during larval growth to produce 90 to 95% of the neurons of the adult thoracic neuromeres. These 25 NBs produce 32 major surviving hemilineages (see "Insect Neurodevelopment," below). Neurons within a hemilineage share certain gene expression patterns during development, send their primary neurites to the same neuropil, and make initial contacts with the same partner lineages. Thus, they meet many of the criteria typically used to identify putative neural classes.

Although the *Drosophila* brain, as noted, has only a fraction of the neurons of a vertebrate brain, it is still a very large and complex network. The VNS contains on the order of 15,000 neurons, and mediates a number of complex behaviors, including grooming, righting, walking, jumping, and flying. All of these behaviors can be observed either spontaneously or in response to an appropriate stimulus in a decapitated fly, indicating that circuitry sufficient to mediate these behaviors is present in the VNS. Thus, the VNS offers rich and complex circuits in a network intermediate in size between a whole fly and a nematode, amenable to all the genetic assets available in *Drosophila*, and with a small set of putative cell classes in the form of its well-characterized secondary hemilineages. It is therefore an attractive system in which to explore the principles underlying neural circuits and behavior, and one worth developing.

Insect Neurodevelopment

In all insects, the neurons of the segmental ganglia are produced by an array of ~30 self-renewing, serially homologous NBs (Thomas et al. 1984). The NBs delaminate from a pool of competent cells in the ventral ectoderm: first, pair-rule and dorsoventral patterning genes specify the boundaries of *achaete-scute*-expressing proneural clusters (Skeath and Carroll 1994), and then a single NB emerges from each cluster via Notch/Delta lateral inhibition (reviewed in Kunisch et al. 1994). Each NB then produces a series of progenitor cells called ganglion mother cells (GMCs). Except for some specialized lineages in the brain (Bello et al. 2008, Bowman et al. 2008, Boone and Doe 2008), the GMCs are not self-renewing: they divide into two terminally differentiated neurons. Notch signaling determines the identity of the two daughter neurons (Spana et al. 1995, Spana and Doe 1996). One is Notch-on, and the other is Notch-off. An NB's progeny are collectively known as its lineage. The Notch-on and Notch-off subgroups are termed the "A" and "B" hemilineages, respectively (Truman et al. 2010).

Specific hemilineages have expanded during insect evolution as behavioral demands changed. For example, the flying locust *Schistocerca* have roughly double the number of thoracic neurons found in the primitively wingless silverfish *Ctenolepisma*, presumably due at least in part to the neural demands of flight (Truman and Ball 1998). Yet these disparate species have the same array of homologous NBs; the different neuron counts arise through changes in the relative length of the NBs' proliferative phases. Of the 31 thoracic NBs, one has a longer proliferative phase in silverfish, 14 have similar proliferative periods in the two species, and 16 proliferate longer in grasshopper (Truman and Ball 1998). Since the grasshopper can fly and the silverfish cannot, one might assume

that the flight circuitry is produced by the 16 lineages that are expanded in grasshopper. Because only a subset of the lineages show expansion, perhaps these lineages were predisposed to filling certain roles in what became the flight circuitry. If elements of the flight circuitry were indeed assembled from lineage components, this would support the hypothesis that neurons in a lineage tend to be functionally related.

In holometabolous insects such as *Drosophila*, neurogenesis is divided into two stages: an embryonic proliferation stage, when the NBs produce neurons that will be active in the larva (called "primary neurons"), and a larval proliferation stage, in which a subset of the NBs reactivates and produces neurons specific to the adult ("secondary neurons") (Booker and Truman 1987, Truman and Bate 1988, Prokop and Technau 1991, Hartenstein et al. 2008, Truman et al. 2010). In *Drosophila,* the NBs that will produce secondary neurons reactivate around the end of the first larval stage and produce neurons through about 12 hours after pupariation. Some primary neurons survive metamorphosis and remodel to function in the adult, but approximately 90-95% of the adult nervous system is made of the neurons that were born during larval growth.

The early neurons produced during the embryonic proliferation period have unique identities. Each NB sequentially expresses the transcription factors Hunchback (Hb), Kruppel (Kr), Pdm, and Castor (Cas), and daughter neurons maintain expression of the transcription factor present at their birth (Isshiki et al. 2001, Novotny et al. 2002). These daughters are easily distinguished and have different functions in the larva. The secondary neurons, however, are much more homogeneous. All of the neurons in a

secondary hemilineage send their initial neurites to the same stereotyped target location. In some cases, hemilineage siblings are also known to share gene expression patterns (e.g., Kumar et al. 2009) and neurotransmitter expression (e.g., Witten and Truman 1998).

As mentioned previously, the secondary neurons of each segment of the *Drosophila* adult VNS are produced by 24 bilaterally paired NBs and an unpaired median NB. This array is repeated, with a few exceptions, in each thoracic segment; subsets repeat in the subesophageal and abdominal ganglia. Each NB lineage (with the exception of lineage 20 vs. 22) can be unambiguously identified in the third instar based on their initial neurite projections (Truman et al. 2004). Together, these NBs produce a maximum of 32 major, distinct hemilineages per hemisegment (20 and 22 are counted together); the majority or all of the neurons in the other hemilineages undergo programmed cell death (Truman et al. 2010).

The thoracic secondary lineages have been characterized and named (numbered) by Truman et al. (2004). This numbering system has not been comprehensively matched back to the identification system for NBs active in the embryo, but when they are, we should be able to assign identity to every neuron of the VNS in terms of its NB of origin and time of birth, insofar as they are distinct individuals. This will also help us to identify homologous hemilineages in different insects, since homologous NBs can be identified in most species (Thomas et al. 1984).

The Insect Ventral Nerve System

Decapitated *Drosophila* can perform a number of relatively complex behaviors. For example, touching a leg bristle results in a leg movement directed away from the stimulus (Vandervorst and Ghysen, 1980); applying dust to the body elicits grooming of the appropriate region (Phillis et al. 1993); if the animal is dropped, "flight" (wing-beating) is initiated (personal observation); and so on (see below). This means the ventral nerve system (VNS) must contain the neural substrates necessary to initiate and coordinate these behaviors.

A rich literature exists on the cell types of the VNS in other insect species, particularly locust and walking stick. There are a number of specific neurons or neural classes that can be reproducibly identified between animals. The ability to repeatedly target these neurons for electrophysiological recordings is highly valuable. In many cases, a great deal is known about their activity under different circumstances, including in response to sensory inputs and during real or fictive behaviors (reviewed in Burrows 1996). Certain guiding principles have emerged:

1. Leg sensory information is processed in parallel by classes of spiking and nonspiking interneurons, as well as by motor neurons directly. These local interneuron networks are sufficient to mediate postural and withdrawal reflexes (reviewed in Burrows 1996).

2. The VNS is capable of producing rhythmic patterns resembling walking (e.g., Ryckebush and Laurent 1993) and flight (e.g., Stevenson and Kutsch 1987) in the absence of sensory feedback. However, sensory feedback strongly modulates the execution of these patterns *in vivo* (e.g., Wendler 1974).

3. Most observed walking gaits can be modeled with an oscillator in each leg that couples to its neighbors in different ways under different circumstances (e.g., Graham 1977, Cruse 1990). These models seem compatible with neural circuits, but no components of such models have been matched to neurons.

4. Flight interneurons are typically intersegmental (reviewed in Burrows 1996); few local flight interneurons have been described. A distinction is typically made between flight-initiating neurons, flight pattern-generating neurons, and wingbeat-modulating neurons, but it is clear that most described interneurons can fall into more than one category depending on the context.

Caution must be exercised in translating information from the locust into *Drosophila*, especially for flight interneurons, because they are phylogenetically quite separate and use different flight mechanisms. However, it seems reasonable to expect that at least some of the described locust interneuron classes will correspond to fly hemilineages. In Chapter 3, I make predictions about homology between a few of the cell classes described in locust and lineages in *Drosophila*.

Standard genetic tools in *Drosophila*

Because this work relies heavily on the sophisticated genetic and transgenic methodologies available in *Drosophila*, a brief summary of the relevant reagents is provided here.

Binary Systems

The single most useful genetic technique available in *Drosophila* is the binary system: heterologous transcription factor/DNA binding site pairs that do not occur naturally in *Drosophila*, but when introduced to its genome, are able to induce transcription of coding sequences placed downstream of the binding site and an appropriate promoter (Brand and Perrimon 1993). The most commonly used binary systems in *Drosophila* are GAL4/UAS, taken from the yeast *Saccharomyces cervisiae* (Brand and Perrimon 1993; Duffy 2002), and LexA/LexAop, taken from *Escherichia coli* (Lai and Lee 2006).

Historically, transgenes were introduced to the genome using *P* elements, resulting in pseudo-random insertions (reviewed in Bachmann and Knust 2008). If a GAL4-containing *P* element happened to insert into an active transcriptional enhancer in the genome, then GAL4 would be transcribed in addition to (or instead of) the native gene, specifically in the cells where that gene was being expressed. If a UAS responder transgene were present in the same animal, then that transgene would also be transcribed. This enhancer-trap method has been used by dozens of labs to create tens of thousands of transgenic *Drosophila* lines that target a huge variety of tissues and cells, repeatably and reliably. (Other methods for introducing binary reagents and other transgenes to the genome now exist; e.g., see "Integrase/Gateway," below.)

The expression pattern of an enhancer-trap line is initially detected using a reporter such as green fluorescent protein (GFP) (Shimomura et al. 1962, Wang and Hazelrigg 1994). Once the pattern is characterized, however, a new responder transgene can be substituted, with the assumption that it will be driven in the same cells as the reporter. A great number of responder transgenes for both GAL4 and LexA have been introduced to the *Drosophila* genome, mediating an astonishing range of cellular manipulations (see "Effectors," below).

The GAL4/UAS binary system can be regulated or modified in a number of ways to attain more specific or otherwise altered expression patterns. Four are used in this thesis:

1. GAL80: GAL80 is a yeast protein that binds the activation domain of GAL4 and suppresses its activity in cells where it is transgenically expressed (Ma and Ptashne 1987, Lee and Luo 1999). Random GAL80 insertions are difficult to use, since GAL80 patterns cannot be visualized directly, but methods of expressing GAL80 in predictable patterns exist (e.g., see "Integrase/Gateway," below).

2. GeneSwitch: In the GeneSwitch method (Roman et al. 2001, Osterwalder et al. 2001), the activation domain of GAL4 is replaced with a truncated version of the human progesterone receptor, which sequesters GAL4 in the cytoplasm except in the presence of the progesterone antagonist RU486. Thus, normally, GAL4 is inactive, since it cannot reach its binding sites in the nucleus; only when the drug is added does it become transcriptionally active. This provides temporal control: for example, if RU486 is not

supplied until adulthood, then expression patterns in the larva are suppressed. This is useful when driving cell death genes, for example.

3. Split GAL4: In the Split GAL4 method (Luan et al. 2006), the GAL4 protein is cleaved between the activation domain and the DNA binding domain, and each half is ligated to half of a "leucine zipper". The two halves are inserted into the genome separately, and can thus be transcribed in independent sets of cells. If the activation domain and DNA-binding domain expression patterns overlap in the same cell, then the two halves will come together with the help of the leucine zipper and drive UAS transgene expression.

4. Flip-On drivers/effectors: It is also possible to make binary system expression contingent on recombinase activity. This technique is described in detail below (see "Recombinases").

Effectors

As noted above, a binary system can be used to drive transcription of anything placed downstream of a binding site and promoter, i.e., virtually anything a genome can encode. A staggering array of UAS effectors exists, and many more are constantly being produced for GAL4/UAS and other binary systems. Transgenes exist to visualize cells morphology, protein localization, and even protein-protein interactions; interference RNA transgenes can be used to manipulate protein levels; ion channels can be expressed to manipulate cell physiology; genetically encoded calcium indicators allow *in vivo* monitoring of neural activity; and the list goes on.

Two major effector categories are used in this thesis:

1. Reporters: These genes allow visualization of cells or subcellular compartments where the driver is active, without (substantially) affecting cellular activity. Examples include green fluorescent protein (GFP) and red fluorescent protein (RFP), which are fluorescent proteins that can be visualized with or without antibody staining, and HA, which is not itself visible but makes an excellent epitope for immunocytochemistry. These proteins can be combined with a number of localization tags, such as mCD8, which binds the reporter to the cell membrane, or TLN (DenMark) (Nicolai et al. 2010), which in neurons causes the reporter to be transported towards postsynaptic compartments. Specific combinations will be explained in the sections where they are used.

2. Neural activators: A number of cation channels have been adapted to depolarize target neurons, either chronically or acutely. *Drosophila* transient receptor potential A1 (dTRPA1) (Parisky et al. 2008, Shang et al. 2008) is a heat-sensitive cation channel that opens at temperatures above 27^{o}C (Hamada et al. 2008). When introduced as a transgene, it can be used to acutely depolarize TRPA1-expressing neurons by rearing flies below the activation temperature, then quickly heating them to > 27^{o}C.

Recombinases

Recombinases are enzymes that catalyze recombination between short, enzyme-specific nucleotide sequences ("recognition sites"). They are found in a variety of organisms, including yeast and bacteria (Grindley et al. 2006). A few have been demonstrated to work as transgenes in metazoans, catalyzing recombination at introduced recognition

sites without causing (too much) harmful recombination at cryptic recognition sites in the host's genome. Site-specific recombination can be used to generate a number of useful genomic rearrangements (e.g. Fig 1.1, adapted from Nern and Pfeiffer et al. 2011).

For example, transgene expression can be made dependent on the presence of a recombinase. A STOP cassette, flanked by recognition sites, is introduced between the transgene and its transcriptional promotor. In most cells, the STOP cassette will prevent transgene transcription. However, where the recombinase is present, it will catalyze recombination between the recognition sites, excising the STOP cassette from the genome and permitting transgene transcription (Fig. 1.1A).

Two other rearrangements relevant to this work are cassette exchange, which is used in the Gateway/Integrase system, and translocation of chromosome arms, which is used in Mosaic Analysis with a Repressible Cell Marker (MARCM). These each receive their own section below.

Gateway/Integrase

Although *P*-element insertion is an excellent way to generate new lines via enhancer trap, it is labor-intensive to determine where the element inserted, and the insertion may disrupt a gene or genes. Moreover, although native enhancer activity is used to drive GAL4 or LexA expression in enhancer trap lines, native activity is problematic in the case of responder insertions, which need to faithfully follow the driver pattern. In the case of reporter constructs, such leak can be detected and compensated. However, in the case

of insertions that cannot be visualized, such as TRPA1 and GAL80, this is a significant obstacle. Expression strength is also highly dependent on insertion site. Finally, there are many applications for which the ability to reproduce a pattern is invaluable. For example, if one had two GAL4 patterns of interest and wished to visualize both in the same animal, it would be very convenient if one of the lines could be converted to LexA, allowing independent driver-responder combinations in the two patterns. This can be done in enhancer trap lines, e.g. through *P*-element-swapping, but it is a labor-intensive process. A better, recombinase-based solution was introduced in the form of the PhiC31 integrase system (Groth et al. 2004).

The site-specific integrase from phage PhiC31 (Thorpe and Smith 1998), a form of recombinase, mediates recombination between two sequences called *attP* and *attB*. A *P*-element containing an *attP* site is hopped into the genome at random, and insertions of interest are selected. Subsequently, any construct flanked by the *attB* sequence can be introduced, along with the PhiC31 integrase, and introduced into that site via recombinase-mediated cassette exchange (Fig. 1.1C). Thus, the pattern of an *attP* insertion could be determined using a GAL4 construct, and used to infer the pattern of GAL80 recombined into the same site. Even better, *attP* sites with very little native expression can be identified, and characterized DNA sequences can be inserted to drive transgene expression. This provides complete control of the transgene environment. It also allows side-by-side comparisons of different sequences' expression patterns or strength, free of confounds associated with different insertion sites. This well-controlled system has been used to optimize many of the drivers and effectors used in *Drosophila*

(e.g. Pfeiffer et al. 2010). It is also the basis of the Rubin GAL4 collection at Janelia Farm (Pfeiffer et al. 2008).

The Rubin Collection

The Rubin GAL4 collection at Janelia Farm is a set of ~8000 GAL4 lines inserted into a selected genomic location, attP2, using the PhiC31 integrase system (Pfeiffer et al. 2008). Each line drives GAL4 under a unique DNA sequence, approximately 3kb in size, taken from the noncoding regions of genes thought to express in the *Drosophila* CNS. That is, rather than make an enhancer trap collection and later try to determine the sequences contributing to patterns of interest, the collection is made from known sequences (putative enhancer elements) and used to assay the resultant expression patterns.

The brain and VNS expression patterns of all 8000 lines have been imaged, in the third instar larva and the adult, in an effort known as the Janelia Fly Light project. In some cases, the expression patterns appear to be subsets of neurons that express the parent genes; in others, the patterns driven by the enhancer fragments from a gene appear completely unrelated to one another or to the parent gene's distribution (Pfeiffer et al. 2008). Moreover, there does not appear to be any correlation between the pattern in the third instar versus the adult CNS: some lines express in many of the same cells, some in completely different cells, and combinations (personal observation). Interestingly, substantial overlap between larval and adult patterns appears to be rare. This probably reflects the phenomenon of gene (and enhancer sequence) reuse for different processes

throughout development. Many of these fragments also drive expression outside the CNS, but for the vast majority of lines this expression has not been characterized.

Janelia also produced a collection of ~2000 LexA lines, derived from the most interesting fragments in the GAL4 collection. Because the sequence driving GAL4 expression is known, it should be possible to recapitulate a desired pattern with a LexA driver using the same enhancer fragment. However, the LexA lines were inserted into a different genomic site, attP40, in order to avoid a phenomenon known as transvection (Mellert and Truman 2012). Although both attP2 and attP40 were selected from a panel of tested sites for their ability to support robust expression with minimal native expression, they are nevertheless different insertion sites, and subject to position effects. In some instances, the expression patterns in attP2 and attP40 are indistinguishable; in others, they are drastically different. This effect has been traced definitively to the insertion site, rather than the GAL4/LexA conversion. Thus, although site-specific integration makes it possible to replicate an expression pattern with a different driver or effector, it still relies on *attP* sites inserted by *P* element, and is subject to some of the same caveats as an enhancer trap collection when switching between insertion sites.

MARCM

Nearly all previous work regarding NB lineages has made use of a technique known as Mosaic Analysis with a Repressible Cell Marker (MARCM). MARCM is an elegant and powerful combination of the tools mentioned above that allows gene expression to be restricted to a stochastic subset of cells in an expression pattern. The standard MARCM

mechanism is outlined in Fig. 1.2 (adapted from Lee and Luo 1999): a heat-shock inducible flippase is used to stochastically induce homologous recombination between homologous chromosomes that each bear an FRT site at the same genomic location (translocation, Fig. 1.1B). One of the chromosomes also bears a pan-cellular GAL4 suppressor such as *tub-GAL80* distal to the FRT site. The other chromosome bears a gene and/or UAS-transgene of interest distal to the FRT site. In progenitor cells in which recombination takes place, at the next cell division, one daughter inherits two copies of *tub-GAL80*, while the other inherits two copies of the gene of interest (Fig. 1.2A). Heat-shock flippase induction can be titrated by changing the duration of the applied heat shock, and the types of cells targeted can be biased by the developmental stage at which the heat shock is applied. For example, one can target secondary hemilineages by applying the heat shock at 24h after egg-laying, when the NBs are finished producing primary neurons but have not yet begun producing secondaries. If recombination occurs in a NB at this stage and it inherits both non-*tub-GAL80* chromosomes at the next division, then all of the secondary neurons it subsequently produces will likewise lack GAL80. If a pan-neuronal driver such as *elav-GAL4* is also present in the fly, then the secondary neurons of the affected NB -- and no other cells -- will express any UAS transgenes present in the genome.

A variant of this technique, called twin-spot (ts) MARCM, uses a similar mechanism, but takes advantage of interference RNA (RNAi) (Fire et al. 1998, Zamore et al. 2000) to express different transgenes in each daughter cell. In place of GAL80 and a transgene, the homologous chromosomes bear 1) UAS-GFP and UAS-RFP-RNAi, and 2) UAS-RFP

and UAS-GFP-RNAi. In cells where recombination occurs, one daughter inherits two copies of UAS-GFP/UAS-RFP-RNAi, and no copies of UAS-GFP-RNAi, and so it expresses GFP (Fig. 1.2B). The other daughter inherits UAS-RFP and UAS-GFP-RNAi, but no RFP-RNAi, and thus expresses RFP.

One advantage of tsMARCM is the ability to visualize the fate of both daughters of the affected cell. For example, if a GMC is hit, one can see the "A" and "B" siblings in GFP and RFP. Another advantage is that if one requires visually sparse preparations, tsMARCM can halve the number of specimens required, because GFP-expressing clones can be imaged independently of RFP-expressing clones in the same preparation.

In Chapter 2, I describe how I have combined different transgenic tools to target genetic manipulation to each of secondary hemilineages of the VNS. In Chapter 3, I use those tools to describe the adult anatomy of the hemilineages. In Chapter 4, I use them to drive dTRPA1 and describe the behaviors associated with activation of each hemilineage.

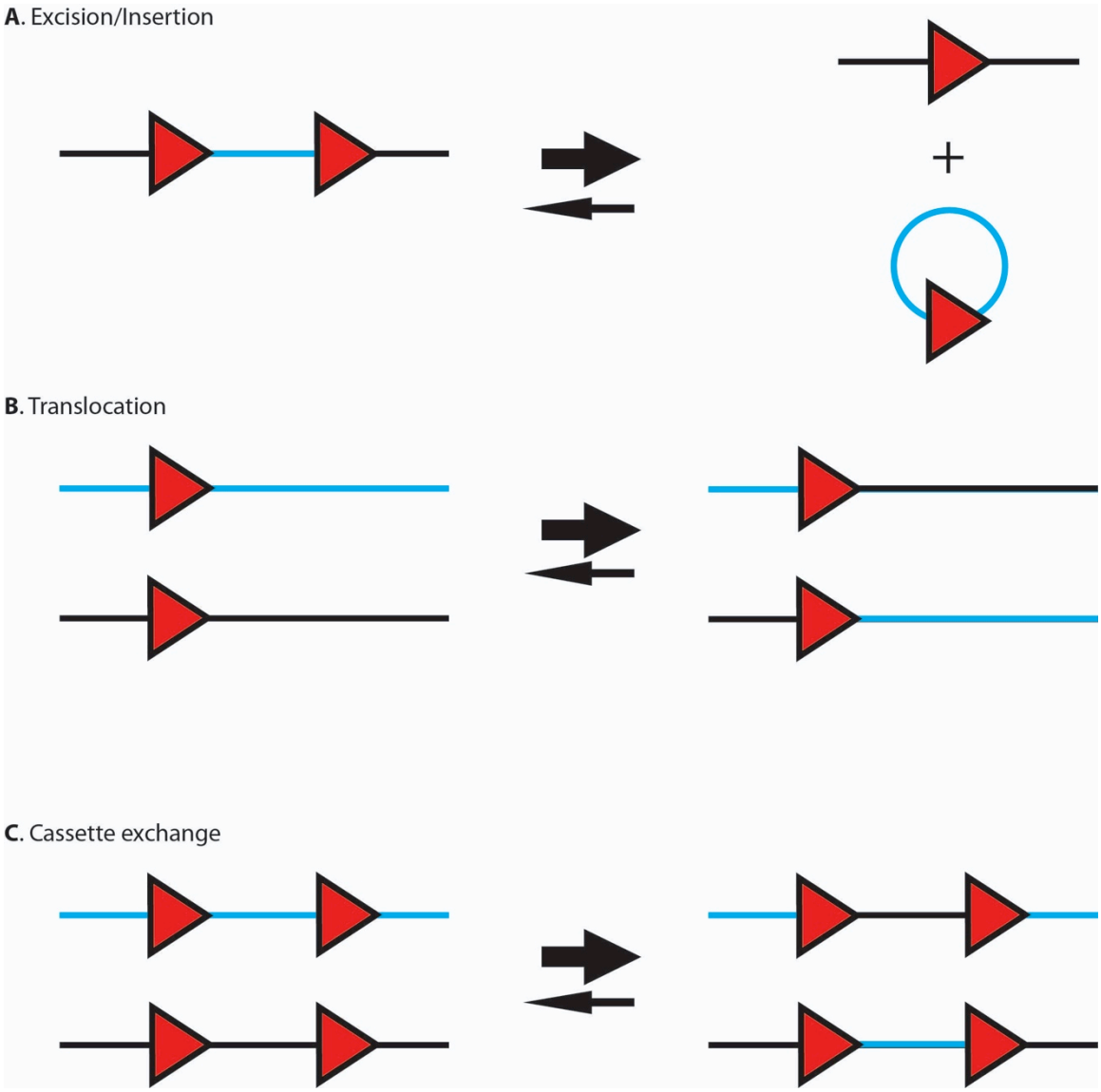

Figure 1.1. DNA rearrangements via site-specific recombinases. Red triangles represent target recognition sites. Excisions (A) are used in flip-on reagents; translocation (B) is used in MARCM; cassette exchange (C) is used in the Gateway integrase system (see text). The reverse reaction, indicated with small arrows, occurs with very low efficiency.

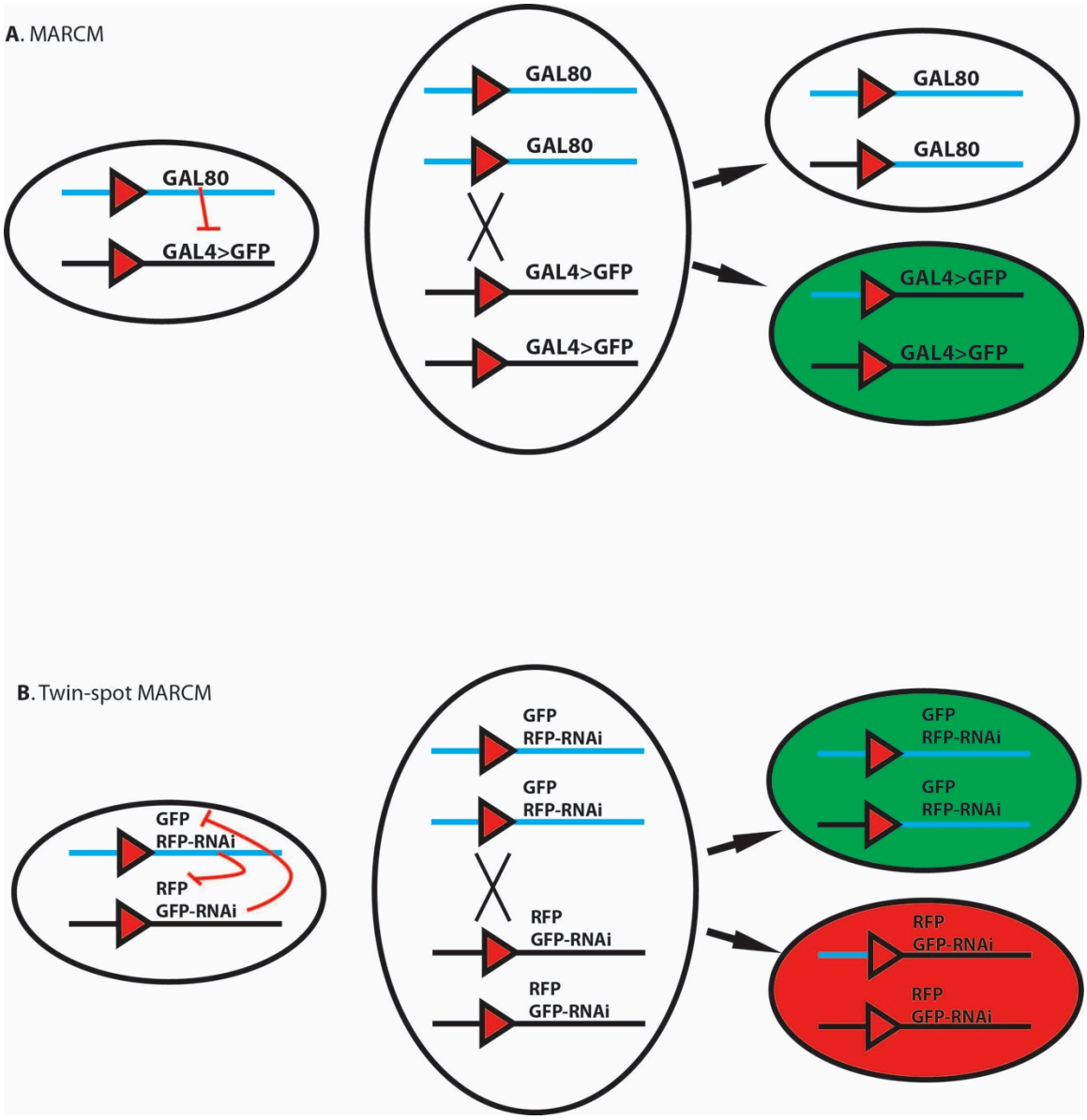

Figure 1.2. Mosaic Analysis with a Repressible Cell Marker (MARCM). Red triangles represent FRT sites. (A) Regular MARCM. Most of the fly is heterozygous (left; blue and black chromosomes), and GAL80 suppresses GAL4-driven transgene expression. In cells where flippase mediates recombination between homologous chromosomes during mitosis, one daughter cell can inherit both copies of GAL80, while the other inherits both copies of GAL4, and no GAL80. In these cells, GAL4 drives transgene expression (e.g., GFP, green cell). (B) Twin-spot MARCM. In tsMARCM, instead of GAL80, each chromosome arm bears a GAL4 responder, plus RNAi against the GAL4 responder on its other homolog (here, GFP and RFP). In cells where mitotic recombination takes place, one daughter inherits two copies of GFP and no GFP-RNAi (green cell), and the other inherits two copies of RFP and no RFP-RNAi (red cell). Adapted from Lee and Luo (1999) (A) and Yu et al. (2009) (B).

Chapter 2

TECHNIQUES FOR TARGETING SECONDARY HEMILINEAGES IN THE ADULT THORACIC VNS

Summary

To facilitate studies addressing the functional cohesion of hemilineages, I collaborated with Barret Pfeiffer (lab of G. Rubin) to design, assemble and test a panel of genetic reagents to target each thoracic hemilineage in the adult. I found that although the Rubin GAL4 collection did not include many lines targeting hemilineages in the adult, there were lines that hit every hemilineage in the third-instar larva. We then tried a number of techniques to refine and immortalize these larval patterns, taking advantage of the modular nature of the Rubin enhancer fragments. Tested methods included variants of the GAL4/UAS and LexA/LexAop binary systems, the GAL4 suppressor GAL80, regular and hormone-dependent flippases, and flip-on reagents. While it is difficult to predict how a given enhancer fragment will behave when GAL4 is replaced with a different effector, I was able to recover useable reagents from many of these attempts. I present a list of the genotypes that best target each hemilineage, and demonstrate how the lines can be used to isolate subsets of neurons in an expression pattern of interest.

Introduction

As outlined in Chapter 1, the basis for the work described in this thesis is the hypothesis that the hemilineages of the VNS can be viewed as 32 circuit elements, each performing a computation necessary for the execution of one or more VNS-mediated behaviors. To test

this hypothesis, I needed to be able to direct gene expression to each hemilineage specifically and reliably. This chapter summarizes my work building, testing and refining reagents towards this goal, in collaboration with Barret Pfeiffer and Gerald Rubin.

Historically, the secondary lineages have been studied using MARCM (Lee and Luo 2001, and see Chapter 1). Although MARCM is a powerful genetic technique, its major drawback is its stochasticity. Clones cannot be directed to a specific neuroblast (NB) or segment, and so experiments tend to require a very large number of animals. Also because it is a stochastic method, clones occur in only one or a few segments per animal, rather than all segments simultaneously. While this is useful for certain studies, it requires post-hoc dissection of every test animal to identify the affected segment(s). Finally, because it affects the neuroblasts (NBs), MARCM will always hit both hemilineages in a clone. I therefore decided to try a different approach, taking advantage of the large-scale screen of the Rubin GAL4 collection (Pfeiffer et al. 2008) to search for lines that showed expression in hemilineage clusters. Such patterns were rare in the adult, but relatively common in the larva. Using Fly Light's imagery database, we identified a set of GAL4 lines strongly targeting each of the 32 distinguishable secondary thoracic hemilineages in the third-instar larva, and then assembled a combination of genetic tools to spatiotemporally refine and immortalize the patterns. Ultimately, I was able to direct expression specifically to every hemilineage, with the exception of 11A and 11B (which are targeted together) and 16 (which I was unable to recover). As a demonstration of the utility and versatility of these lines, I used my hemilineage 12A line to direct responder

expression to the vPR6 cluster of *fruitless*-expressing neurons, hypothesized to regulate the inter-pulse interval of courtship song (von Philipsborn et al. 2011).

Materials and Methods

Fly stocks

Unless otherwise noted, flies were reared on standard cornmeal and molasses food at 25^{o}C. All GAL4 lines are from the Rubin GAL4 collection (Pfeiffer et al. 2008). *fru*-LexA refers to *fru*$^{P1.LexA}$ (Mellert et al. 2010). Unless noted otherwise, all other constructs were designed and built by Barret Pfeiffer and are listed in Table 1.

RU486/estradiol feeding

Hormone-sensitive reagents were tested under a variety of conditions. Treatments were as follows:

Larvae expressing a fusion protein of ligand binding domain (LBD) of the human estrogen receptor fused to GAL4 (hER-GAL4) were treated with water-soluble β-estradiol (Sigma). A vial containing ~15mL of cornmeal-molasses food was melted in the microwave, and then a solution containing either 20 or 40mg of β−estradiol in 1.5 ml distilled water was added, resulting in a final concentration of 200 or 400μM β-estradiol, respectively. Early third instars bearing UAS-GFP and R24B02-hER-GAL4 were floated out of food using 20% sucrose, collected with a paintbrush, and transferred to treated food vials. 24h later, wandering third instars were collected and dissected.

GeneSwitch constructs are a fusion of the human progesterone receptor LBD with GAL4 (Osterwalder et al. 2001, Roman et al. 2001). GeneSwitch animals were treated with the progesterone mimic mifepristone (RU486, Sigma). Food containing either 1.5 or 7mg RU486 dissolved in 1.5 ml 70% ethanol was made and fed to larvae as described above. For experiments in which adults were fed RU486, 10-20 flies were placed in a food vial with RU486, allowed to feed for three days, then collected and dissected.

For timed experiments, 10, 20, or 40µl of a ~10mM RU486 stock solution (10mg RU486 dissolved in 2ml 70% ethanol) were added to 500µl of 20% sucrose solution in an Eppendorf tube, for test concentrations of ~200, 400, or 800µM RU486, respectively. Third-instar larvae were collected as described above and transferred to the Eppendorf tube. Larvae were left floating in the sucrose-RU486 solution for either 5h or 20h, then transferred to a clean food vial. Animals were dissected 24h after the start of drug exposure.

For DMSO experiments, 5mg of RU486 was dissolved directly in 1ml of the tissue-penetrating solvent dimethyl sulfoxide (DMSO, Sigma). Wandering third instars were collected with a brush and dipped into the RU486-DMSO solution for 5-120s, then wiped clean and transferred to a fresh (non-treated) food vial until dissection. To allow time for the reporter to be transcribed and translated, animals were dissected 24h after exposure to drug, by which time, most had pupariated.

For surface application of RU486, parents were allowed to lay eggs in a food vial for a few days, then transferred to a fresh vial. Approximately 4 days after egg-laying, 60µL of a ~10mM RU486 stock solution (10mg RU486 dissolved in 2mL 95% ethanol) was applied to the surface of the food. At 24h after treatment, any larvae that had

wandered and/or pupariated were discarded to ensure that test animals had fed on RU486 for at least 24h. 48h after treatment, the subsequent wandering larvae and pupae (which had all fed on RU486 for 24-48h) were collected and transferred to an untreated food vial. These animals were then dissected at various times thereafter.

Preparation and examination of tissues

Tissues were dissected in PBS (phosphate-buffered saline, pH 7.8, Cellgro by MediaTech, Inc.) and fixed in 4% buffered formaldehyde overnight at 4°C. Fixed tissues were rinsed in PBS-TX (PBS with 1% Triton X-100, Sigma), then incubated in a cocktail of 10% normal donkey serum (Jackson ImmunoResearch), 1:1000 rabbit anti-GFP (Jackson ImmunoResearch), 1:40 rat anti-N-Cadherin (Developmental Studies Hybridoma Bank), and 1:40 mouse anti-Neuroglian (Developmental Studies Hybridoma Bank) overnight at 4°C. Tissues were then rinsed in PBS-TX and incubated with 1:500 AlexaFluor 488-conjugated donkey anti-rabbit, AlexaFluor 594-conjugated donkey anti-mouse, and AlexaFluor 649-conjugated donkey anti-rat (all from Invitrogen) overnight at 4°C. Tissues were then washed in PBS-TX, mounted onto poly-Lysine-coated coverslips, dehydrated through an ethanol series, cleared in xylenes, and mounted in DPX mountant (Sigma-Aldrich). Nervous systems were imaged on a Zeiss LSM 510 confocal microscope at 40x with optical sections taken at 2µm intervals. LSM files were contrast-enhanced as necessary and *z*-projected using ImageJ (http://rsbweb.nih.gov/ij/).

Results and Discussion

Identifying hemilineage-specific expression patterns

The Rubin collection of enhancer lines is based on a collection of about 7200 *cis* regulatory modules (CRMs). For each fly line a transgene including one of the CRMs, a core promoter, and the GAL4 protein coding region are inserted into a unique integration site on chromosome III (attP2) (Pfeiffer et al. 2008). I screened the Janelia Fly Light imagery database for CRMs driving expression in thoracic hemilineages. Very few lines (~9/7200, 0.1%) showed clean hemilineage expression in the adult, and of these, most were obviously incomplete. However, GAL4 expression patterns tend to change through development, and in the third-instar larva, a large proportion of Rubin lines (~30%) expresses GAL4 in one or more hemilineages. For the 32 distinguishable hemilineages, I was able to identify at least one GAL4 line that hit the target hemilineage and no other secondary neurons in the third-instar VNS. However, even the cleanest hemilineage GAL4 lines express in some off-target cells, including primary neurons in the larval VNS, primary and/or secondary neurons in the larval brain and/or peripheral targets at other stages.

Thus, I faced two related problems: how to refine these larval expression patterns, and how to immortalize this expression to maintain it into the adult, where I could then manipulate neuronal function. Towards both of these ends, I explored variations on two major transgene themes: binary systems (GAL4/UAS and LexA/LexAop), and flip-on reagents. As discussed in more detail in Chapter 1, the Rubin GAL4 collection was built so that a CRM that generated a GAL4 pattern of interest could be recloned to drive a different effector, such as LexA, then re-integrated into the same genomic location (or a

different location of choice) using phiC31 integrase, theoretically yielding LexA expression in the original pattern. While this is not always true (Pfeiffer et al. 2010, and see below), the reproducibility is sufficiently reliable that I collaborated with B. Pfeiffer in the Rubin lab to remake the enhancer fragments from our best GAL4 lines to drive a variety of effectors, including variants of GAL4 and LexA, and the GAL4 suppressor GAL80.

I used flip-on strategies to immortalize expression levels in selected neurons. For these strategies, a STOP cassette (a transcriptional terminator and insulating sequence) is flanked by flippase recognition target (FRT) sequences and placed between a promoter and a responder gene, thereby blocking responder transcription. Flippase expression is then directed to the cells of interest, excising the STOP cassette in those cells and allowing the responder sequence to be transcribed (Fig. 2.1) (e.g., Struhl and Basler 1993, Pignoni and Zipursky 1997, and Ito et al. 1997). Within this framework, every component can be modified. I found that the most effective approach was to test each component individually, then combine reliable reagents. Thus, I have organized this section in terms of the relative efficacy of single components. At the end, I discuss the most reliable combinations for obtaining lineage-specific expression in the adult.

Binary systems: GeneSwitch

The GAL4 protein can be split into two functional domains: the activation domain that controls transcriptional activity, and the DNA-binding domain that determines activator

sequence-specificity (Brent and Ptashne 1985, Keegan et al. 1986). These domains can be manipulated independently to generate chimeric proteins with different activation and/or DNA-binding properties. This modularity is the basis for most of the binary system variants I tested.

In the case of GeneSwitch, the "native" GAL4 activation domain is replaced with a truncated version of the human progesterone receptor (hPR) (Osterwalder et al. 2001, Roman et al. 2001). This truncated receptor binds the progesterone antagonist mifepristone (RU486). In the absence of RU486, the receptor sequesters the protein outside of the nucleus, rendering it transcriptionally inactive. However, after binding RU486, the receptor changes conformation and the protein enters the nucleus, where it drives transcription of UAS transgenes. A related system replaces the GAL4 activation domain with the human estrogen receptor (hER), and activates in the presence of β-estradiol (Han et al. 2000). I tested both systems as means of temporally restricting transgene expression.

I wanted to use GeneSwitch/hER-GAL4 constructs to drive UAS-flippase (UAS-flp) specifically in the third instar, to activate flip-on reagents. Without the temporal specificity provided by GeneSwitch, a hemilineage GAL4 line driving UAS-flippase in a flip-on strategy induces expression in unwanted cells, reflecting flippase activity in the embryo and adult, in addition to the larval targets (e.g. Fig. 2.2A). Thus, B. Pfeiffer remade 19 of our best larval GAL4 CRMs as GeneSwitch and/or hER-GAL4 lines.

For unknown reasons, we could not induce transgene expression using hER constructs (data not shown), but the GeneSwitch constructs worked well. Our tester construct, R24B02-GeneSwitch, did not drive GFP expression in the absence of RU486, whereas robust expression was observed in larvae or adults transferred to food containing approximately 50μM RU486 for 24h (larvae) or 72h (adults) (Fig. 2.3). I then used a broader CRM pattern, R20B05, to compare different drug concentrations and exposure times. Third-instar larvae were floated in 20% sucrose containing 200, 400, or 800μM RU486 for either 5h or 20h. After a 5h exposure, 800μM RU486 resulted in the most robust transgene expression; after a 20h exposure, both 400μM and 800μM RU486 yielded strong expression (Fig. 2.4C-D).

Due to the difficulty involved in collecting and transferring feeding larvae, I tested two additional methods. First, I exposed newly wandering larvae to ~10mM RU486 dissolved in dimethyl sulfoxide (DMSO) for 5, 30, 60, or 120s, and dissected them 24h later. The 60 and 120s treatments were usually lethal. A 5 or 30s exposure to RU486 in DMSO sufficed to induce robust expression in most cells (Fig. 2.4E). This treatment has the advantage of being effective in non-feeding stages such as wandering larvae and pupae. A second method involved applying different amounts of ~10mM RU486 to the surface of a vial of food containing larvae. The net (whole-vial) RU486 concentrations tested were up to 100μM, but since larvae tend to live in the top few millimeters of food in a vial, the relevant exposure concentrations were likely much higher. I found that 60μl of a 10mM stock solution of RU486 applied to the food surface induced expression comparable to that observed with food containing 50μM RU486 (Fig. 2.4B) and with

higher surface treatments of RU486 (data not shown). This last method became my standard RU486 treatment.

My next concern was whether RU486 applied using that method persists through metamorphosis to activate the (unwanted) adult expression pattern. I transferred larvae to food containing ~ 1mM RU486 at 24h prior to wandering, then removed them from the vial at the onset of wandering, transferred them to non-RU486 food, and dissected them at different time points. As shown in Fig. 2.3C, expression in the larval pattern persists until approximately 48h APF, but no expression is observed in the adult. This is in accord with Osterwald et al. (2001), who found that expression of elav-GeneSwitch in first instar larvae decreases to undetectable levels within ~24h of being transferred to RU486-free food, although a similar decay is not observed in fed adults (Roman et al. 2001). For the GAL4 lines I used, this was sufficient to eliminate unwanted expression.

Finally, I wanted to know whether this hormone-dependent expression was sufficient to refine UAS-flp expression, since theoretically a single molecule of flippase could excise a STOP cassette and permanently activate transgene expression in a cell. GeneSwitch appears to be highly effective in the context of flip-on immortalization: compared to the parent GAL4 line, R24B02-GeneSwitch eliminates nearly all off-target expression in the VNS (Fig. 2.2).

I tested 19 CRM-GeneSwitch constructs. Seven worked reliably in the larva; examples are shown in Fig. 2.5. Of those, 5 worked in flip-on immortalization pathways. One

possible reason for the 12 failed constructs is that for some lines, the pattern observed in the third-instar larva might reflect perduring GFP molecules that were transcribed at an earlier time. If the CRM is not actively driving GAL4/GeneSwitch expression in the third instar, that could explain why exposure to drug at this time does not induce the expected expression pattern. It should also be noted that all of the GeneSwitch constructs share ectopic expression in the optic lobes (Fig. 2.5). Since they were inserted into the same integrase site as the parent GAL4 lines, which do not show this pattern, this is not a position effect (see next section), but likely reflects activity inherent to the GeneSwitch sequence.

Binary systems: Split GAL4

Luan et al. (2006) showed that one can drive transcription of the GAL4 activation domain (AD) and DNA-binding domain (DBD) separately, then bring them together with a leucine zipper, a system they call Split GAL4. The advantage of Split GAL4 is that the AD can be driven in one pattern and the DBD in another, and only in cells where the two patterns overlap do the two halves come together to drive transgene expression.

For each hemilineage, I selected two CRMs that overlapped in that hemilineage and nowhere else in the larva, and B. Pfeiffer made one into a Split GAL4 AD (utilizing the strong activation domain p65, rather than the "native" GAL4 AD) and the other into a Split GAL4DBD. Where possible, I chose combinations that did not overlap in the adult.

I also selected three CRMs that drove expression in all secondary neurons, but no primary neurons, and B. Pfeiffer made them into Split ADs and/or DBDs.

Out of 11 hemilineage-specific pairs, 2 worked. An example is shown in Fig. 2.6A. There were no obvious features of the parent CRMs that correlated with successful versus failed Split pairs. I also crossed the three pan-secondary ADs to DBDs made from CRMs expressing in various lineages. Of 10 tested lines, 6 worked when crossed to the pan-secondary R20B05-AD (e.g. Fig. 2.6B). Unfortunately, although many lineage/pan-secondary combinations did restrict expression to the intersection of the parent CRMs, most of the CRMs I chose expressed in multiple hemilineages, and thus the combinations were not particularly useful. Additionally, although the three pan-secondary CRMs had seemingly identical expression patterns as GAL4 lines, I found differences in their efficacy as Split GAL4 ADs. R20B05-AD appeared to work as expected, preserving hemilineage expression while excluding primary expression from the intersected CRM pattern (Fig. 2.7). R10G10-AD did not work at all. R17C04-AD preserved hemilineage expression but also allowed expression in primary neurons. I did not specifically determine the reason for this with R17C04, but speculate that the change is related to the pattern expansion sometimes observed when the GAL4 AD is replaced with the strong p65 AD (e.g., Pfeiffer et al. 2010). Because R20B05 did not suffer from this pattern, this effect appears to depend on the CRM used to drive expression.

I then gathered the strongest Split GAL4 combinations and used them to drive UAS-flp expression to activate a flip-on immortalization pathway. This step likewise yielded

mixed results; examples are shown in Fig. 2.6 (A" and B"). Again, there was no obvious pattern that explained why some combinations worked while others did not.

B. Pfeiffer and I attempted to troubleshoot our Split GAL4 failures. One candidate was the genomic location of the insertion site. To facilitate stock-building and avoid transvection (see below), Split-GAL4 DBDs were inserted into the same site as the parent GAL4 lines (attP2), but the ADs were inserted into a different integrase site, attP40, on chromosome II. In many cases, insertion of the same CRM into a different integrase site altered the expression pattern, due to various local chromatin influences collectively called position effects (Pfeiffer et al. 2010). To probe the range of position effects on my Splits, I compared the insertion of R20B05-AD at three different chromosomal sites: attP40 (where the other ADs were inserted), attP2 (where the parent GAL4 constructs were inserted), and VK000027. When crossed to the R24B02-DBD, the attP40 and VK000027 transgenes were equally weak, and did not drive expression in the target hemilineage, hemilineage 12A (Fig. 2.8), but the attP2 insertion of R20B05-AD did show expression in the target hemilineage when crossed to R24B02-DBD. However, when I crossed R20B05-AD to R23G07-DBD (attP2), I saw expression in the target lineage, but also in off-target primary neurons present in the R23G07-GAL4 expression pattern (Fig. 2.8).

The above result was perplexing, because the R20B05 CRM does not drive expression in primary neurons. Consequently, I did not expect to get functional Split GAL4 in those cells. The unexpected expression was likely due to transvection, a phenomenon in which

the regulatory region of a gene can influence transcription on its paired chromosomal homolog (i.e., in *trans*). Mellert and Truman (2012) demonstrated that when two transgenes are inserted into the same integrase site, the enhancer for one can sometimes drive expression of the other. In this case, it appears that the R23G07 CRM drives expression of both the DBD in *cis* and the AD in *trans,* allowing the reconstitution of active Split GAL4 in the full pattern. I observed this pattern with several other DBDs that were inserted in the same chromosomal site as the AD (data not shown). Thus, although integrating Split GAL4 halves into different attP sites can change their expression patterns in unexpected ways, inserting both halves into the same integration site is not an option due to the prevalence of transvection.

I then gathered the strongest Split GAL4 combinations and used them to drive UAS-flp expression to activate a flip-on immortalization pathway. This step likewise yielded mixed results; examples are shown in Fig. 2.6(A", B"). Off-target expression could be due to unexpected expression at different stages, since patterns were not examined for overlap at all developmental stages.

Binary systems: GAL80

In yeast, GAL80 binds and inactivates GAL4 in the absence of galactose. In *Drosophila,* GAL80 has been used to refine GAL4-driven transgene expression patterns by inactivating GAL4 in a subset of cells. Historically, while there were a few well-defined GAL80 patterns (e.g., pan-cellular *tubulin*-GAL80 and VNS-specific *teashirt*-GAL80),

most GAL80 lines were generated as enhancer traps, and thus their expression patterns had to be deduced from crosses to characterized GAL4 lines. The modular nature of the Rubin GAL4 collection, however, allows the creation of targeted CRM-GAL80 lines that should theoretically express GAL80 in the same cells as that CRM's parent GAL4 line.

As noted, GAL4 lines driving expression in secondary hemilineages in the third-instar larva are relatively common in the Rubin GAL4 collection. I took four GAL4 lines that expressed in the majority, but not all, of the secondary lineages, and had them remade as GAL80 lines. The goal was to use these GAL80 lines to restrict multi-lineage patterns to single or a few hemilineages.

The selected CRMs were made into three types of GAL80 construct: "traditional" GAL80, which contains no intron and uses an hsp70 3'-untranslated (UTR) sequence; GAL80v5, which contains an intron (IVS) to improve translational efficiency (Huang and Gorman 1990, Duncker et al. 1997) and the SV40 3'-UTR to improve RNA stability (Lee and Luo 2001); and GAL80-WPRE, which contains an IVS and a viral woodchuck post-transcriptional regulatory element to improve protein expression (Zufferey et al. 1999, Pfeiffer et al. 2010). All three types of construct performed similarly. To test the GAL80 lines, I crossed them to flies bearing a GAL4 line that expresses in all secondary neurons, R20B05-GAL4, and a UAS-GFP reporter. All four enhancers produced effective suppression in the targeted lineages when crossed to R20B05-GAL4, resulting in the predicted expression pattern. For example, R15E07-GAL4 drives expression in all secondary hemilineages except those that project in the anterior intermediate commissure

(lineages 7B, 8B, 10B, and 18B). When R15E07-GAL80 is crossed to R20B05-GAL4, expression is suppressed in all but those lineages, and we are left with a clean 7B/8B/10B/18B driver line (Fig. 2.9D).

In addition to CRM-GAL80 constructs, I found another GAL80 that could isolate lineages: nSyb-GAL80. The neuronal synaptobrevin promoter (nSyb) (DiAntonio et al. 1993) is traditionally used as a pan-neuronal driver (e.g., Pauli et al. 2008, von Philipsborn et al. 2011). However, when expressing nSyb-GAL4 in larvae, I found that it drives expression in the functioning primary neurons but not in the clusters of arrested, immature secondary neurons (Fig. 2.10A). Given this expression pattern, I reasoned that nSyb-GAL80 (which has been published as a pan-neural GAL4 suppressor in the adult, e.g. Rubinstein et al. 2010) could be used in the larva to eliminate off-target expression in primary neurons in our hemilineage GAL4 lines, without affecting larval hemilineage expression. Indeed, I found that when nSyb-GAL80 was crossed to flies homozygous for R15D11-GAL4 and UAS-GFP, the primary neurons that are normally seen in that line were suppressed, leaving clean expression in hemilineage 12B in all three thoracic segments (Fig. 2.10C). This is the first use of nSyb-GAL80 in such a developmental context. In addition, I could then use the GAL4/nSyb-GAL80 combination to drive UAS-flp expression with a flip-on LexA: the LexA, lacking the GAL4 AD, is GAL80-insensitive, but the nSyb-GAL80 suppresses the (unwanted) adult pattern of the GAL4 line. Thus, nSyb-GAL80 eliminates off-target expression in both the larva and the adult, resulting in much-improved flip-on results (e.g. Fig. 2.10E). This proved to be the most effective strategy for reliably refining larval hemilineage GAL4 lines.

Hormone-activated flippase (UAS-hPR-Flp)

Flippase is an enzyme that catalyzes recombination between specific DNA sequences, called flippase recognition target (FRT) sites (Broach et al. 1982). Thus, just like transcriptional activators, flippase needs to be in the nucleus to have an effect. In order to keep flippase out of the nucleus until needed, B. Pfeiffer suggested a strategy similar to GeneSwitch GAL4 and fused the ligand-binding domain of hPR to flippase. B. Pfeiffer made several fusions of the hPR and flippase. I found that a version with the hPR fused to the N-terminus of the flippase protein reliably catalyzed STOP cassette excision in the presence of RU486, but showed very little activity in the absence of the drug (Fig. 2.11).

I then tested whether UAS-hPR-flp could be used to restrict STOP cassette excision to the third-instar larva in a flip-on immortalization scheme. Indeed, I found that compared to UAS-flp, UAS-hPR-flp yielded a cleaner, more hemilineage-specific pattern when crossed to the same immortalization scheme (Fig. 2.10F). This is presumably because off-target cells from other developmental stages were eliminated. This strategy has a major advantage for our flip-on schemes: by making the flippase hormone-dependent, rather than using a binary system, the UAS-hPR-flp can be used with any GAL4 line. By contrast, with a GeneSwitch strategy, each CRM of interest must be remade into a GeneSwitch line and tested.

The best methods and CRMs to target each hemilineage are summarized in Table 1. (Hemilineage nomenclature is after Truman et al. 2010). I have genotypes that yield reasonably reliable adult expression in nearly all of the hemilineages. I was unable to recover good lines for lineage 0 or lineage 16, and I have a clean line that targets lineage 11, but not its separate hemilineages. I assigned qualitative cleanliness and reliability rankings to the lines as follows: Category I (best, expression is totally restricted to the lineage/hemilineage), II (expression is sometimes observed in other lineages or neurons, and/or the lineage of interest is sometimes missing from hemisegments), and III (adequate, but consistently expresses in a characteristic set of off-target cells, and/or the lineage of interest is consistently missing from one or more hemisegments).

Case study: Using hemilineage lines to target and determine the developmental origin of the vPR6 cluster of fruitless*-expressing neurons*

It is commonly held that an ontogenetic nomenclature system is the only practical way to assign identities to the overwhelming diversity of neurons in the insect brain (e.g., Rowell 1989). Thus, it would be convenient to have a way to assign developmental origin to a particular neuron or neural class, e.g. a hit in a behavioral screen, or neurons that express a gene of interest. Under certain circumstances, the toolset described here can be used to dissect broad gene expression patterns in the VNS into subsets that come from a common NB, and/or to assign NB origin to a neural class of interest. As proof of principle, we demonstrated that a previously identified subset of the *fruitless (fru)*-expressing neurons are all produced in hemilineage 12A, and cleanly isolated the entire cluster, which has not been previously published.

The *fru*-expressing neurons are necessary and sufficient to drive most aspects of male courtship behavior in the fly, and their anatomy, genetics, and function have been dissected in detail. Yu et al. (2010) divided the *fru* expression pattern into ~100 groups of cells, including ~40 in the VNS. von Philipsborn et al. (2011) subsequently identified lines targeting those groups using a screen of ~1000 GAL4 lines intersected with *fru*-Flp. The largest cell cluster in the VNS, which Yu et al. (2010) terms vPR6, projects to a structure they call the thoracic triangle and may be involved in shaping the courtship song. In their GAL4 screen, von Philipsborn et al. (2011) recovered 5 lines that each captured 2-5 of these cells in the male, and none in the female. These lines clearly did not hit all of the cells in the vPR6 cluster, since Yu et al. estimated that it should contain approximately 6-10 cells in the male and 4-6 cells in the female (2010).

Based on the projection pattern of these cells, J. Truman determined that the vPR6 cluster was made up of progeny of hemilineage 12A. I used my hemilineage 12A combination (including the 12A driver R24B02, nSyb-GAL80, UAS-flippase, and LexAop>stop>GFP) to restrict LexAop>GFP expression in the VNS to the neurons of hemilineage 12A, then used $fru^{P1.LexA}$ (Mellert et al. 2010) to drive GFP expression in the subset of 12A neurons that are part of the *fru* pattern. This technique reliably captured a group of approximately 12 cells in males, whereas lines from previous screens captured only ~ 5 cells (von Philipsborn et al. 2011). The male vPR6 cluster is estimated to include 6-10 cells according to Yu et al. (2010), while I observed 14-16 cells in the cluster when using $fru^{P1.LexA}$ to drive LexAop-GFP. (The difference in total cell counts may be due to

differences in the *fru*-Flp vs. *fru*-LexA driver expression patterns.) The intersected pattern was quite clean in the VNS (Fig. 2.12C), similar to the lines published by von Philipsborn et al. (2011) but with more cells. Expression was also observed in a few *fru*-expressing neurons in the brain, again similar to the levels of brain expression exhibited by the lines of von Philipsborn et al. (2011). Using my lines, I was able to confirm that the shape of the full vPR6 arbor in both sexes matches the digitally masked arbor assigned to vPR6 in Yu et al. (2010). Thus, it is possible to identify the developmental origin of secondary neurons of interest and isolate those neurons using the toolkit presented here, provided one has a GAL80-insensitive driver for the chosen cells.

I have made a comparative assessment of various genetic strategies for targeting the hemilineages of the *Drosophila* VNS. Using a combination of Rubin GAL4 lines (in the adult and in the larva), flip-on reagents, and variations thereof, I have assembled genotypes to direct transgene expression to nearly all the lineages of the VNS, strongly and specifically. I hope that the reagents described in this chapter will prove of use to future studies of the development and function of the secondary lineages of the VNS, in addition to the experiments described in subsequent chapters of this thesis.

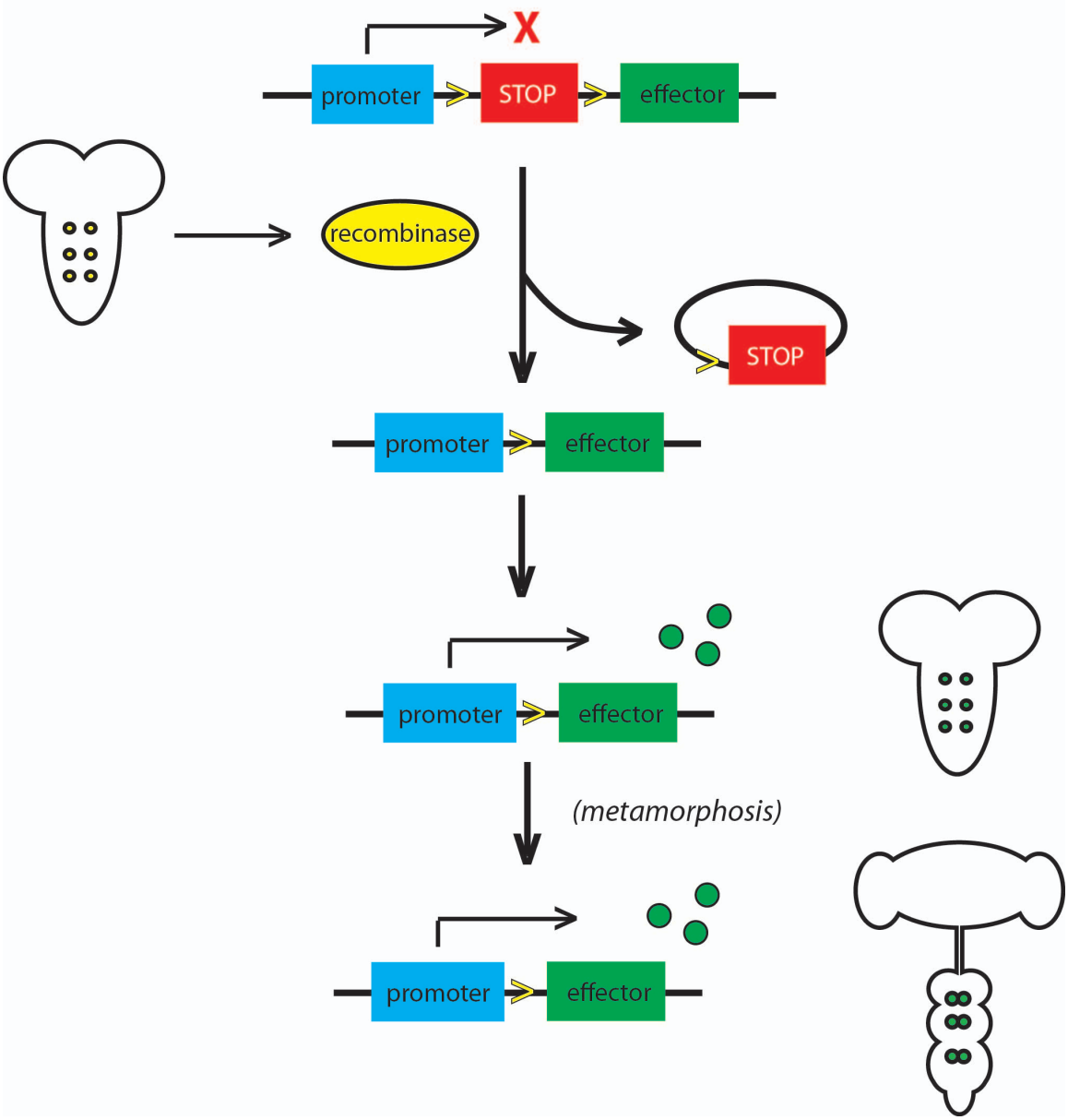

Figure 2.1. A flip-on strategy to immortalize larval expression patterns. Flippase-dependent ("flip-on") transgenes have a STOP cassette flanked by FRT sites (yellow arrowheads) inserted between a promotor and a coding sequence of choice, preventing transcription (top). Flippase is driven in cells of interest in the larval CNS, indicated in yellow on the left. Flippase excises the STOP cassette, permitting transcription specifically in the cells of interest. The use of a constitutive promoter, such as the actin promoter, results in continual expression following excision (bottom, indicated in green).

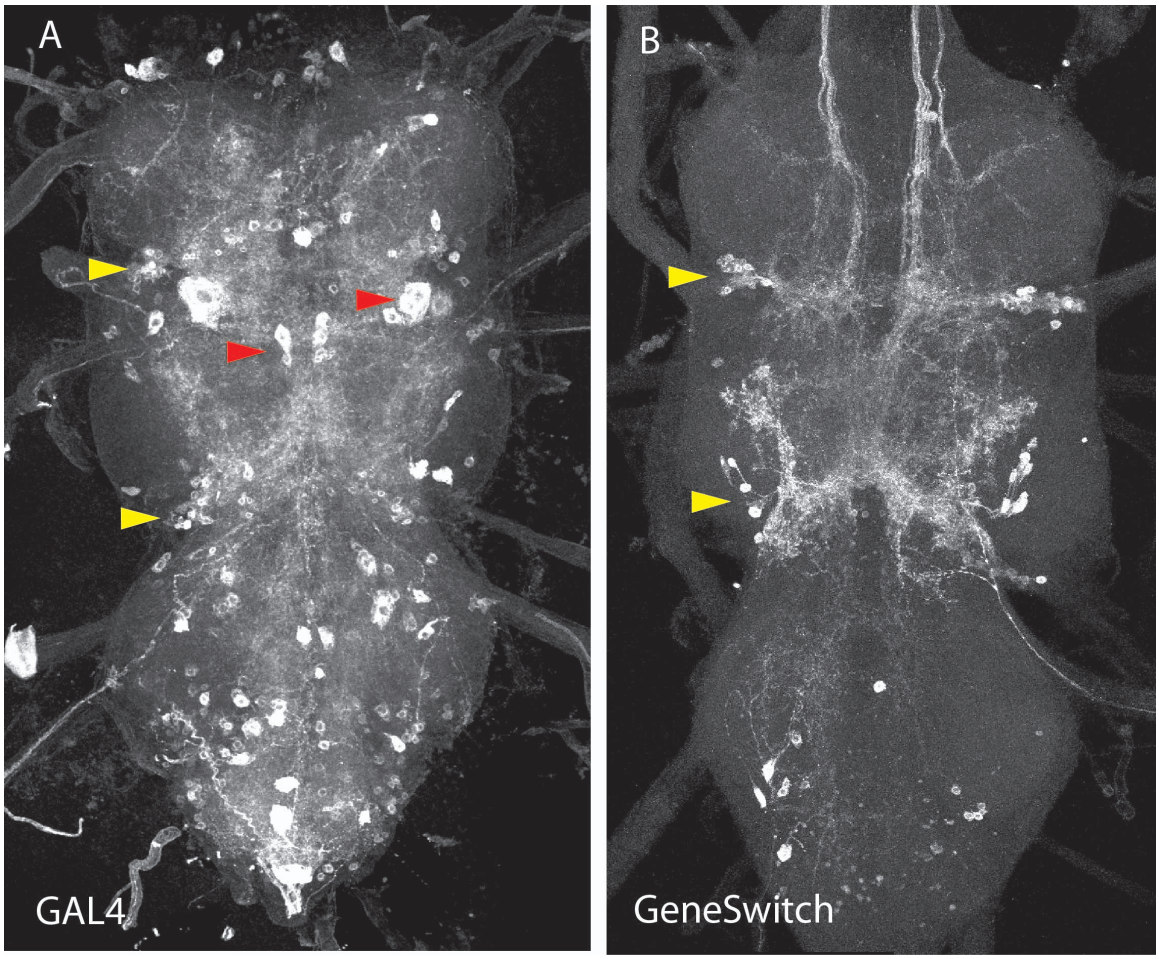

Figure 2.2. R24B02-GeneSwitch restricts UAS-flp expression to target cells. Adult VNSs bearing act>STOP>GAL4; UAS-flp; UAS-GFP crossed to R24B02-GAL4 or R24B02-GeneSwitch. (A) In the case of R24B02-GAL4, cells from driver activity at all stages of development, embryo to adult, are flipped on. Expression is observed in many cells, including hemilineage 12A (yellow arrowheads) and off-target cells (e.g., red arrowheads). (B) When R24B02-GeneSwitch is used and larvae are fed on RU486 food as third-instar larvae, flippase activity is restricted to the larval expression pattern, hemilineage 12A (yellow arrowheads).

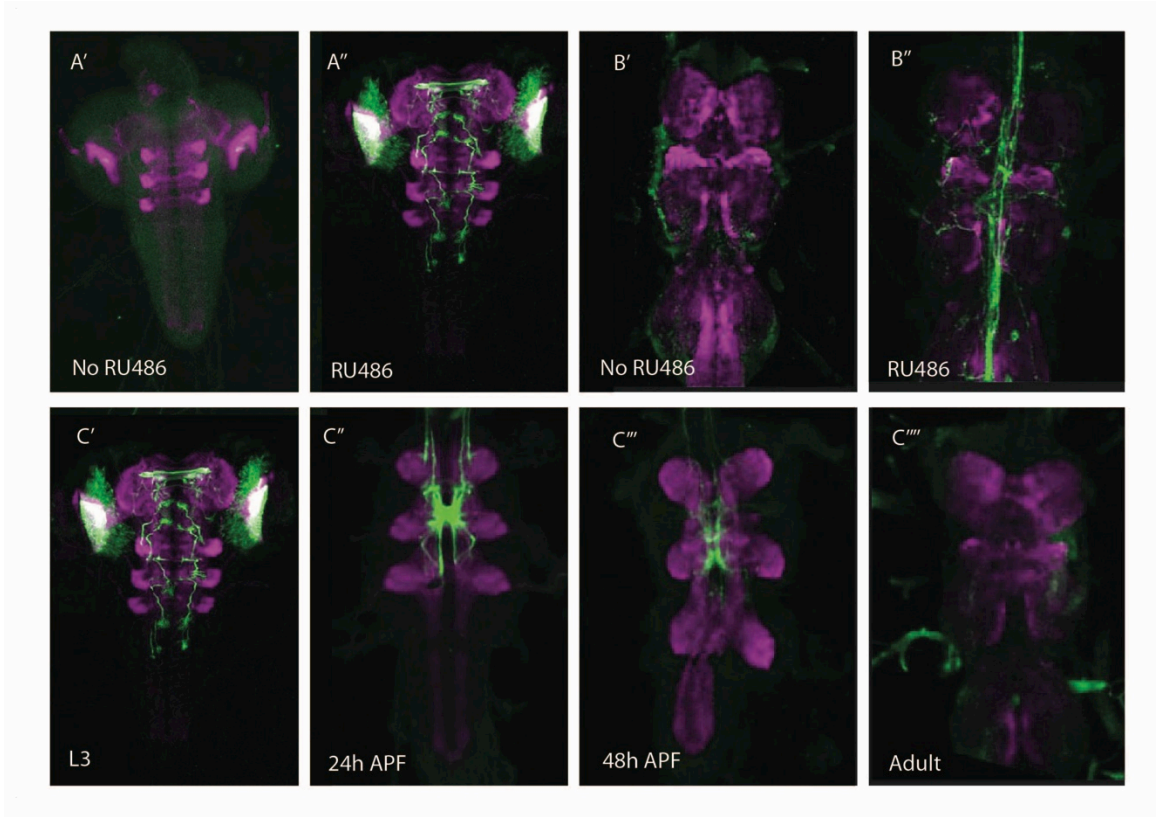

Figure 2.3. GeneSwitch-driven GFP expression is dependent on administration of RU486. All flies are w; +; R24B02-GeneSwitch/pJFRC2-UAS-GFP. (A) L3 CNS: untreated (A') vs. fed on 1mM RU486 food for 24h as L3 (A''). (B) Adult VNC: untreated (B') vs. fed on 1mM RU486 food for 72h as adults (B''). (C) Animals fed on RU486 food for 24h during L3 show robust expression in the larval pattern at wandering L3 (C'). This expression persists at 24h APF (C'') and 48h AFP(C'''), but disappears by the adult stage (C''''). L3, third-instar larva; VNC, ventral nerve cord; APF, after puparium formation. Green: anti-GFP; magenta: anti-nCadherin.

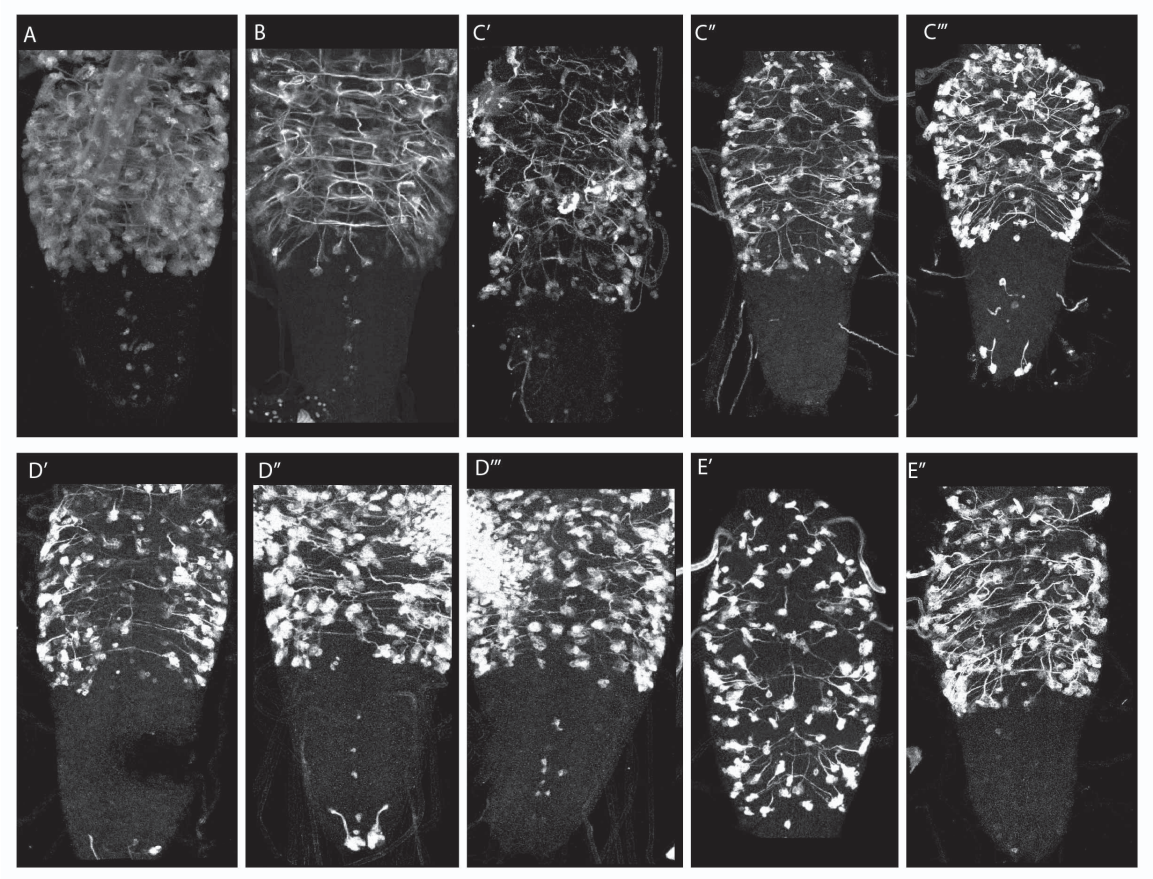

Figure 2.4. Comparison of RU486 administration methods for third-instar larvae. VNSs from third-instar larvae (A, B) or pupae 0-24h APF (C-E). (A) R20B05-GAL4 drives expression in all secondary hemilineages. B-E: GFP expression driven by R20B05-GeneSwitch after different doses and methods of RU486 administration. All flies are w; +; R20B05-GeneSwitch/pJFRC2-UAS-GFP. (B) Larva from a vial treated with 60uL of ~1mM RU486 for 24h. (C) Feeding (pre-wandering) L3s floated for 5h in 20% sucrose solution containing ~200uM (C'), 400uM (C''), or 800uM (C''') RU486. Larvae/prepupae were dissected 24h after the start of treatment. (D) As in (C), but L3s were floated for 20h. (E) Treated with a 5s (E') or 30s (E'') exposure to ~10mM RU486 in DMSO as L3w, then dissected 24h after treatment. All treatments induce UAS-GFP expression in the expected pattern. L3w, wandering third instar. APF, after puparium formation.

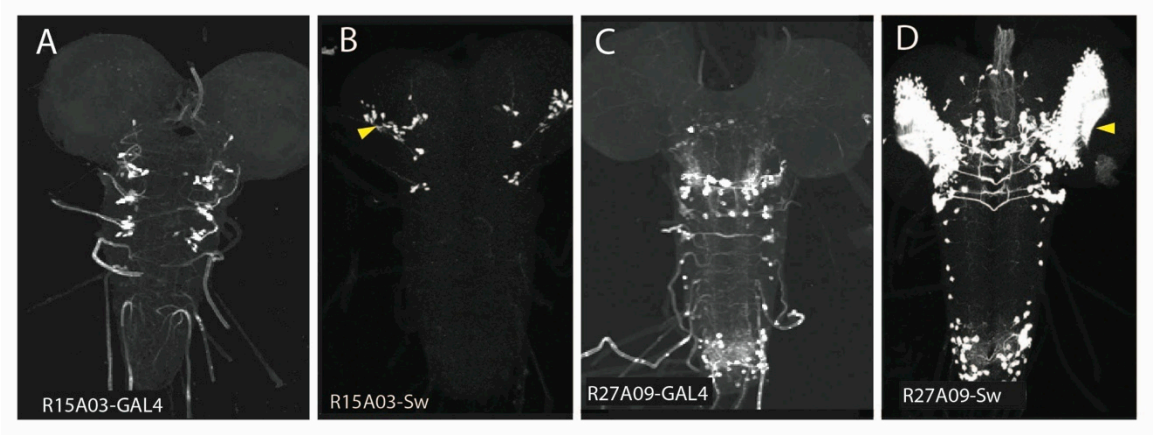

Figure 2.5. Examples of CRM-GeneSwitch lines. (A) R15A03-GAL4 drives expression in lineage 24. (B) R15A03-GeneSwitch, fed on RU486 food for 24h, also drives expression in lineage 24. (C) R27A09-GAL4 drives expression in lineage 18B plus primary neurons. (D) R27A09-GeneSwitch, fed on RU486 food for 24h, drives expression in the same pattern.Yellow arrowheads, background optic lobe expression found in all GeneSwitch lines, but not the parent GAL4s (see text).

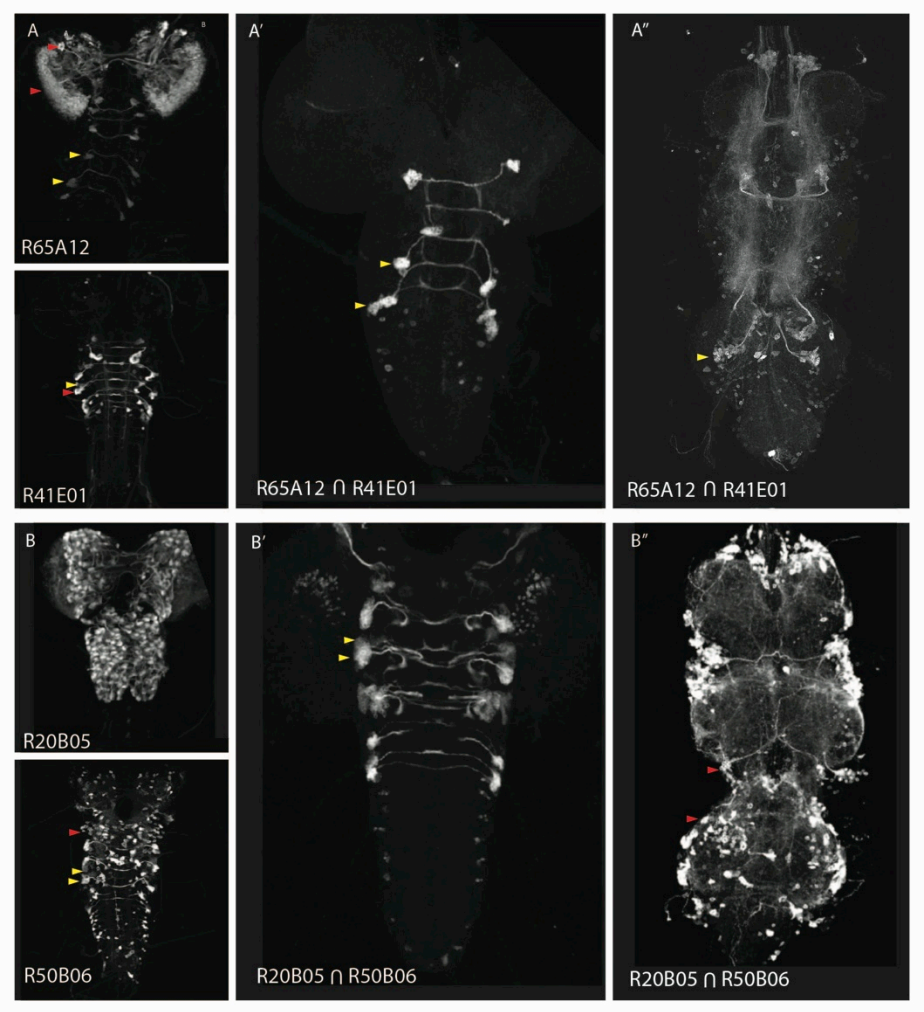

Figure 2.6. Split GAL4 constructs. Left panels, "parent" CRM-GAL4s (upper panel, Split-GAL4-AD; lower panel, Split-GAL4-DBD). Images from the Janelia FlyLight database. Center panels, Split-GAL4-driven GFP expression in third-instar larvae. Right panels, Split-GAL4s crossed to a flip-on stock. Genotype: act>STOP>GAL4(attP18)/w; CRM1-AD(attP40)/UAS-flp(attP40); CRM2-DBD(attP2)/pJFRC2-UAS-GFP(attP2). (A) A dedicated hemilineage 7B pair, R65A12-AD and R41E01-DBD. In the larva, R65A12 drives expression in hemilineage 7B (yellow arrowheads) and several brain lineages (red arrowheads). R41E01 drives expression in hemilineages 7B (yellow arrowheads) and 23B (red arrowheads). The Split-GAL4 intersection drives expression specifically in hemilineage 7B in the larva (A') and successfully immortalized hemilineage 7B in a flip-on strategy in the adult (A''). (B) An example of intersection with the pan-secondary CRM R20B05 eliminating expression in primary neurons. R50B06 drives expression in hemilineages 9A and 17A (yellow arrowheads), plus primary neurons (red arrowheads). The Split-GAL4 intersection drives expression specifically in those lineages in the larva (B'), but picks up off-target cells in the adult when used with an immortalization strategy (B'', e.g. red arrowheads).

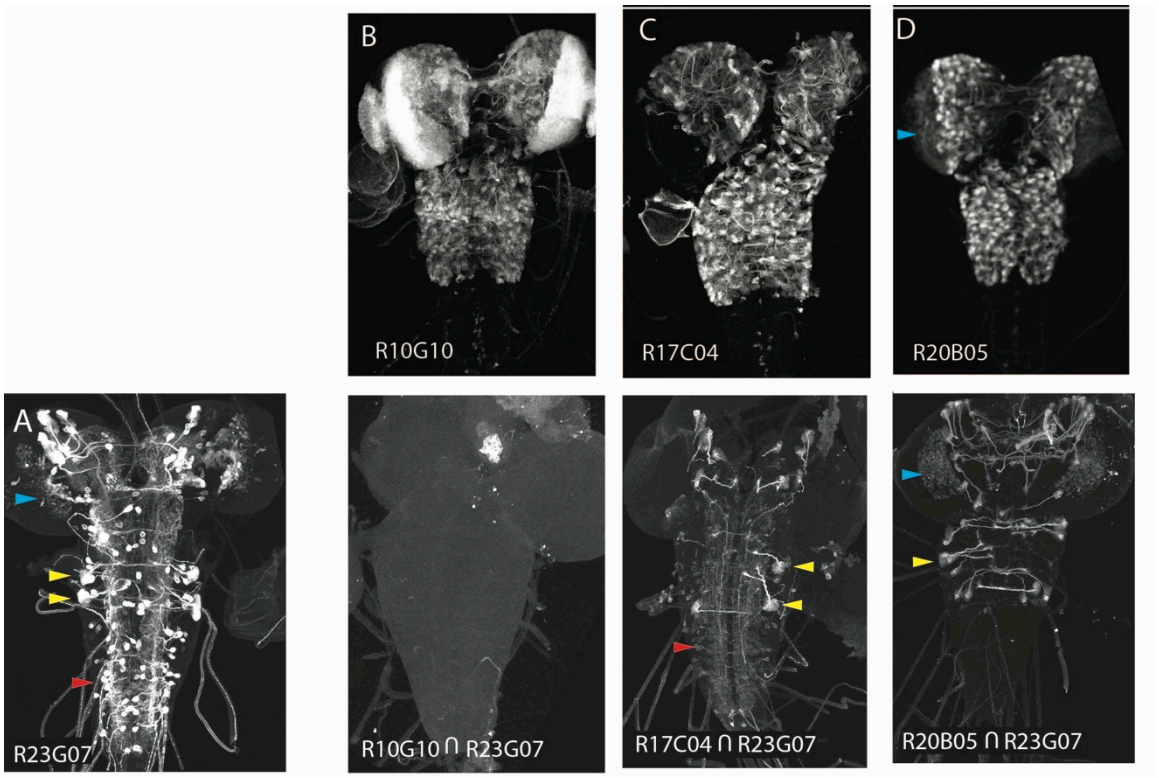

Figure 2.7. Three pan-secondary Split ADs yield different intersection results. (A) R23G07-GAL4 drives expression in secondary lineage 11 (yellow arrowheads), primary neurons (red arrowheads), and the optic lobe (blue arrowhead). Image from the Janelia Farm FlyLight database. (B-D) Three CRMs that drive expression in all secondary neurons. Upper panels, expression pattern driven by the CRM-GAL4; lower panels, R23G07-DBD (attP2) intersected with each CRM-AD (attP40). (B) R10G10-AD drove no CNS expression with R23C07-DBD. (C) R17C04-AD with R23G07 drove expression in lineage 11 (yellow arrowheads), but also unexpectedly drove expression in primary neurons (red arrowheads). (D) R20B05-AD with R23G07-DBD drove expression in lineage 11 (yellow arrowheads) and the optic lobe (blue arrowhead), but not in primary neurons.

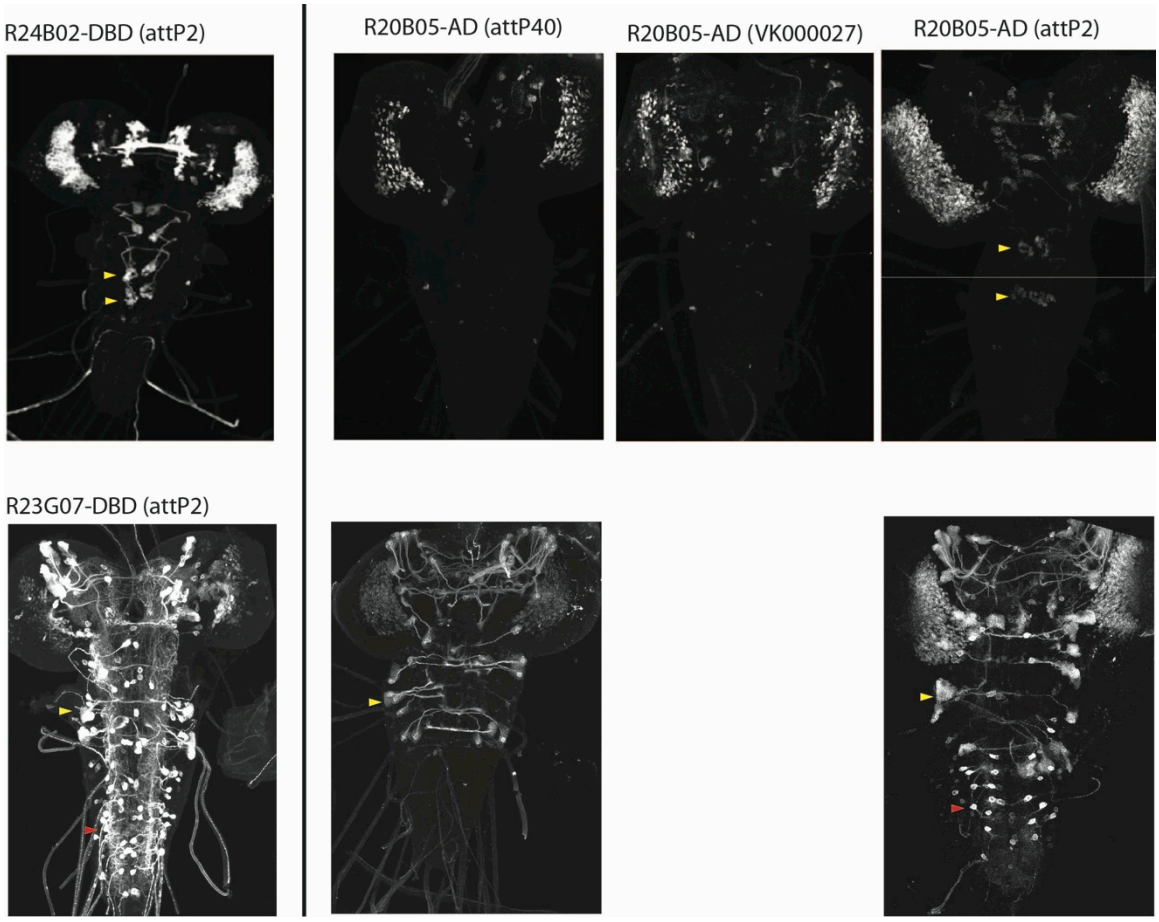

Figure 2.8. Split GAL4 expression depends on integration site. Split GAL4 DBDs integrated into attP2 were crossed to the pan-secondary R20B05-AD insertion noted at top (integrase site in parentheses). GAL4 expression patterns of the DBD parent CRMs are shown at left (images from the Janelia Farm FlyLight database). Upper row: R24B02-DBD. Expression in hemilineage 12A is only recovered from the attP2 insertion of R20B05-AD (yellow arrowheads). Lower row: R23G07-DBD. The attP40 insertion of R20B05-AD drives expression in secondary lineage 11 but not primary neurons; the attP2 insertion of R20B05-AD drives expression in both secondary lineage 11 (yellow arrowheads) and primary neurons from the R23G07 pattern (red arrowheads). The unexpected expression in primary neurons is likely due to transvection (see text).

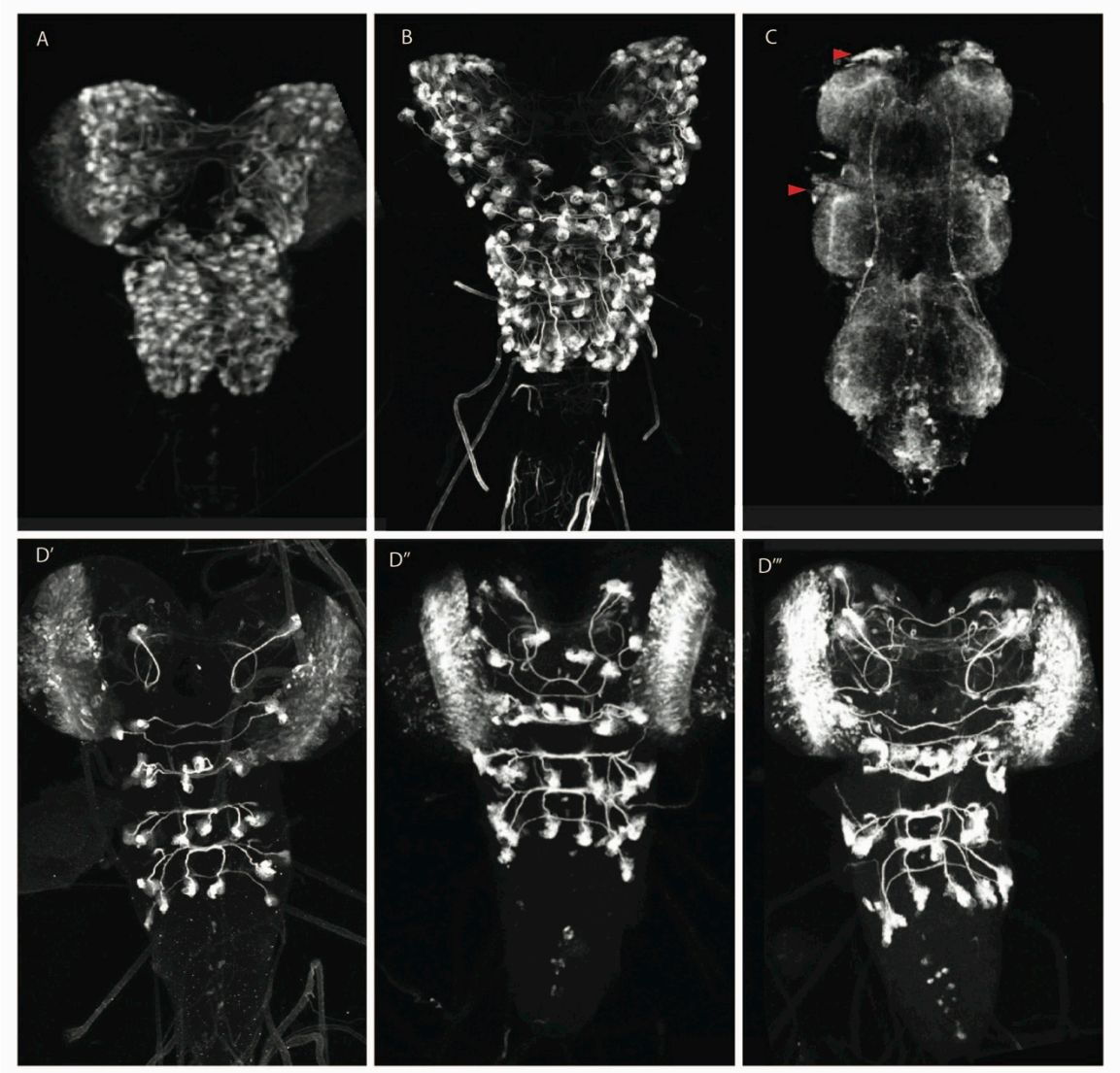

Figure 2.9. Targeted restriction of GAL4 expression using CRM-GAL80. (A) R20B05-GAL4 drives expression in all secondary hemilineages. GAL80-restricted patterns in C and D are crossed to this driver. (B) R15E07-GAL4 drives expression in most lineages in the larva, with the exception of hemilineages that project in the aI commissure. (C) When R15E07-GAL80-restricted R20B05 expression was used to drive UAS-flp in a flip-on immortalization pathway, the resultant expression patterns did not hit the target lineages; e.g., hemilineage 15B is not present in the restricted larval pattern (D), but it appears in the immortalized pattern (red arrowheads). Genotype: act>STOP>GAL4(attP18)/+; R15E07-GAL80v5(attP40)/+; R20B05-GAL4/pJFRC2-UAS-GFP(attP2). (D) When R20B05-GAL4 expression is restricted by R15E07-GAL80 constructs with different posttranscriptional modifiers, expression is restricted to the expected cells (i.e., hemilineages projecting in the aI commissure). (D') "Traditional" 15E07-GAL80, (D'') 15E07-GAL80v5, (D''') 15E07-GAL80-WPRE-SV40 (see text). Genotype: +; R15E07-GAL80(attP40)/+; R20B05-GAL4/pJFRC2-UAS-GFP(attP2).

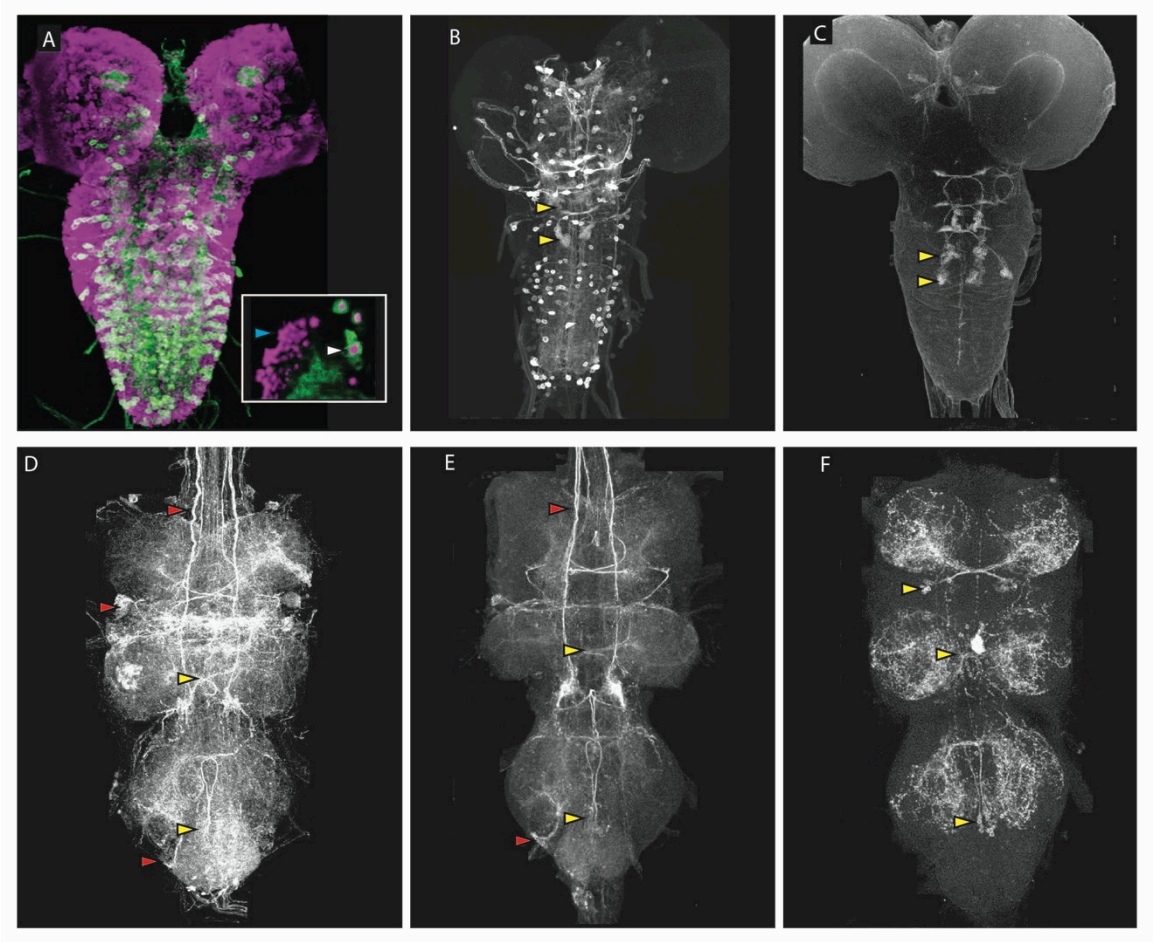

Figure 2.10. nSyb-GAL80 suppresses GAL4 expression specifically in mature neurons. (A) In the third-instar larva, nSyb-GAL4 drives expression in primary neurons, but not secondary neurons. Inset: single optical slice showing colocalization of anti-GFP (green) and the pan-neural marker anti-elav (magenta) in primary neurons (e.g., white arrowhead), but not in immature secondary neurons (e.g., blue arrowhead). (B) R15D11-GAL4 drives expression in secondary hemilineage 12B (yellow arrowheads) and various primary neurons. (C) R15D11-GAL4 with nSyb-GAL80: expression is suppressed in primary neurons, and only 12B expression remains. (D) When used to drive UAS-flp in a flip-on immortalization strategy, R15D11-GAL4 yields expression in hemilineage 12B (yellow arrowheads), but also numerous off-target cells (red arrowheads). Genotype: w; UAS-flp (attP40)/+; R15D11-GAL4/nSyb-LexA, LexAop-GFP. (E) Same genotype as (D), but also bearing nSyb-GAL80(su(Hw)attP8) on the X chromosome. Expression in off-target cells is much reduced. A small amount of off-target expression is observed in secondary neurons and descending neurons (e.g., red arrowheads). (F) Adult VNC expression pattern using both nSyb-GAL80 and UAS-hPR-flp to restrict expression to the targeted cells in (C). No off-target expression is observed.

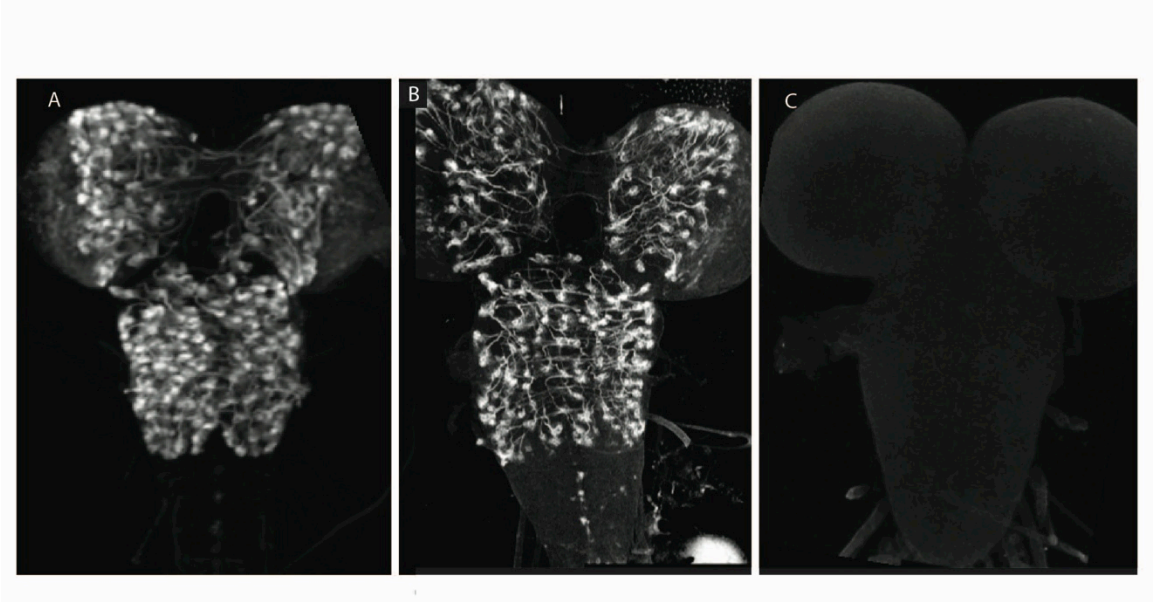

Figure 2.11. UAS-hPR-flp is fully active in the presence of RU486, but inactive without drug. (A) R20B05-GAL4 drives UAS-GFP expression in all secondary neurons. (B) A larva bearing the genotype pJFRC2-UAS>STOP>GFP(attP18)/w; +; UAS-hPR-flp(VK00005)/R20B05-GAL4 and fed on RU486 food for 24h prior to dissection. GFP expression is present in nearly all of the expected cells, indicating that the STOP cassette has been excised by UAS-hPR-flp with high efficiency. (C) A larva of the same genotype as (B), but never treated with RU486. No GFP expression is observed, meaning UAS-hPR-flp was completely inactive in the absence of drug.

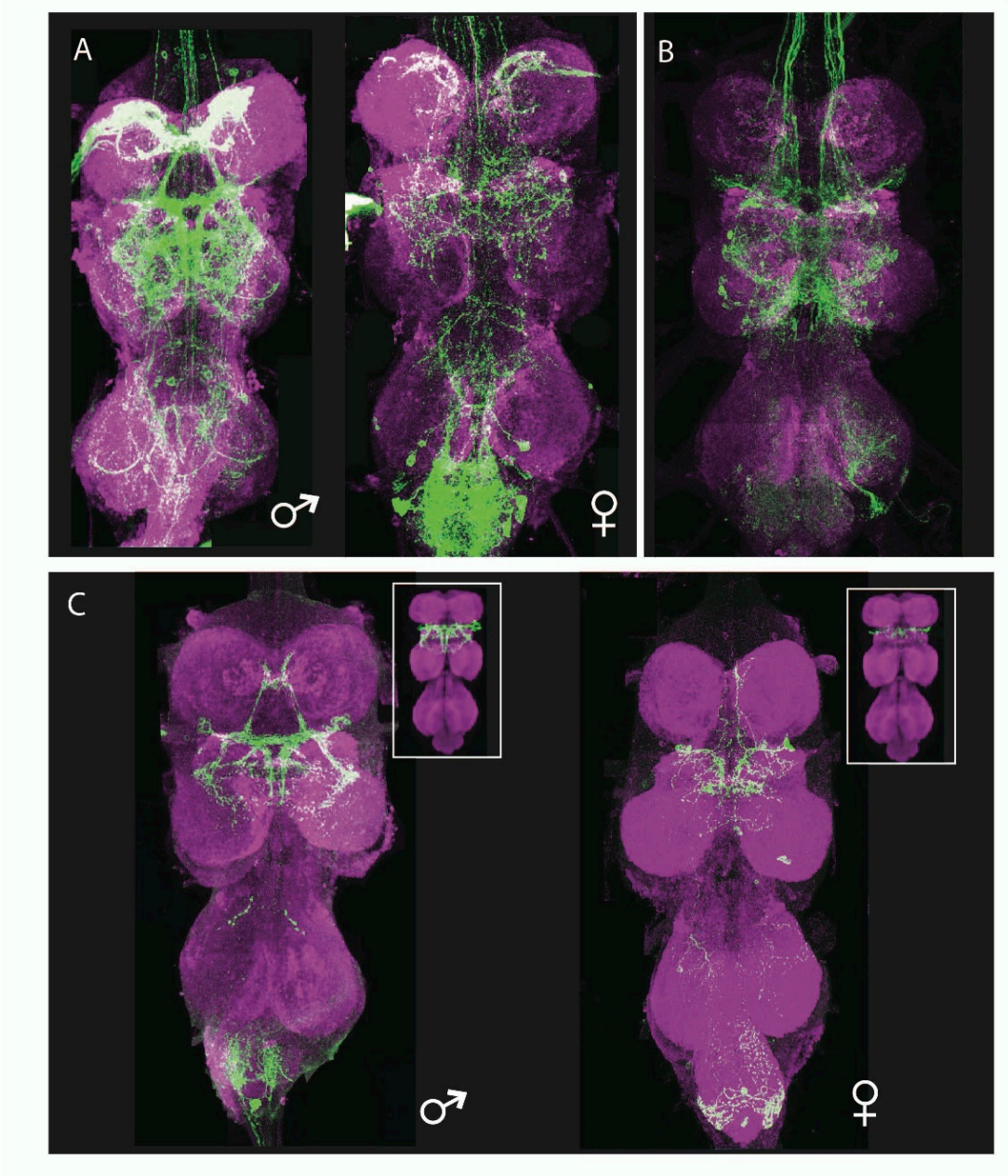

Figure 2.12. Generation of a vPR6-specific line by intersecting hemilineage 12A and fru-LexA. (A,B) Parental expression patterns. (A) The fru-LexA expression pattern. The female pattern (right) is a subset of the male pattern (left), and many of the neurons have dimorphic arbors. (B) Hemilineage 12A. Genotype: nSyb-GAL80 (su(Hw)attP8)/+; UAS-flp(attP40)/+; R24B02-GAL4/nSyb-LexA, LexAop>STOP>GFP. This hemilineage contains the vPR6 cluster of fru-expressing neurons. (C) The intersection of A and B, isolating the vPR6 neurons. Genotype: nSyb-GAL80(su(Hw)attP8); UAS-flp(attP40)/LexAop>STOP>GFP(attP40); R24B02-GAL4(attP2)/fru-LexA. Insets: the arbors and numbers of cells match digital representations of the complete vPR6 pattern in males (left) and females (right), adapted from Yu et al. 2010.

Table 2.1. Summary of genotypes used to address the hemilineages.

Hemilineage	CRM	Genotype	Rating
0A	R39D01	R39D01-GAL4, UAS-GFP	II
1A	R22G11	R22G11-GAL4, nSyb-GAL80, UAS-hPR-flp, act>STOP>LexA, LexAop-GFP	III
	R22G11	R22G11-LexA, LexAop-GFP	II
1B	R58F02	R58F02-GAL4, nSyb-GAL80, UAS-[hPR]-flp, act>STOP>LexA, LexAop-GFP	III
	R13G06	R13G06-GAL4, nSyb-GAL80, UAS-[hPR]-flp, act>STOP>LexA, LexAop-GFP	III
2A	R50G08	R50G08-GAL4, nSyb-GAL80, UAS-flp, act>STOP>LexA, LexAop-GFP	I
	R50G08	R50-G08-GAL4, UAS-IVS-GFP	I
3A	R31H10	R31H10-GAL4, nSyb-GAL80, UAS-flp, act>STOP>LexA, LexAop-GFP	III
3B	R41G09	R41G09-GAL4, nSyb-GAL80, UAS-[hPR]-flp, act>STOP>LexA, LexAop-GFP	II
	R23B05	R23B05-LexA, LexAop-GFP	II
4B	R51D02	R51D02-GAL4, nSyb-GAL80, UAS-flp, act>STOP>LexA, LexAop-GFP	II
5B	R86D02	R86D02-GAL4, nSyb-GAL80, UAS-flp, act>STOP>LexA, LexAop-GFP	I
6A	R35A03	R35A03-GAL4, nSyb-GAL80, UAS-flp, act>STOP>LexA, LexAop-GFP	I
6B	R46C11	R46C11-GAL4, nSyb-GAL80, UAS-flp, act>STOP>LexA, LexAop-GFP	I
7B	R65A12	R65A12-GAL4, nSyb-GAL80, UAS-flp, act>STOP>LexA, LexAop-GFP	I
	R41E01	R65A12-AD, R41E01-DBD, act>STOP>GAL4, UAS-flp, UAS-GFP	II
	R75H06	R75H06-GAL4, nSyb-GAL80, UAS-flp, act>STOP>LexA, LexAop-GFP	
8A	R69H11	R69H11-GAL4, UAS-GFP	II
8B	R09D08	R09D08-GAL4, nSyb-GAL80, UAS-[hPR]-flp, act>STOP>LexA, LexAop-GFP	II
9A	R48H02	R48H02-GAL4, nSyb-GAL80, UAS-[hPR]flp, act>STOP>LexA, LexAop-GFP	I
	R52E12	R52E12-GAL4, UAS-GFP	II
10B	R13B08	R13B08-GAL4, nSyb-GAL80, UAS-[hPR]flp, act>STOP>LexA, LexAop-GFP	I
11A	R26B05	R26B05-GAL4, nSyb-GAL80, UAS-[hPR]-flp, act>STOP>LexA, LexAop-GFP	I*
11B	R26B05	R26B05-GAL4, nSyb-GAL80, UAS-[hPR]-flp, act>STOP>LexA, LexAop-GFP	I*

Table 2.1, continued

12A	R24B02	R24B02-GAL4, nSyb-GAL80, UAS-[hPR]-flp, act>STOP>LexA, LexAop-GFP	I
	R24B02	R24B02-GeneSwitch, act>STOP>GAL4, UAS-flp, UAS-GFP	I
12B	R15D11	R15D11-GAL4, nSyb-GAL80, UAS-[hPR]-flp, act>STOP>LexA, LexAop-GFP	I
13A	R49C05	R49C05-GAL4, nSyb-GAL80, UAS-flp, act>STOP>LexA, LexAop-GFP	III
13B	R41G09	R41G09-GAL4, UAS-IVS-GFP	II
14A	R80G10	R80G10-GAL4, nSyb-GAL80, UAS-hPR-flp, act>STOP>LexA, LexAop-GFP	III
	R73H04	R73H04-GAL4, nSyb-GAL80, UAS-hPR-flp, act>STOP>LexA, LexAop-GFP	III
15B	R12F11	R12F11-GAL4, nSyb-GAL80, UAS-flp, act>STOP>LexA, LexAop-GFP	II
16	N/A	N/A	N/A
17A	R78A08	R78A08-GAL4, nSyb-GAL80, UAS-flp, act>STOP>LexA, LexAop-GFP	III
18B	R27A09	R27A09-GAL4, nSyb-GAL80, UAS-flp, act>STOP>LexA, LexAop-GFP	II
	R27A09	R27A09-GeneSwitch, act>STOP>GAL4, UAS-flp, UAS-GFP	
19A	R50C03	R50C03-GAL4, nSyb-GAL80, UAS-[hPR]-flp, act>STOP>LexA, LexAop-GFP	III
	R32E04	R32E04-GAL4, UAS-GFP	II
19B	R84E06	R84E06-GAL4, nSyb-GAL80, UAS-flp, act>STOP>LexA, LexAop-GFP	III
20A/22A	R19A07	R19A07-GAL4, nSyb-GAL80, UAS-flp, act>STOP>LexA, LexAop-GFP	III
	R19H10	R19H10-GAL4, UAS-GFP	I
	R24G06	R24G06-LexA, LexAop-GFP	I
21A	R51H05	R51H05-GAL4, nSyb-GAL80, UAS-[hPR]-flp, act>STOP>LexA, LexAop-GFP	II
	R26H05	R26H05-AD, R51H05-DBD, act>STOP>GAL4, UAS-flp, UAS-GFP	II
23B	R35C09	R35C09-GAL4, nSyb-GAL80, UAS-flp, act>STOP>LexA, LexAop-GFP	I
	R67A11	R67A11-GAL4, nSyb-GAL80, UAS-flp, act>STOP>LexA, LexAop-GFP	II
	R77C10	R77C10-GAL4, UAS-GFP	I
24B	R73B01	R73B01-GAL4, nSyb-GAL80, UAS-flp, act>STOP>LexA, LexAop-GFP	I

* R26B05 hits both hemilineages of NB11.

Chapter 3

CHARACTERIZATION OF HEMILINEAGE ANATOMY IN THE ADULT THORACIC VNS

Summary

Although the anatomy of the throacic neuroblast lineages has been characterized in the third-instar larva (Truman et al. 2004), the transition from these initial projection patterns to the mature adult morphology of the corresponding hemilineages is difficult to trace because of the structural changes that occur in the thoracic CNS during metamorphosis (e.g. Brown and Truman 2009). I used the lines described in Chapter 2 to characterize the anatomy of the 32 distinguishable adult-specific hemilineages. Where possible, this includes data on their presumed polarity and the neurotransmitter they express. I have also created a simple tool to easily visualize and compare the hemilineages' adult arbors, and describe how potential connections based on arbor proximity compare to predicted overlap based on initial contact patterns in the larva.

Introduction

A map is necessary for understanding a circuit, although it is far from sufficient. If we posit that the secondary hemilineages represent 32 elements in the circuits underlying behaviors mediated by the thoracic ventral nervous system (VNS), then we need a catalog of their morphology so we can identify them and their inputs and outputs, and ultimately map their connectivity. In this chapter, I use MARCM clones and the genetic tools

described in Chapter 2 to characterize the adult anatomy of each hemilineage and make a putative connectivity map based on regions of arbor overlap.

This task is made feasible by the work of Truman et al. (2004) establishing the morphology and initial contact partners of the hemilineages in the third-instar larva. By the onset of larval wandering, NBs have produced most of the neurons they are going to make, although divisions continue until approximately 12h APF (Brown and Truman 2009), and the characteristic lineage-specific projection patterns of the secondary neurons have been established. At this stage, these initial neurites express the cell adhesion protein neurotactin (de la Escalera et al. 1990), and anti-neurotactin staining reveals a stereotyped scaffold of bundles present in each thoracic segment. Truman et al. (2004) mapped the thoracic secondary lineages in the third-instar larva to this neurotactin scaffold. Most hemilineages can be unambiguously identified based on 4 criteria: general location of the somata, whether they cross the midline, where in the neuropil their bundle terminates, and/or which neurotactin tract they follow.

Unfortunately, neurotactin expression fades soon after the onset of adult development, so this marker cannot be used to track the cell groups through metamorphosis. However, the larval bundles also express the adhesion protein neuroglian, and this expression is maintained into the adult (D. Shepherd and D. Williams, unpublished data). Thus, the larval neurotactin landmarks can be identified at later stages using anti-neuroglian staining. However, the neurotactin/neuroglian scaffold undergoes considerable deformation during metamorphosis, and we found that the major, multi-lineage tracts all

separate in the adult into single-lineage bundles. Fortunately, the flip-on strategies described in Chapter 2 allow us to confirm a lineage's identity in the larva, then map its tract in the adult, and thereby define the lineage origins of the bundles in the adult neuroglian scaffold.

Truman et al. (2004) noted that the initial neurite projected by each hemilineage in the larva tended to arrest and produce a small defasciculation near the neurites from other lineages. They hypothesized that these contact points had functional significance, possibly indicating future synaptic partners. I made a map of putative synaptic connections between lineages based on the large-scale overlap of their arbors, and compared this to the predictions made by Truman et al. (2004). With a few exceptions, these connections appear plausible in the adult, and I have greatly expanded on that network.

It has been suggested that many insect neurons form a proximal arbor that is largely postsynaptic, and a distal arbor that is mostly presynaptic, although inputs and outputs are commonly mingled (e.g., Burrows 1996). For some projection neuron lineages that clearly display proximal-distal organization, I have designated dendritic vs. axonal arbors. For a subset of lineages, I was able to confirm this designation using the presynaptic marker GFP-tagged n-synaptotagmin (nSyt-GFP) (Zhang et al. 2002). This information should help to interpret the flow of information in our putative network.

Another important feature of neural circuits is sign, i.e. whether connections are excitatory or inhibitory. One major inhibitory neurotransmitter is γ-aminobutyric acid (GABA) (reviewed in Burrows 1996). The distribution of GABAergic neurons appears to be well-conserved in the thoracic nervous system. Immunocytochemical studies of species from across the Insecta show seven apparently homologous clusters of GABA-reactive cell bodies in the thoracic segments (Witten and Truman 1998). Witten and Truman (1998) determined that the cells in each cluster are clonally related, and correspond to specific postembryonic lineages in *Manduca sexta*. I assigned lineage identity to these clusters in *Drosophila*, and identified an additional cluster that may not be present in other taxa.

Finally, I compiled this information into two databases: a MATLAB graphical user interface that allows one to quickly compare arbor morphology between two or three lineages, and a Neuroptikon network map of the thoracic lineages.

Materials and methods

Fly stocks

Flies were reared on standard cornmeal and molasses food at 25^{o}C. For GFP-expressing flies, transgenic constructs and hormone feeding of hormone-inducible reagents are discussed in Chapter 2. The presynaptic marker nSyt-GFP (Zhang et al. 2002), membrane-bound RFP, and/or the nonfluorescent epitope tag membrane-bound HA were

directed to hemilineages using the hemilineage-specific driver genotypes described in Chapter 2 (all constructs, generous gift of B. Pfeiffer).

The genotype for twin-spot MARCM flies (Yu et al. 2009) was *hsflp[1]/yw; FRT40A, UAS-mCD8-GFP, UAS-rCD2-miRNA/ FRT40A, UAS-rCD2-RFP, UAS-GFP-miRNA; nSyb-GAL4/ +*.

Eggs were collected over a 24h period and heat-shocked at 37^{o}C for 10-30 minutes. Progeny were reared to adults, aged for 10-14 days, and dissected. Clones were detected by immunocytochemistry.

The general scheme for visualizing sensory neuron-lineage interactions involved the following genotype:

LexAop-GFP (su(Hw)attP8), UAS-RFP (attP18)/w; CRM1-LexA (attP40)/+; CRM2-GAL4/+. In this example, CRM1 and CRM2 are both Rubin enhancer fragments; CRM1 drives expression in a class of sensory neurons and CRM2 drives expression in a lineage or lineages. R46C11-LexA and R54E06-LexA were used to drive expression in leg chordotonal afferents, R13F12-LexA was used to drive expression in leg gustatory receptor neurons, and R49C06-LexA was used to drive expression in leg tactile afferents. Sensory neuron driver lines were selected based on the pattern of sensory projections in the ventral CNS, then confirmed using confocal microscopy of the sense organs in the periphery. Leg chordotonal afferent lines were identified based on Kamikouchi et al. (2010). Leg gustatory receptor neuron lines were identified based on Boll and Noll (2002). Leg tactile afferent lines were identified based on Murphey et al. (1989).

Immunocytochemistry

Tissues were dissected in PBS (phosphate-buffered saline, pH 7.8, Cellgro by MediaTech, Inc.) and fixed in 4% buffered formaldehyde overnight at 4°C. Fixed tissues were rinsed in PBS-TX (PBS with 1% Triton X-100, Sigma), and then incubated in primary antibodies overnight at 4°C. Tissues were then rinsed in PBS-TX four times and incubated in secondary antibodies overnight at 4°C. Tissues were then washed four times in PBS-TX, mounted onto poly-Lysine-coated coverslips, dehydrated through an ethanol series, cleared in xylenes, and mounted in DPX mountant (Sigma).

For determining the adult anatomy of the hemilineages, I used a primary antibody mixture of 1:1000 rabbit anti-GFP (Jackson ImmunoResearch), 1:40 rat anti-nCadherin (Developmental Studies Hybridoma Bank, DSHB), and 1:40 mouse anti-Neuroglian (DSHB) in 10% normal donkey serum (Jackson ImmunoResearch) in PBS-TX, Secondary antibodies were 1:500 AlexaFluor 488-conjugated donkey anti-rabbit, AlexaFluor 594-conjugated donkey anti-mouse, and AlexaFluor 649-conjugated donkey anti-rat (all from Invitrogen).

For anti-GABA staining, the primary antibody mixture consisted of 1:1000 sheep anti-GFP (AbD Serotec), and 1:1000 rabbit anti-GABA (Sigma) in 10% normal donkey serum (Jackson ImmunoResearch) in PBS-TX. Secondary antibodies were 1:500 AlexaFluor 488-conjugated donkey anti-sheep and AlexaFluor 594-conjugated donkey anti-rabbit (both from Invitrogen).

For twin-spot MARCM, nSyt/DenMark, and double-lineage experiments, primary antibody mixture consisted of 1:1000 sheep anti-GFP (AbD Serotec), 1:1000 rabbit anti-dsRed (Clontech), 1:40 mouse anti-neuroglian (most preparations; DSHB) or 1:100 rat anti-HA (nSyt/DenMark/HA staining; Roche), and 10% normal donkey serum (Jackson ImmunoResearch) in PBS-TX. Secondary antibodies were 1:500 AlexaFluor 488-conjugated donkey anti-sheep, AlexaFluor 594-conjugated donkey anti-rabbit, and AlexaFluor 649-conjugated donkey anti-mouse/rat (all from Invitrogen).

Microscopy and image processing

Nervous systems were imaged on a Zeiss LSM 510 confocal microscope at 40x with optical sections at 2um intervals. LSM files were converted into TIFF files, *z*-projected, and resliced (for transverse sections) using ImageJ (http://rsbweb.nih.gov/ij/). Neuroglian tracts and arbors were hand-traced and hand-overlaid using Neuroglian and n-Cadherin landmarks, by projecting the reference image in Vaa3D (Peng et al. 2010, http://www.vaa3d.org/) and performing the rendering in Adobe Illustrator.

Graphical user interface (GUI) and connectivity map generation

The GUI summarizing the Neuroglian and arborization data was generated using MATLAB 2008a (v.7) (The Mathworks). The xyz coordinates of the neuroglian tracts and arbors were manually converted to line segment coordinates for visualization in the GUI. Connectivity maps were created using Neuroptikon visualization software (https://openwiki.janelia.org/wiki/display/neuroptikon/Home).

Results

Metamorphosis of the neuroglian scaffold

In the larva, there are five major neurotactin commissures crossing the midline in each thoracic segment: anterior and posterior dorsal commissures (aD and pD, respectively), anterior and posterior intermediate commissures (aI and pI), and an anterior ventral commissure (aV) (Truman et al. 2004). Lineages can be identified by the location of their cell bodies and the commissure through which they project. However, during metamorphosis, the thoracic neuropil increases in volume by severalfold due to the expansion and growth of the adult arbors of the arrested secondary neurons and the ingrowth of adult sensory axons. This expansion leads to considerable distortion of the larval tracts and commissures. Also, lineage clusters can be pulled apart as neuropils expand and different hemilineages are anchored at different insertions sites into the neuropil (Brown and Truman 2009, D. Shepherd pers. comm.). In extreme cases, the somata of neurons that projected contralaterally in the larva can be pulled across the midline, so that they appear to project ipsilaterally in the adult. Thus, it is not always trivial to match a neurotactin tract to its adult neuroglian equivalent.

The flip-on strategies described in Chapter 2 allowed me to identify a lineage in the larva, then document its anatomy in the adult. I mapped the adult tract of each lineage to the neuroglian scaffold. The results are summarized in Fig. 3.1. I traced the neuroglian tracts based on a confocal stack from a randomly chosen VNS at approximately 10μm *z*-

intervals (Fig. 3.1B). There is a certain amount of variation between preparations, both biologically and due to differences in mounting angle. Aligning dorsoventral landmarks in preps that were slightly tilted was especially challenging. Landmarks of particular value in orienting oneself between specimens include the following:

The medial cluster: As the sole unpaired lineage, lineage 0A is an unmistakable marker at the posterior midline of every segment. The tracts of lineages 5B, 6A, 6B, 12B, and 23B project dorsoventrally through much of the ventral VNS, and their position relative to one another is diagnostic of relative dorsoventral location throughout this region (Fig. 3.1, slices 2-10). I refer to this grouping as the medial cluster.

Insertion of the leg and wing nerves: Nerve insertions are particularly useful in describing the differences between segments. The neuromeres distort in segment-specific ways so that while the relative relationship of tracts generally remains constant, there are segmental variations in positions relative to the body axis. In T2, which I use as the standard in describing the relative position of tracts, the leg nerve insertion defined the most ventral landmark in that segment. In T1, the leg nerve insertion is more dorsal and at the anterior end of the segment. In contrast, the T3 leg nerve insertion is usually found at the far posterior end of the segment. This shift in the position of the leg nerve entry affects the segmental position of other tracts. For example, the tract for hemilineage 13B is the ventral most neuroglian landmark in T2. In T1, by contrast, the neuropil has rotated anterodorsally, and the 13B bundle is found more dorsally, along the anterior

edge of the neuropil. In T3, the leg neuropil has rotated posteroventrally, and hemilineages 13B and 14A typically cross the midline in the same optical slice.

Wing nerve insertion generally defines the nominal boundary between leg and wing neuropil, but in T1 the lineages have shifted anterodorsally and some leg lineages extend their arbors up to the level of the neck connective.

The T1 peninsula: Approximately halfway between where the leg neuropils fuse and where the wing nerve inserts, a finger of cell bodies invades T1 neuropil at the midline, from the anterior (Fig. 3.1, slice 8). It is flanked by the lineage 10B neuroglian tracts. This landmark is helpful in distinguishing the various lineages that insert just below the neck connective in T1.

To demonstrate the degree of stereotypy between image stacks, Fig. 3.1C shows a single optical section from a neurotactin-stained specimen from tissue that was dissected and imaged independently of the one shown in Fig. 3.1B. In T1 and T2, only a few tracts remain in the midline cluster, which places the image between slices 10 and 11 of the reference CNS (Fig. 3.1B). The identification of the other tracts in these segments is then fairly straightforward. In T3, however, the section shows the midline cluster lineages still forming long tracts, placing us closer to slice 8 from the reference CNS for this segment. This illustrates that due to variable tilt in the mounted nervous systems, one must consult landmarks from several adjacent *z*-slices in the original confocal stack to confirm tract identity.

Adult anatomy of the thoracic secondary lineages

The following sections describe the adult morphology of the thoracic lineages. As mentioned above, some of the larval neurotactin tracts pull apart in the adult, so the cell bodies of the two hemilineages become considerably displaced from each other. Where possible, I have described the hemilineage anatomy in terms of soma location, main neurite trajectory, and location of the proximal and distal arbors. In a broad sense, adult morphology generally resembles the larval projection but with a large synaptic arbor emerging where the initial neurite arrested. The only secondary lineages that are missing from this analysis are lineages 0 and 16.

Lineage 1

Lineage 1 is the anteriormost lineage in each segment. In the larva, the lineage 1 cell cluster is located ventrolaterally. The cell bodies of hemilineage 1A translocate dorsally during metamorphosis so that in the adult, the 1A cell cluster is in the dorsal third of the VNS. The 1A tract follows the aV commissure in the larva. In the adult, it is still among the most ventral tracts in the VNS, but it expresses neuroglian only weakly and is not a good landmark. MARCM clones (Fig. 3.2) show that the neurons from the 1A cluster produce both dorsal and ventral ipsilateral arbors. After crossing the midline, the bundle makes a distinctive posterior "hook," also evident in the larval form of the hemilineage, and then bifurcates to form a dorsal projection and a ventrolateral projection. The ipsilateral and contralateral arbors project into similar neuropil areas so that the ipsilateral ventral arbor of the left hemilineage 1A cluster appears to overlap with the contralateral

arbor from the right hemilineage 1A cluster, and the left and right dorsal arbors likewise appear to overlap. nSyt-GFP localization indicates that the main output regions of the hemilineage are concentrated around the ventral arbors (Fig. 3.2C), although due to the overlap mentioned above, I cannot determine whether the enrichment is in the ipsilateral or contralateral arbor or both.

In the larva, hemilineage 1B projects to the next-anterior segment. In the adult, its cell body cluster is pulled anteriorly, and ends up at the ventral, posterior edge of the next-anterior segment. The hemilineage 1B arbor projects throughout the posterior half of the ventral third of the neuropil. As with other lineages that make local leg interneurons, no clear proximal-distal or polar organization is apparent.

Lineage 2

Hemilineage 2A survives, while hemilineage 2B undergoes programmed cell death, resulting in an apparently monotypic lineage (Truman et al. 2010). In both the larva and the adult, the cell bodies of hemilineage 2A are paired ventromedial clusters at the anterior margin of each neuromere, and the 2A neurites project to the dorsal surface of the neuromere and make a sharp lateral turn. As described in Brown and Truman (2009), MARCM clones show that in T2, hemilineage 2A makes a proximal "interstitial" arbor and a distal arbor, both in the dorsal third of the neuropil (Fig. 3.3). The interstitial arbor stays in the medial third of the neuropil on each side. The major projection is ipsilateral and extends into the next-anterior segment. The interstitial arbor also has a weak contralateral component that stays within the neuromere of origin. The distal arbor is

dorsal to the interstitial arbor, broader, and stays within its neuromere of origin. nSyt-GFP concentrates in the distal arbor (Fig. 3.3C). In T1 and T3, only the distal arbor is present. In the lineage 2 line shown in Fig. 3.3A, only the distal arbor is seen in T2. This suggests that the construct used to label this hemilineage may not drive expression in all of the lineage cells.

Lineage 3

In the larva, the cell body cluster of lineage 3 is ventromedial. The A and B neurites project together dorsally to the mid-neuropil, then diverge. The hemilineage 3A neurite bends laterally to the dorsal portion of the ipsilateral leg neuropil, while the 3B neurite continues dorsally and arrests near the bundles from 12A and 11B. In the adult, the cell bodies of hemilineage 3A remain ventral, just posterior to the leg nerve insertion. The lineage forms an arbor throughout the ventral third of the neuropil (Fig. 3.4).

The cell bodies for the hemilineage 3B neurons translocate dorsally during metamorphosis. In T1, they end up in the middle third of the VNS, slightly ventral to the wing nerve insertion. In T2, they are found at the dorsal surface of the VNS (Fig. 3.4). Lineage 3 is found near the posterior border of each thoracic segment in the larva. In the adult, the arbor of the 3B neurons in T1 extends most of its branches into T2, and those in T2 extends into the anterior T3 neuropil. The arbors are restricted to the dorsal third of the neuropil. The T1 arbor has two layers: a dense, midline-crossing upper layer at the dorsal surface of the neuropil, and a thinner lower layer that projects towards the midline but does not appear to cross (Fig. 3.4F). The T2 arbor is similar, although it is difficult to

distinguish layers. I did not find hemilineage 3B neurons in T3. Since a T3 cluster is present in the third-instar larva, the cells may die during metamorphosis.

Lineage 4

Hemilineage 4A undergoes programmed cell death in the larva (Truman et al. 2010). The cell body cluster of hemilineage 4B is ventromedial in the larva, and it sends its initial neurite to the lateral part of the ipsilateral leg neuropil. In the adult, the cell body cluster stays ventral, wrapping around the leg nerve insertion. Hemilineage 4B extends a short tract dorsally, then makes a thin arbor in the upper part of the ventral third of the VNS, mostly in the posterior half of the leg neuropil (Fig. 3.5).

Lineage 5

In the larva, hemilineage 5A undergoes programmed cell death (Truman et al. 2010). The hemilineage 5B somata are ventrolateral, and their initial neurites project to the pI commissure, cross the midline and arrest. In the adult, the cell bodies are pulled towards the midline. The bundled neurites cross the midline at a posterior intermediate position, and appear to form a major ipsilateral arbor just prior to crossing (Fig. 3.6D). The lineage makes a compact arbor that projects up and down the medial region of the neuropil and up the neck connective (Fig. 3.6). I recovered no MARCM clones for this lineage.

Lineage 6

Lineage 6 is unique in that both of its hemilineages project contralaterally in the larva, with neurites of the hemilineage 6A forming the pD commissure and neurites of 6B

crossing the midline in the pI commissure. During metamorphosis the cell bodies of the two hemilineages separate into distinct clusters, but stay ventral (Fig. 3.7), as described in Brown and Truman (2009). Hemilineage 6A clusters are found in T1 through A1 (Fig 3.7A). In keeping with its dorsal larval projection, hemilineage 6A forms one of the dorsalmost arbors in the adult. In segment T2, the proximal arbors of these neurons are ipsilateral to the cell bodies but are largely confined to the segment of origin. The distal arbors are contralateral to the cell body cluster and the axons from clusters in the three thoracic segments and A1 converge in the dorsal neuropil of T2. nSyt-GFP localizes to the lateral portions of the contralateral arbor.

The neurons of hemilineage 6B are found in T1 to T3 but are typically missing from segment A1. They produce another long dorsoventral tract, near that of hemilineage 5B. As in the larva, the 6B bundle stays just posterior to the 5B bundle throughout most of its length, and extends a little farther dorsally. The point at which the 6B tract crosses the midline and disappears from neuroglian staining is the dorsal limit of the medial cluster. The hemilineage 6B neurons have no substantial ipsilateral arbor. After crossing the midline, they branch profusely in the dorsal third of the neuropil. Their presynaptic sites seem to be concentrated in the distal portions of the contralateral arbor (Fig. 3.7K). As with 6A, the T1 and T3 clusters tend to converge onto T2.

Lineage 7

In the larva, only hemilineage 7B survives (Truman et al. 2010). It has a ventrolateral cell cluster. The hemilineage 7B neurite bundle crosses the midline in the aI tract, then makes

an ascending projection. The basic morphology is much the same in the adult (Fig. 3.8), as described in Brown and Truman (2009). The neurites project dorsally, forming a bushy ipsilateral (proximal) arbor in the dorsal third of the neuropil, then crossing the midline to form two contralateral (distal) projections: one in the lateral part of the ventral third of the neuropil in its segment of origin, and another that forms a fine ascending arbor that runs in a dorsal tract all the way to the neck connective. In the larva, hemilineages 7B and 8B both project in the aI commissure, and in the adult the tract for hemilineage 7B parallels that of hemilineage 8B throughout the middle third of the neuropil, forming a distinctive neuroglian landmark (Fig. 3.8C). Hemilineage 7B is also found in A1, and the A1 homolog is clearly visible in Fig. 3.8A-B.

Lineage 8

In the larva, lineage 8 forms a ventrolateral cell cluster in the anterior part of each thoracic segment. Hemilineage 8A projects to the dorsal region of the ipsilateral leg neuropil, while hemilineage 8B projects contralaterally across the aI commissure. In the adult, the somata are found in approximately the same location; the A and B clusters separate, but not by much (Fig. 3.9). Neurons of the 8A hemilineage are confined to the ipsilateral leg neuropil, where they arborize throughout the middle third of the VNS (Fig. 3.9), near the level at which the motoneurons from lineages 15B and 24B arborize. Its neuroglian tract is an important neuroglian landmark in the leg neuropil: it is easy to identify based on its insertion near the tract for 8B and its pronounced lateral bend.

The neurons in hemilineage 8B produce multi-part, midline-crossing, intersegmental arbors (Fig. 3.9). Proximal arbors include an intrasegmental lateral arbor and an ascending medial arbor in the dorsal third of the ipsilateral neuropil. The hemilineage also makes symmetric ascending projections in the upper part of the dorsal neuropil. The T2 and T3 homologs send these projections to T1, while the T1 homolog sends projections up the neck connective. nSyt-GFP localization suggests that the proximal arbors are mostly dendritic, and the dorsal ascending projections are axons.

In T3, hemilineage 8B produces the contralateral haltere interneurons (cHINs) (Strausfeld and Seyan 1985), with their distinctive "bowtie" arbor (Fig. 3.9E,F). These neurons receive sensory inputs from the haltere nerve, in their lower, intrasegmental ipsilateral arbor, then make an ascending projection on the contralateral side. (This tells us that the matching ipsilateral projection seen in MARCM clones must be produced by a separate subclass of 8B cells.) The homologous arbor in T2 is found where the wing nerve inserts, and may receive wing sensory inputs. A reduced homologous arbor is also found in T1, although it is unclear what inputs it might receive.

Lineage 9

In the larva, lineage 9A is the dorsalmost cell cluster in the anterior half of the neuromere, and sends its neurite to the dorsomedial part of the leg neuropil. Hemilineage 9B undergoes programmed cell death (Truman et al. 2010). In the adult, the 9A somata are found in the middle third of the VNS. The hemilineage arborizes in the far ventral leg neuropil (Fig. 3.10), as described in Brown and Truman (2009). Hemilineage 9A is made

up of local leg interneurons whose arbors overlap with afferents from leg chordotonal organs (Fig. 3.10C).

Lineage 10

In the larva, only hemilineage 10B survives (Truman et al. 2010). The cell body clusters of 10B are just lateral to those of lineage 2 and their neurite bundle projects across the aI commissure. The hemilineage 10B cell bodies remain anteromedial in the adult. The neuroglian tract projects to the middle of the VNS, then forms two arbors: a fingerlike ventral arbor that starts medial and projects ventrally almost to the leg nerve insertion, forming fine branches along its entire length, and an intersegmental dorsal arbor near the midline at the middle of the neuropil (Fig. 3.11). In total, the intersegmental arbors project all the way from the abdominal ganglia up the neck connective. I did not recover MARCM clones of lineage 10, so I could not determine the extent of the intersegmental projections of 10B from each segement.

Lineage 11

I was unable to construct lines to target hemilineages 11A and 11B independently, but R26B05 targets the whole lineage quite cleanly (Fig. 3.12). Lineage 11A is found in T1 and T2, whereas lineage 11B is found only in T2. Both are absent from T3. This makes it the most segmentally specialized lineage, with a unique combination of siblings present in each thoracic segment. This property enabled me to assign parts of the T2 arbor to 11A vs. 11B, based on the 11A projection pattern in T1.

In the larva, the lineage 11 cell cluster is found at the posterior edge of the neuromere, lateral to the leg neuropil and dorsal to most other cell clusters. Hemilineage 11A projects medially but stops well short of the midline; 11B extends dorsally to the edge of the pD commissure, but likewise does not cross the midline.

In the adult, the cell bodies move to the dorsal surface of the VNS. Hemilineage 11A has a broad, asymmetric, multipartite arbor. The most proximal arbor is formed in the dorsal third of the neuropil, near the ipsilateral edge. Slightly ventral to that, the ipsilateral arbor continues, but another projection crosses the midline and arborizes in the medial part of the middle third of the VNS on the contralateral side. In both T1 and T2, this arbor projects into T2. nSyt-GFP localizes to this arbor; it appears to be an output region (Fig. 3.12C). This output branch appears situated to contact the other branch of its contralateral homolog. Still farther down, 11A makes a projection into the ipsilateral leg neuropil. In T1, this branch projects anteriorly throughout the lateral T1 leg neuropil. In T2, the branch projects posteriorly into T3 and arborizes throughout the T3 leg neuropil.

Hemilineage 11B projects across the midline and contacts its contralateral homolog, forming a relatively simple arbor in the dorsalmost part of the VNS (Fig. 3.12). The 11B arbor has two parts: an anterior projection that crosses the midline, and and a posterior projection that stays ipsilateral. nSyt-GFP localizes to the posterior portion of the arbor.

Lineage 12

In the larva, the lineage 12 cell body cluster is ventromedial. Hemilineage 12B projects to the pI commissure, crosses the midline and arrests. The larval branching pattern of hemilineage 12A is the quite variable. Using a GAL4 driver line that targets this hemilineage in every segment, the larval morphology of the hemilineage clusters were as follows: It is present in segments S2 to T2 and A1. Sometimes, a few 12A cells survive in T3. In T1, the neurite bundle bifurcates, forming both a dorsal and a medial branch. In the T2 cluster, a dorsal branch is almost always present, and a medial branch may or may not be present. The presence or absence of the medial branch is affected by genetic background, but largely stochastic. In S2, S3, and A1, only a dorsal branch is present. Because of the variable and stochastic nature of the branches, I did not attempt to characterize them differentially in the adult.

In the adult, the cell body clusters for 12A and 12B remain ventral but move slightly more lateral. Hemilineage 12A arborizes throughout the dorsal third of the neuropil. The arbors from the T1 and T2 homologs converge on T2, and overlap their contralateral and segmental homologs extensively (Fig. 3.13). nSyt-GFP localizes to the medial portions of the dorsal arbors, plus a small region in the lateral part of the lower arbors (Fig. 3.13C). I did not recover a MARCM clone containing hemilineage 12A in the adult, so I could not determine the extent of arbor overlap.

The neuroglian tract for hemilineage 12B forms part of the medial cluster (Fig. 3.1). The fasciculated neurites cross the midline and then arborize in ventroposterior regions of the contralateral leg neuropil (Fig. 3.13). nSyt-GFP localizes to the lateral portion of this

contralateral arbor. 12B also sends a weak projection to the dorsal part of the ipsilateral leg neuropil, in the middle third of the VNS.

Lineage 13

Both hemilineages of lineage 13 project to the leg neuropil in the larva, 13A to the ipsilateral leg and 13B to the contralateral leg. The lineage 13 cell body cluster is located ventrolaterally, in the middle of the neuromere.

The 13A neuroglian tract is the ventralmost neuroglian landmark in T2. In all segments, it is the tract nearest the leg nerve insertion (Fig. 3.1). The 13A arbor then extends along the edges of the leg neuropil, from the nerve insertion throughout the ventral third of the neuropil.

The cell bodies of 13B are pulled towards the midline as the neuropil expands during metamorphosis, because the cells are anchored in the contralateral leg neuropil. The neuroglian tract of hemilineage 13B is the ventralmost midline-crossing neuroglian landmark (Fig. 3.14, but see below). The hemilineage 13B neurons have no ipsilateral arbor. Their contralateral arbor is restricted to the ventralmost parts of the leg neuropil. The cell bodies for hemilineage 13B are sometimes pulled across the midline during metamorphosis (Fig. 3.14D).

Lineage 14

In lineage 14, almost all of the 14B neurons die, so the cluster is comprised almost exclusively of hemilineage 14A neurons (Truman et al. 2010). The neuroglian tract for these cells is the second-most ventral neuroglian landmark in the neuropil, just dorsal and anterior to the tract for hemilineage 13B (Fig. 3.1). As with 13B, the 14A neuroglian bundle projects across the midline to the contralateral leg neuropil in the larva, but its somata are sometimes pulled across the midline during metamorphosis. Hemilineage 14A has no ipsilateral arbor. Its contralateral processes arborize throughout the ventral half of the leg neuropil, somewhat anterior to those from hemilineage 13B (Fig. 3.15).

Lineage 15

Hemilineage 15A undergoes programmed cell death (Truman et al. 2010). Leg motor neurons are produced by five lineages (Brierley et al. 2012), but hemilineages 15B and 24B are unique in that they produce leg motor neurons exclusively. Accordingly, they project through the leg neuropil and out the leg nerve in the larva. The adult morphology of hemilineage 15B matches expectations based on previous characterizations of the leg motor neurons of the fly (e.g., Nassel et al. 1986) (Fig. 3.16). 15B produces a subset of the motor neurons innervating distal leg segments (femur and tibia) (Brown and Truman 2009), while 24B produces motor neurons that innervate proximal leg segments (coxa, trochanter and femur) (Baek and Mann 2009). The dendritic arbors for hemilineage 15B project throughout the dorsolateral part of the ipsilateral leg neuropil.

Lineage 17

In lineage 17, only the 17A sibling survives (Truman et al. 2010). I had difficulty isolating a good line for lineage 17. My best genotype hits 17A most of the time, but also reliably hits lineage 11, and occasionally other lineages. However, even in the presence of other lineages, the neuroglian tract for 17A was easy to distinguish (Fig. 3.17). In the larva, its cell body cluster is at the dorsoanterior border of the neuromere, and its neurite bundle projects medially through intermediate neuropil, but before the midline it turns sharply dorsal and hooks back laterally. In the adult, this shape is even more pronounced, forming a large loop in the anterior part of the segment. Hemilineage 17A is found in T2 and T3, but not T1.

I recovered MARCM clones of this lineage (Fig. 3.17) and determined that it produces a proximal dorsal arbor in the dorsomedial parts of the ipsilateral leg neuropil and two distal dorsal arbors (at the far end of the loop): an ascending branch that projects into the neck connective, and a descending lateral branch. There is also a ventral arbor that branches off of the bottom of the loop and projects posteriorly in the ventral parts of the ipsilateral leg neuropil.

Lineage 18

Hemilineage 18A undergoes programmed cell death (Truman et al. 2010). Like 17A, hemilineage 18B is missing from T1 and situated at the dorsal, anterior edge of segments T2 and T3. In the larva, it projects in the aI commissure. In the adult, its T2 neuroglian tract forms a distinctive landmark at the posterior edge of the wing nerve insertion neuropil. It forms an elaborate, midline-crossing arbor that extends into the dorsalmost

region of the neuropil (Fig. 3.18). A major proximal branch extends from the cell body cluster towards the midline, at the level of wing nerve insertion. This branch then apparently crosses the midline and continues to the contralateral border of the neuropil along a more dorsal and posterior route. This projection arborizes near the cell body cluster of its contralateral homolog. Hemilineage 18B also produces intersegmental projections near the midline. Without MARCM clones, I cannot be certain whether the projections from each segment are ascending or descending, but they appear to converge on the posterior part of T2. Finally, at the dorsal surface of the neuropil, the lineage makes a thin, elaborate midline-crossing arbor. nSyt-GFP appears to localize to the dorsomedial portions of this arbor (Fig. 3.18C). The T3 arbor is similar to that of T2, but slightly reduced.

Lineage 19

In the larva, the lineage 19 cell body cluster is found in the dorsal third of the VNS, at the posterior border of the neuromere. 19A descends to the ipsilateral leg neuropil, while 19B projects in the pI commissure, then turns anteriorly. The adult morphology is similar: the 19A and 19B cell body clusters stay close together in the dorsal posterior part of the neuromere, and 19A projects to the ipsilateral ventral neuropil, while 19B stays dorsal and makes ascending projections. Hemilineage 19B is greatly reduced in T1.

The adult arbor of hemilineage 19A has two major parts: a descending projection that arborizes throughout the ventral part of the leg neuropil, and a medial projection at the level of the cell bodies (halfway up the VNS) that extends to the midline but does not

cross. The medial projections in T1 and T2 converge on the midline in T2 and appear to overlap (Fig. 3.19). nSyt-GFP localizes to the most medial (distal) parts of the medial projection. The 19A medial arbor appears to overlap with axons of the leg chordotonal afferents (Fig. 3.19C).

The adult arbor of hemilineage 19B has many parts (Fig. 3.19). It forms an ipsilateral ventral arbor that descends into the ipsilateral leg neuropil. It also forms a complex, bilaterally symmetric arbor with both multiple ascending projections. The lateral ascending projections are larger, more dorsal, and do not make many fine branches; they are referred to as the "major" dorsal branches in Fig. 3.19. nSyt-GFP localizes primarily to these projections (Fig. 3.19J). The medial paired arbors are smaller and make fine, dense projections medial to and overlapping with the lateral projections. These are the minor dorsal branches (Fig. 3.19G-J). In T3, the dorsal part of the neuromere is pulled anterior to accommodate the fused abdominal neuromeres. The 19B cluster in this segment is reduced, with only a few axons crossing the midline. The overall structure of its arbor is similar to that in T2.

Lineage 20/22

In these lineages the first few B sibs become motoneurons and the remainder die (Truman et al. 2010). In the larva, 20A and 22A are adjoining lineages in the posterior half of the neuromere. Their A sibs both send very short projections to the ventral leg neuropil, and it is difficult to tell them apart. I was unable to recover lines that distinguished them, and treat them as a single entity in the adult. The adult morphology of 20A/22A is not much

changed (Fig. 3.20). The cell body cluster is found at the posterolateral border of each thoracic segment. The neuroglian tract projects straight into the leg neuropil, where it arborizes throughout the middle portion of the leg neuropil, at the upper border of the ventral third of the neuropil. The arbor has a distinctive "Y" shape in the adult, with a lateral and a medial branch.

Lineage 21

The larval morphology of lineage 21A is similar to that of lineage 20A/22A. In the adult, the cell body cluster of 21A remains close to that of lineage 20/22. Its neuroglian tract projects dorsally into the middle of the leg neuropil, where it forms an expansive spray of arbor that virtually fills the ipsilateral leg neuropil (Fig. 3.21). Hemilineage 21B undergoes programmed cell death (Truman et al. 2010).

Lineage 23

In the larva, only the hemilineage 23B siblings survive (Truman et al. 2010). The hemilineage 23B cell bodies are located ventrolaterally. They project across the pI commissure and terminate soon thereafter. In the adult, however, the 23B somata translocate and become very dorsolateral. The bundled primary neurites project ventrally to the mid-VNS, paralleling the tract of 19B. Since both of these lineages project in the pI commissure in the larva, it appears that during metamorphosis the entire tract curls dorsomedially, bringing the lineage 23 cell bodies with it. The 23B projection sends off a robust branch just prior to crossing the midline that arborizes throughout the ipsilateral leg neuropil. This branch continues to the ventralmost portions of the leg neuropil, where

it appears to overlap with multiple classes of leg sensory neuron (Fig. 3.22F-H). The hemilineage then crosses the midline and extends a small intersegmental medial process. The MARCM clone in Fig. 3.22E shows hemilineage 23B in T2 extending these processes to the dorsal leg neuropils of T1 and T3. MARCM clones of lineage 23 in T1 show that in this segment, the medial processes are descending, bilaterally symmetric, and extend to the posterior border of T2. I did not recover a MARCM clone of lineage 23 in T3.

23B is one of the only hemilineages whose neuroglian tract transits the neuropil dorsal-to-ventral, rather than ventral-to-dorsal. It is the single longest dorsoventral tract in the neuropil and forms an important landmark in the medial cluster (Fig. 3.1).

Lineage 24

As with lineage 15, hemilineage 24A dies in the larva (Truman et al. 2010), while hemilineage 24B produces leg motor neurons. Lineage 24 was described in Brown and Truman (2010). 24B produces motor neurons that innervate proximal leg segments (coxa, trochanter and femur) (Baek and Mann 2009), while 15B produces the motor neurons for more distal leg segments. The adult morphology of 24B is in accord with other descriptions of leg motor neurons (e.g., Nassel et al. 1986), and is similar to that of hemilineage 15B in both the larva and the adult. Its arbor is slightly more complex that that of 15B, though it has fewer neurons. Part of the neuroglian tract parallels that of hemilineage 15B, but it also forms a projection towards the midline, where it may form a

small midline-crossing branch that projects dorsally (Fig. 3.23). Without a MARCM clone, I could not confirm this.

Hemilineage adult anatomy is summarized in Fig. 3.24.

Lineage origin of GABAergic clusters in the thoracic VNS

The GABA-immunoreactive cells in the VNS occur in discrete clusters, rather than being scattered throughout the cortex. Colocalization of hemilineage drivers and anti-GABA staining showed that these GABA-reactive clusters corresponded to identified lineages and hemilineages, and 8 such clusters were found in segment T2 (Fig. 3.25). The anterior dorsal cluster of GABA cells comes from hemilineage 9A. The lateral dorsoposterior cluster comes from hemilineage 19A, while the medial dorsoposterior cluster comes from 11B. The anterior ventral cluster comes from lineage 13: the "A" and "B" siblings are both GABA-immunoreactive. The paired ventromedial clusters are part of hemilineage 6B and hemilineage 5B. The unpaired, posterior ventromedial cluster comes from hemilineage 0A. The posterior ventrolateral cluster comes from hemilinage 12B.

A database and interface for comparing the adult arbors of the thoracic lineages

I created a MATLAB graphical user interface (GUI) to visualize this data on the adult hemilineages. The GUI displays a schematized VNS with neuroglian tracts marked as in Fig. 3.1, and allows the user to visualize the tracts, arbors, and/or neurotransmitter identity of up to three different lineages at a time by selecting them with checkboxes (Fig.

3.26). This is a simple way to test whether two hemilineages project to the same region, and can quickly identify pairs that could not possibly synapse onto one another.

A putative map of lineage overlap

Using the GUI, I established the degree of overlap between each pair of lineages. I then used the network visualization software Neuroptikon to generate a map of overlapping arbors in the thoracic neuropil from this data (Fig. 3.27). (Most errors will be wrongly predicted connections, rather than missed connections.) Neuroptikon allows the user to quickly visualize all of the partners assigned to a lineage by clicking on it (e.g., Fig. 3.27B,C). While not definitive, this map can facilitate hypothesis generation for more in-depth case-by-case testing.

Discussion

The tools developed in Chapter 2 enabled me to make the first comprehensive characterization of the adult anatomy of the secondary hemilineages of the thoracic CNS. In addition to being a valuable resource for identifying neurons based on the neuroglian tract in which they run, my data reveal some interesting information about the organization of the thoracic neuropil.

Metamorphosis of the neuroglian scaffold

Truman et al. (2004) described the architecture of the larval VNS in terms of an intricate scaffold of tracts and commissures that express neurotactin and neuroglian. These tracts

consist largely of the initial neurites of the secondary hemilineages. The scaffold undergoes dramatic warping and deformation during metamorphosis, such that it is difficult to identify the adult counterpart. I determined that the primary neurites within a hemilineage bundle remain tightly fasciculated in the adult, but the individual bundles dissociate from one another and the commissures are no longer discrete entities. For example, in the larva, the bundles from lineages 7B, 8B, 10B, and 18B are closely associated in the aI commissure; in the adult, the tracts for 7B and 8B still cross the midline together, but 10B and 18B have been displaced anteriorly and do not form a cohesive tract.

It is curious that this commissural structure dissolves in the adult, because the larval neurotactin scaffold is homologous to the major tracts and commissures of the VNS in more basal species. Perhaps lineages that are markedly different from their commissure-mates, such as the neurons in hemilineage 1A, are lineages whose function has changed dramatically over evolutionary time; e.g., perhaps the ancestral morphology and function of 1A more closely resembled that of 13B and 14A. The lineages recruited to build the flight neuropil are obvious examples of lineages whose function has changed over time. As these hemilineages diverged functionally, they could have been pulled farther from their original targets, until hemilineages that were adjacent in ancestral insects became widely separated in the fly. (The evolution of flight is simply an illustrative example. Grasshoppers retain the ancestral VNS organization, so flight alone clearly does not account for the observed changes.) Another issue is why the neurons in the hemilineages are still bundled in the adult. They appear to be bundled in glial sheaths, because if the

neurons are killed, the tracts still appear in neuroglian staining (personal observation). One could speculate that neurons within a lineage are recruited to new functions as a unit, and so although the commissures pull apart in the adult fly, the lineages remain cohesive units.

My map of the adult neuroglian scaffold and annotated landmarks should be of practical use in identifying the lineage of origin of thoracic interneurons. Secondary neurons can now be assigned to their lineage of origin by the neuroglian tract in which they project. This will allow cross-referencing to information about likely neurotransmitter expression, potential synaptic partners, etc.

Larval vs. adult projection overlap

In describing the initial projections of the secondary lineages, Truman et al. (2004) noted that lineage neurites typically arrested near or touching the projections of specific other lineages. They hypothesized that these initial connections prefigured adult connectivity. I generated a tool to easily compare the arbors of two or three hemilineages to determine whether they might overlap, and therefore whether they could potentially be synaptic partners. Using this tool, I checked their predictions against adult anatomy. With two exceptions, all of their predicted connections seem possible in the adult.

The exceptions are hemilineage 1A and lineage 10B. In the larva, hemilineage 1A projects across the midline in the ventralmost commissure and contacts the ventral surface of the leg neuropil. Consequently, Truman et al. predicted that 1A would connect

with leg lineages in the adult. However, during metamorphosis, 1A turns dorsally and elaborates along the leg-wing neuropil border, and does not connect with ventral leg lineages at all. Lineage 10B projects in the aI commissure in the larva, and Truman et al. predicted that it would connect with other aI lineages. However, while the other aI lineages (0A, 7B, 8B, and 18B) ultimately project to the far dorsal neuropil, 10B sends arbors into the ventral leg neuropil and is pulled well away from these lineages in the adult. Thus, while initial contacts between lineages do largely correlate with adult connectivity, these exceptions demonstrate that initial proximity does not automatically lead to synaptic connections, nor does it constrain the lineages to nearby partners. Why these two lineages behave unexpectedly is unknown.

A counterpoint is provided by lineages 9A and 14A. Truman et al. (2004) documented initial contact between these two lineages, although lineage 9A projected to intermediate leg neuropil, while 14 projected more ventrally. In the adult, presumably as leg sensory neurons invade the neuropil, the arbors of both of these lineages are displaced to the far ventral neuropil, but remain in close proximity despite this massive rearrangement. This suggests that in some cases, initial contacts between lineages may prefigure connectivity patterns (rather than coincidental anatomical proximity), because some associations survive substantial anatomical deformation and thus must be maintained through either co-regulation or physical coupling.

Hemilineages as neural classes

One goal of characterizing the hemilineages was to identify neural classes that would help us to understand the functional organization of the thoracic ganglia. In some cases, the neurons in a hemilineage share obvious similarities, such as hemilineage 15B, which produces only leg motor neurons. Another example is the progeny of NB4-1 in the grasshopper, homologous to hemilineage 14A in the fly, most of which become midline spiking interneurons (Shepherd and Laurent 1992). These neurons are all inhibitory local interneurons that receive leg mechanosensory inputs and synapse onto leg motor neurons. It seems reasonable to regard both of these as examples of lineages that produce a neural class. Hoever, other lineages in the brain and VNS have been found to produce multiple distinct neural classes (e.g. Kao et al. 2012, Lai et al. 2008, Nagayama 1989).

At a minimum, cells that belong to the same neural class should project to similar regions of the neuropil. I did not perform any single-cell analyses, so I cannot say for certain whether all the cells within a hemilineage project to the same regions. However, the arbors of certain hemilineages are so complex, it seems unlikely that all of the regions would be contacted by a single neuron. Thus, these hemilineages likely comprise at least two neural classes. Conversely, some hemilineage arbors are so simple that it seems probable that a single neural class is represented.

Most hemilineages that arborize in the dorsal third of the neuropil appear to belong to the former category, while most that arborize in the ventral third appear to belong to the latter. It appears likely that all of the hemilineages that produce local leg interneurons, produce a single type of local leg interneuron. This includes 1B, 3A, 4B, 8A, 9A, 12B,

13A, 13B, 14A, 19A, 20A/22A, and 21A. A few dorsally projecting lineages also produce very simple arbors, namely 2A, 3B, and 11B, and may represent single neural classes.

Most of the other hemilineages produce complex projections that likely arise from the combined arbors of multiple neural classes. Hemilineages 0A, 1A, 5B, 6A, 6B, 7B, 8B, 11A, 12A, 18B, and 19B all probably encompass cells that project to nonoverlapping regions. Hemilineages 10B, 17A, and 23B are intermediate in complexity. It is plausible that individual neurons could project to all of the observed target regions, but they would be particularly complex neurons.

It would be interesting to explore whether arbor complexity and/or intralineage heterogeneity correlated with the complexity and/or evolutionary history of the behavioral function associated with a given hemilineage. For example, the hemilineages associated with flight must have served rather different functions in wingless ancestral taxa. Perhaps the complex arbors observed among the dorsal lineages are the result of recent expansion and divergence within a single ancestral neural class.

Polarity and arbor morphology

It has been suggested that many insect neurons form a proximal arbor that is largely postsynaptic, and a distal arbor that is mostly presynaptic (e.g., Burrows 1996). The leg-specific lineages typically cannot be divided into proximal and distal sections, so this relationship cannot be tested for these cells. In the case of intersegmental lineages, testing

this idea becomes an interesting problem because the lineages overlap with their contralateral and segmental homologs, and so it was often very difficult to distinguish presynaptic and postsynaptic arbor regions (e.g., using nSyt-GFP). MARCM clones allowed us to visualize lineages in a single hemisegment, but I did not combine MARCM with nSyt-GFP. Using MARCM, I observed two types of intersegmental arbors: asymmetric and bilaterally symmetric.

The neurons in hemilineages 1A, 2A, 5B, 6A, 6B, 7B, 8B, 17A, 19B, and 23B had distinctly asymmetric arbors, and most of these could be divided into proximal and distal sections. (This list is not comprehensive; other lineages may have asymmetric arbors, as well.) In most tested cases, the presynaptic marker nSyt-GFP localized mostly to the distal arbor. However, there were exceptions. For example, nSyt-GFP distributes throughout the asymmetric arbor of hemilineage 12B, with the exception of a small region near the ventral midline. MARCM clones show that this ventral projection corresponds to the most distal parts of the 12B arbor. Thus, hemilineage 12B appears to have a distal dendritic arbor, with presynaptic sites scattered throughout the proximal branches.

For lineages with symmetric arbors, such as 1A, one would need MARCM clones containing nSyt-GFP to determine whether input/output zones are also bilaterally symmetric. One could envision two scenarios: in the first, the ipsilateral (proximal) branches could be dendritic and the contralateral (distal) branches axonal, so the lineage transmits information about its ipsilateral side to its contralateral neighbor. Alternatively,

the lineage could receive information from the left and right sides and/or transmit that information to both the left and right homologs of its downstream targets. My lineage lines cannot be used to distinguish these possibilities.

Identification of GABAergic interneurons

If, as proposed, hemilineages correspond to neural classes, then one would expect the neurons within a hemilineage to express the same neurotransmitter, or at least of the same sign (i.e., excitatory vs. inhibitory). GABA is a major inhibitory transmitter in *Drosophila* as well as vertebrates, and GABA-immunoreactive cells occur in clusters that are clonally related in *Manduca* (Witten and Truman 1998) and likely *Drosophila*. I used my hemilineage-specific lines to identify the *Drosophila* homologs of the seven clonally related clusters of GABAergic neurons described in Witten and Truman (1998). A few homologies were easy to identify: the *Manduca* "E" cluster corresponds to hemilineage 9A; the "N" cluster is hemilineage 12B; the "T" cluster is hemilineage 19A; and the "X" cluster is hemilineage 0A, which was already known.

The composition of the *Manduca* "M" cluster is unclear. Hemilineage 6B contains a large number of strongly GABA-immunoreactive cells near the midline, as does hemilineage 5B. Both lineages are in the correct location to be part of the cluster designated "M" by Witten and Truman (1998). They attribute this cluster to embryonic NB 5-5 based on the work of Wolf and Lang (1994), whereas Truman et al. (2004) proposed that lineage 6 is produced by embryonic NB 5-2. The embryonic NB that produces lineage 5 has not been determined. In grasshopper, some GABA clusters are thought to result from the fusion of

two adjacent lineages (O'Dell and Wakins 1988), but in *Manduca,* this is not the case (Witten and Truman 1991). It seems safest to say that hemilineage 5B produces the "M" GABAergic cluster as described by Witten and Truman, and postulate that in *Drosophila*, unlike *Manduca*, the cluster may also contain cells produced by hemilineage 6B.

The "K" cluster of Witten and Truman (1998) is probably lineage 13. Witten and Truman (1998) reported that the K_L and K_M clusters correspond to the two hemilineages of a single neuroblast, whose cell body clusters are mingled in the larva but pull apart during metamorphosis. K_L and K_M likely correspond to 13A and 13B. Both of the latter are GABAergic. However, the morphology of 13A neurons may not match the anatomy of the K_L cluster from other species. The other possibility is that the K cluster corresponds to hemilineage 14A, and that lineage 13 represents a population that is GABAergic in flies but not in moths.

I also identified hemilineage 11B as GABAergic. A GABA-positive cell cluster corresponding to this hemilineage has not been previously described. As with the K lineage above, this could be a case of differential transmitter expression between taxa.

One final pattern to emerge from the anatomy data is the tendency for lineages to contact their contralateral and segmental homologs. This is the case for all lineages that make projection neurons, with the possible exception of hemilineage 17A. (I was unable to determine whether 17A in T3 makes an ascending projection that contacts 17A in T2.)

This could reflect some developmental rule involving self-recognition that enables neurons to establish correct connections over long physical distances.

As predicted, the hemilineages of the thoracic VNS make unique, highly stereotyped arbors that carve out distinct territories in the neuropil. Based on projection patterns and neurotransmitter staining, most hemilineages probably contain one or a few neural classes. The array of neuroblasts that produces the thoracic ganglia is conserved beyond the Insecta, and so these classes must have homologs in all insect taxa. The form and function of some of these classes is doubtless quite different in divergent taxa, but the concept of tracing hemilineages across taxa to identify homologous neurons is a powerful one. Interestingly, the major tracts and commissures of the thoracic ganglia are also conserved at least from grasshopper to fly, but only in the fly larva. Prior to metamorphosis, the neuroglian scaffold of the larval VNS is organized with clear homology to the structure of the grasshopper tracts and commissures. During metamorphosis, this scaffold is distorted and the major tracts and commissures are pulled apart, and the homologous structures are quite difficult to discern in the adult fly. However, with the information in this chapter, we should now be able to determine the anatomical correspondence between classes of neurons in different species. We should also be able to ascribe any secondary neuron in the thoracic VNS to its lineage of origin, based on the neuroglian tract in which it projects. This provides a convenient identification system, as well as allowing us to cross-reference the neurons to the polarity, neurotransmitter, and arbor overlap data provided here, and potentially even

functional data inferred from homology to neurons in the grasshopper and other insects. In summary, this chapter should provide a useful reference for future studies of the VNS in a variety of contexts.

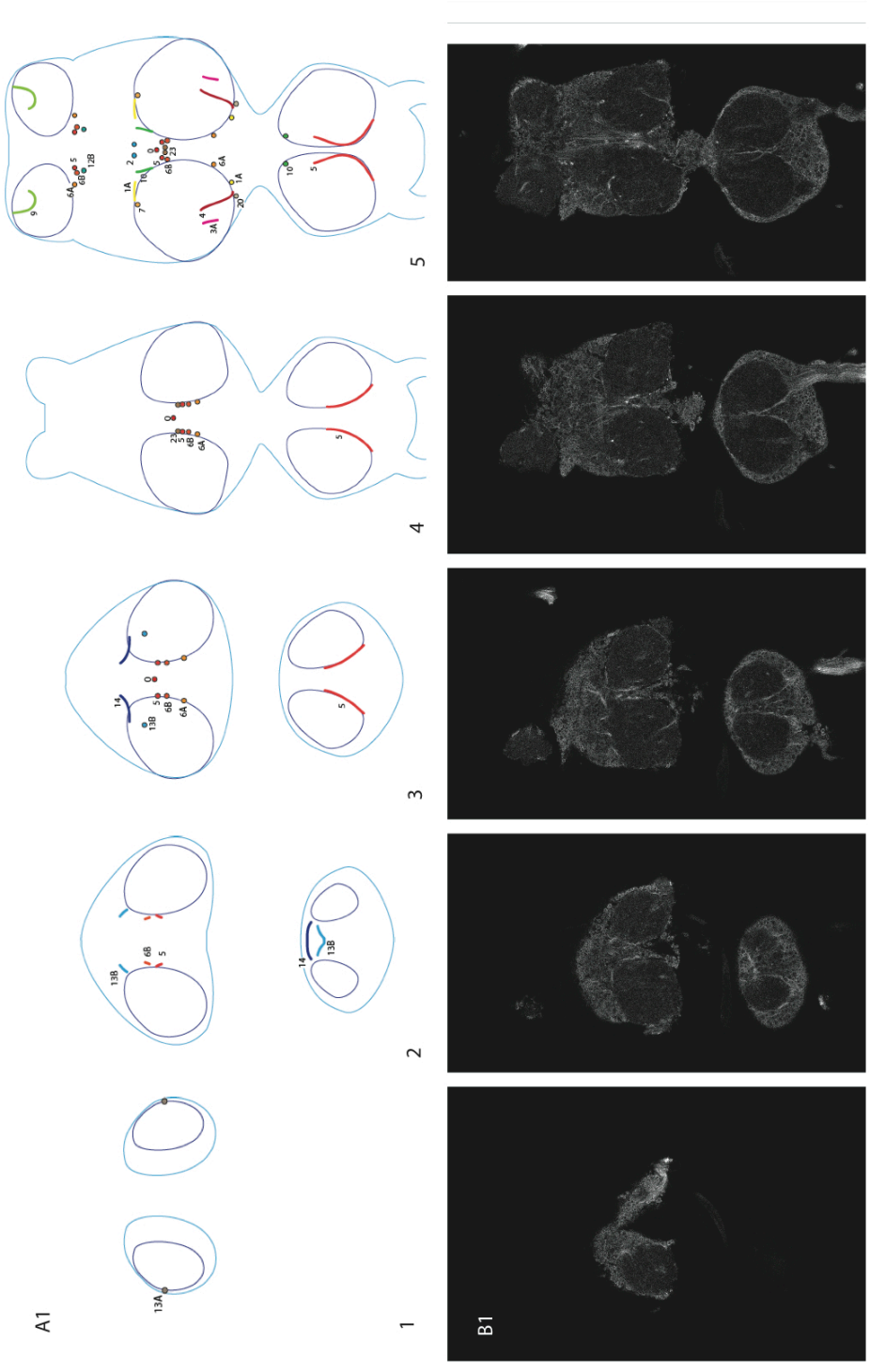

Figure 3.1. Summary of the hemilineage origins of the neuroglian scaffold in the adult. (A) Schematics of 15 optical slices of the VNS (10µm intervals) with color-coded neuroglian tracts, annotated on the left. Nomenclature is after Truman et al. (2004). (B) The original confocal slices from which schematics in (A) were traced. (C) Optical slice from another specimen, demonstrating the stereotypy of the scaffold. (B) and (C) are stained for anti-neuroglian.

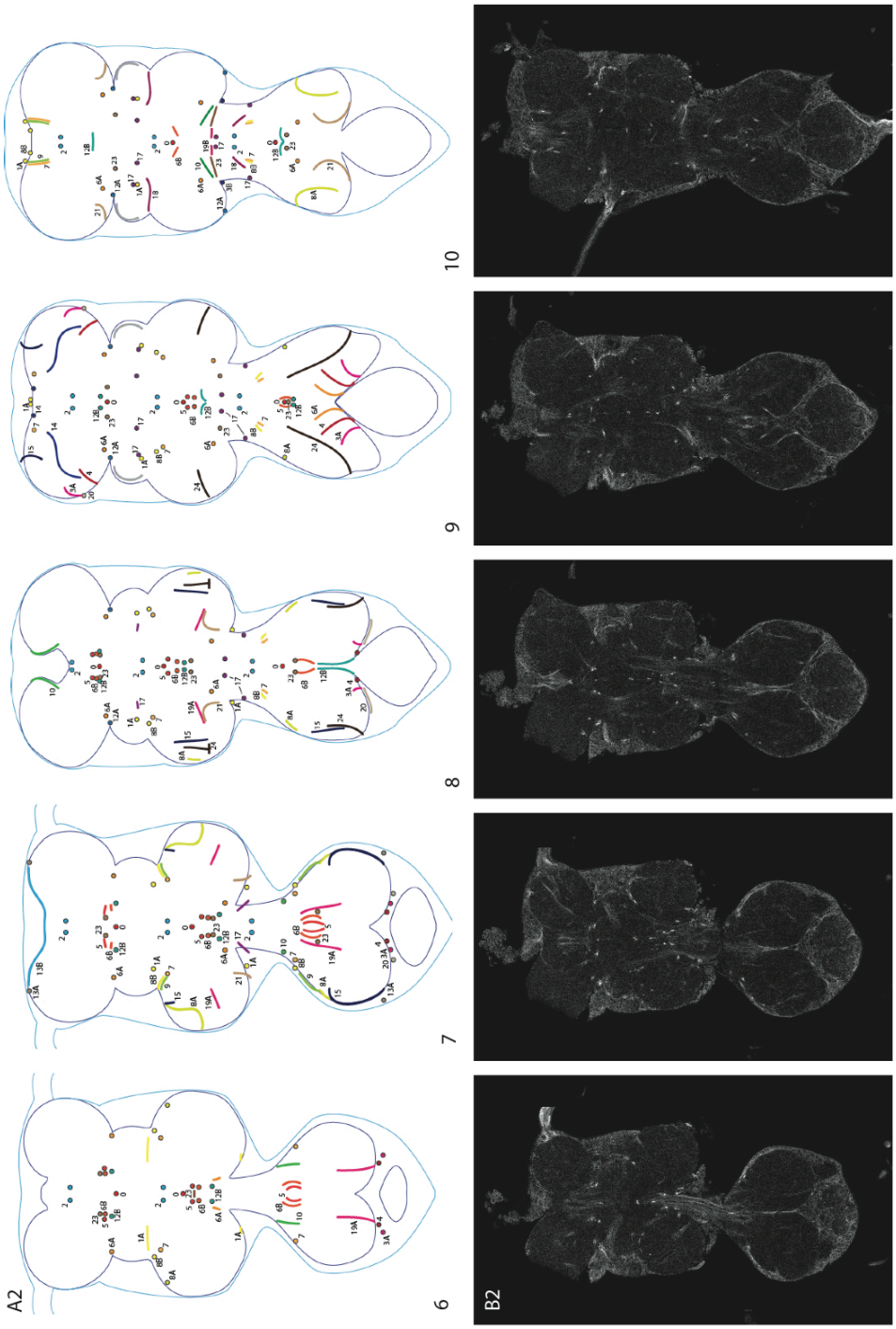

Figure 3.1, continued (2/3).

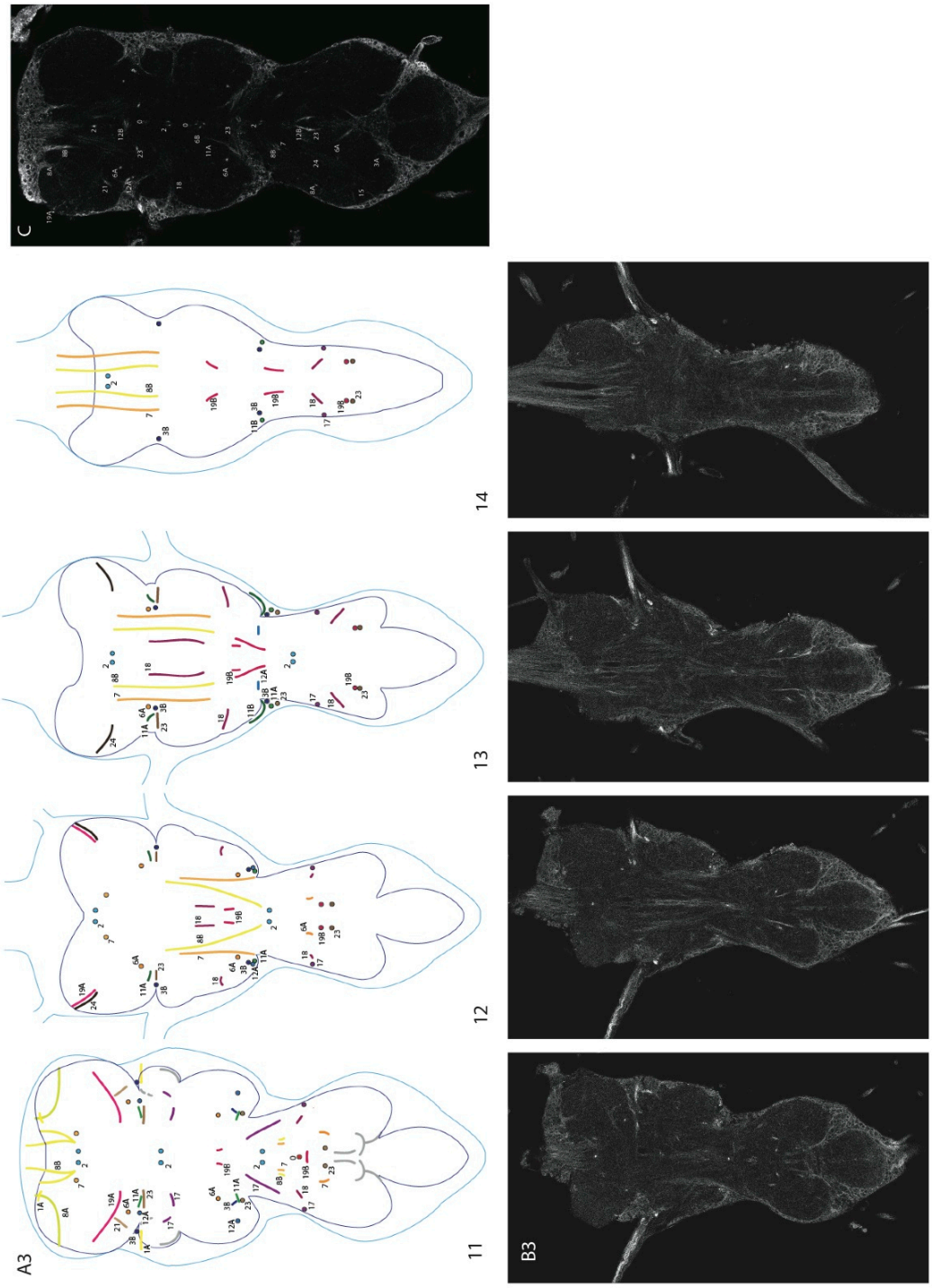

Figure 3.1, continued (3/3).

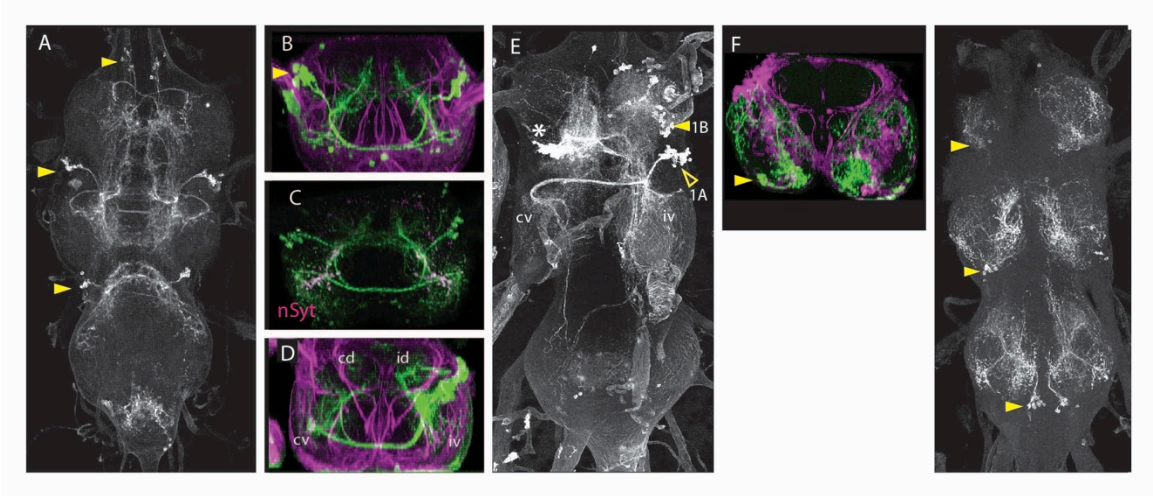

Figure 3.2. The adult anatomy of lineage 1. Yellow arrowheads: cell body clusters. (A) z-projection of the ventral CNS showing the location of hemilineage 1A clusters and arbor. (B) Transverse projection of T2 showing the right and left A1 clusters and their overlapping arbors. (C) T2 transverse projection showing that nSyt-GFP (magenta) localizes to the ventral parts of the 1A arbor. (D) Transverse section of a lineage 1 MARCM clone in T2, showing the arbor of hemilineage 1A. The cells produce a dorsal (id) and ventral (iv) ipsilateral projection and dorsal (cd) and ventral (cv) contralateral projections. (E) z-projection of a lineage 1 MARCM clone in T2. Open arrowhead, hemilineage 1A cell cluster; filled arrowhead, hemilineage 1B cell cluster. Note that the 1B cell body cluster has been pulled into T1. A lineage 6 clone is also present (*). (F) Transverse section of T1 showing the two hemilineage 1B clusters projecting to the ventromedial leg neuropil . (G) z-projection the ventral CNS showing the location of the 1B hemilineages. Note that the cell body cluster in T3 originated in anterior A1. (B,D,F) Green, anti-GFP; magenta, anti-neuroglian. Genotypes: (A,B) w; R22G11-LexA (attP40)/+; LexAop-GFP (attP2)/+. (C) LexAop-RFP (su(Hw)attP8)/w; R22G11-LexA (attP40)/+; LexAop-nSyt-GFP (su(Hw)attP1)/+. (D,E) tsMARCM clones (see Materials and Methods). (F,G) nSyb-GAL80 (su(Hw)attP8)/act>STOP>LexA (attP18); LexAop-GFP (attP40)/+; R48B01-GAL4 (attP2)/UAS-hPR-flp (VK00005).

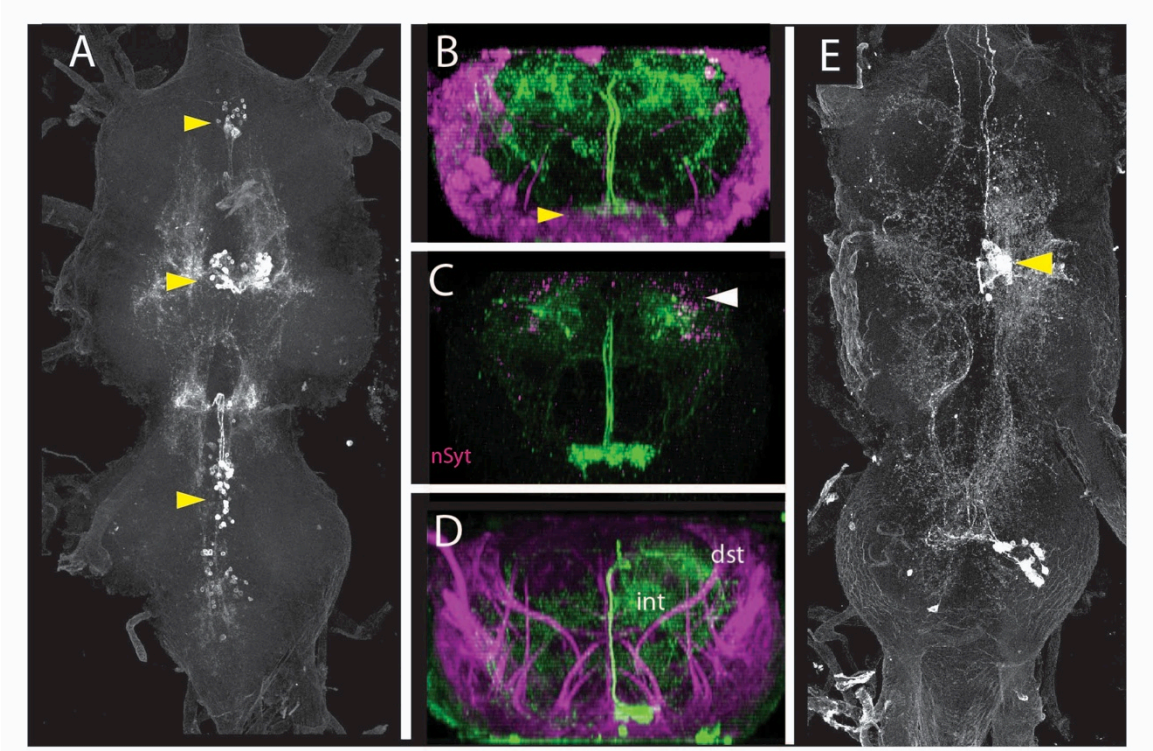

Figure 3.3. The adult anatomy of lineage 2. Yellow arrowheads indicate cell body clusters. Hemilineage 2B undergoes programmed cells death. (A) z-projection the VNS showing hemilineage 2A clusters in segments T1, T2, and T3. (B) Transverse section of hemilineage 2A in T2. Optical slices from the MARCM clone shown in (F). (C) nSyt-GFP (magenta) localizes to the dorsal, distal parts of the arbor (white arrowhead). (D, E) MARCM clone of lineage 2 in T2; (D) Transverse section of T2 showing the lineage 2 clone and indicating the interstitial (int) and distal (dst) arbors (E) z-projection of a MARCM clone of lineage 2 in T2. A clone from another lineage is in T3 (*). (B,D) Green, anti-GFP; magenta, anti-neuroglian. Genotypes: (A,B) w; +; R50G08-GAL4 (attP2)/pJFRC2-UAS-GFP (attP2). (D,E) tsMARCM clone (see Materials and Methods). (C) UAS-nSyt-GFP (attP18)/w; +; R50G08-GAL4 (attP2)/UAS-HA (VK00005).

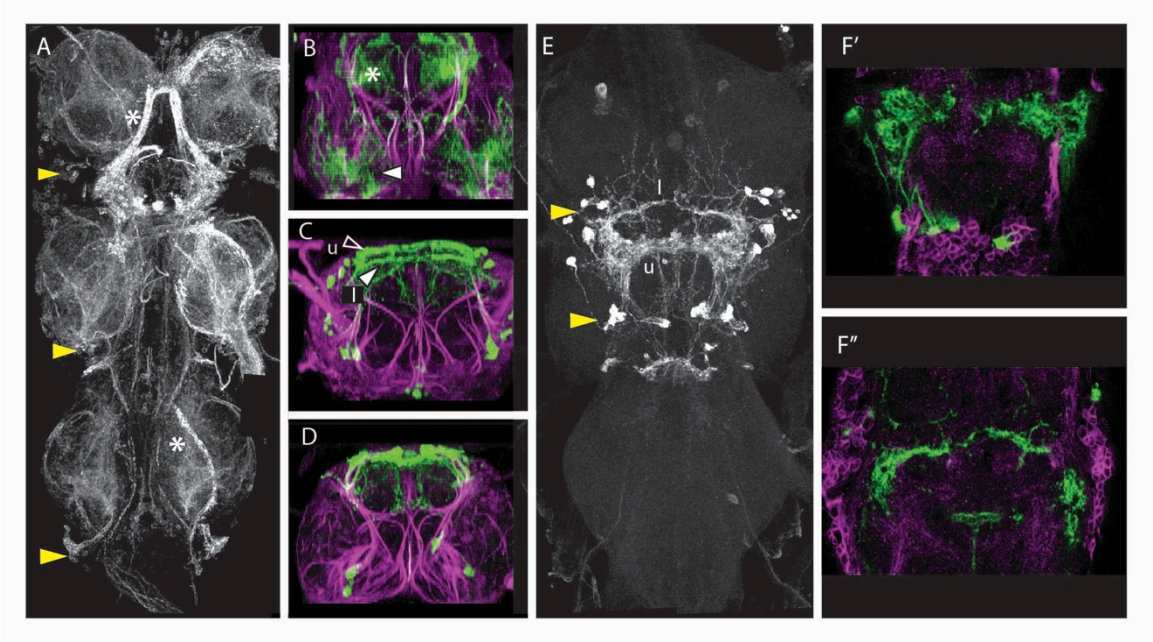

Figure 3.4. The adult anatomy of lineage 3. Yellow arrowheads indicate cell body clusters. (A,B) Hemilineage 3A. (A) z-projection of 3A showing hemilineage 3A clusters in T1, T2, and T3. This line also expresses in the strong sensory projections from the wings and halteres (*). (B) Transverse section of hemilineage 3A in T2 showing its ventral projection (arrowheads). *: Wing and haltere sensory projections. (C-F) Hemilineage 3B. (C) Transverse section of hemilineage 3B in T1 showing the separation between the upper (u, open arrowhead) and lower (l, filled arrowhead) arbors. (D) Transverse section of hemilineage 3B in T2. (E) z-projection of ventral CNS showing hemilineage 3B clusters in only T1 and T2. (F') Optical slice from the dorsal surface of the VNS, showing the shape of the upper arbor. (F'') Optical slice 15µm ventral to (F'), showing the shape of the lower arbor. (B-D, F) Green, anti-GFP; magenta, anti-neuroglian. Genotypes: (A,B) nSyb-GAL80 (su(Hw)attP8)/w; UAS-flp (attP40)/+; R31H10-GAL4 (attP2)/nSyb-LexA (attP2), LexAop>STOP>GFP (VK00005). (C-F) w; R23B05-LexA (attP40)/+; LexAop-GFP (attP2)/+.

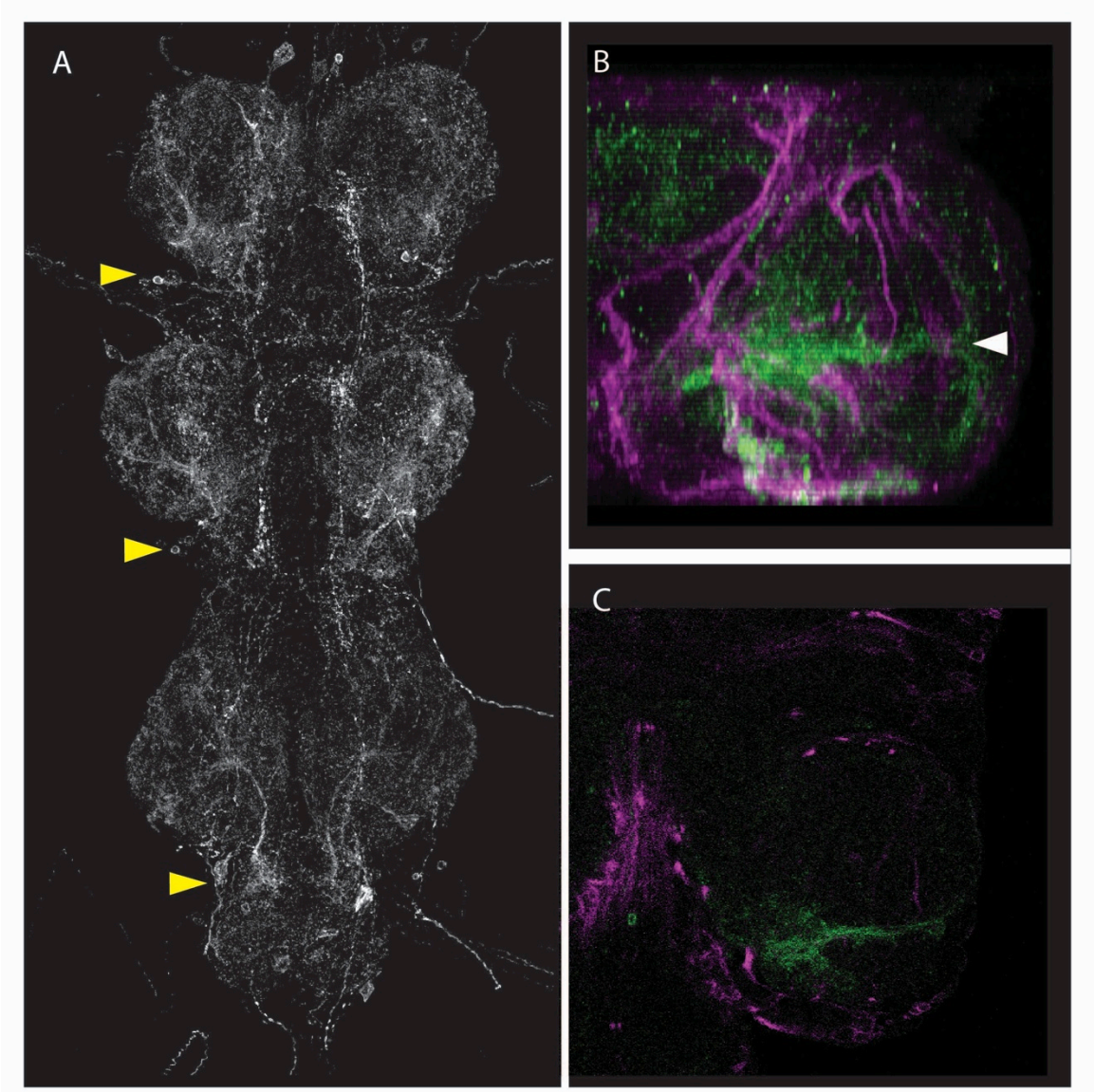

Figure 3.5. The adult anatomy of lineage 4. Yellow arrowheads, cell body clusters. Hemilineage 4A undergoes programmed cell death. (A) z-projection of the ventral CNS showing hemilineage 4B clusters in T1 through T3. (B) Transverse section of the right side of the T2 neuromere showing arbor in the intermediate leg neuropil. (C) Single optical slice from the level of the white arrowhead in (B), showing the shape and location of the main arbor. (B,C) Green, anti-GFP; magenta, anti-neuroglian. Genotypes: (A) nSyb-GAL80 (su(Hw)attP8)/w; UAS-flp (attP40)/+; R51H05-GAL4 (attP2)/nSyb-LexA (attP2), LexAop>STOP>GFP (VK00005). (B,C) act>STOP>GAL4 (attP18)/w; UAS-flp (attP40)/+; R11A03-GeneSwitch (attP2)/pJFRC2-UAS-GFP (attP2).

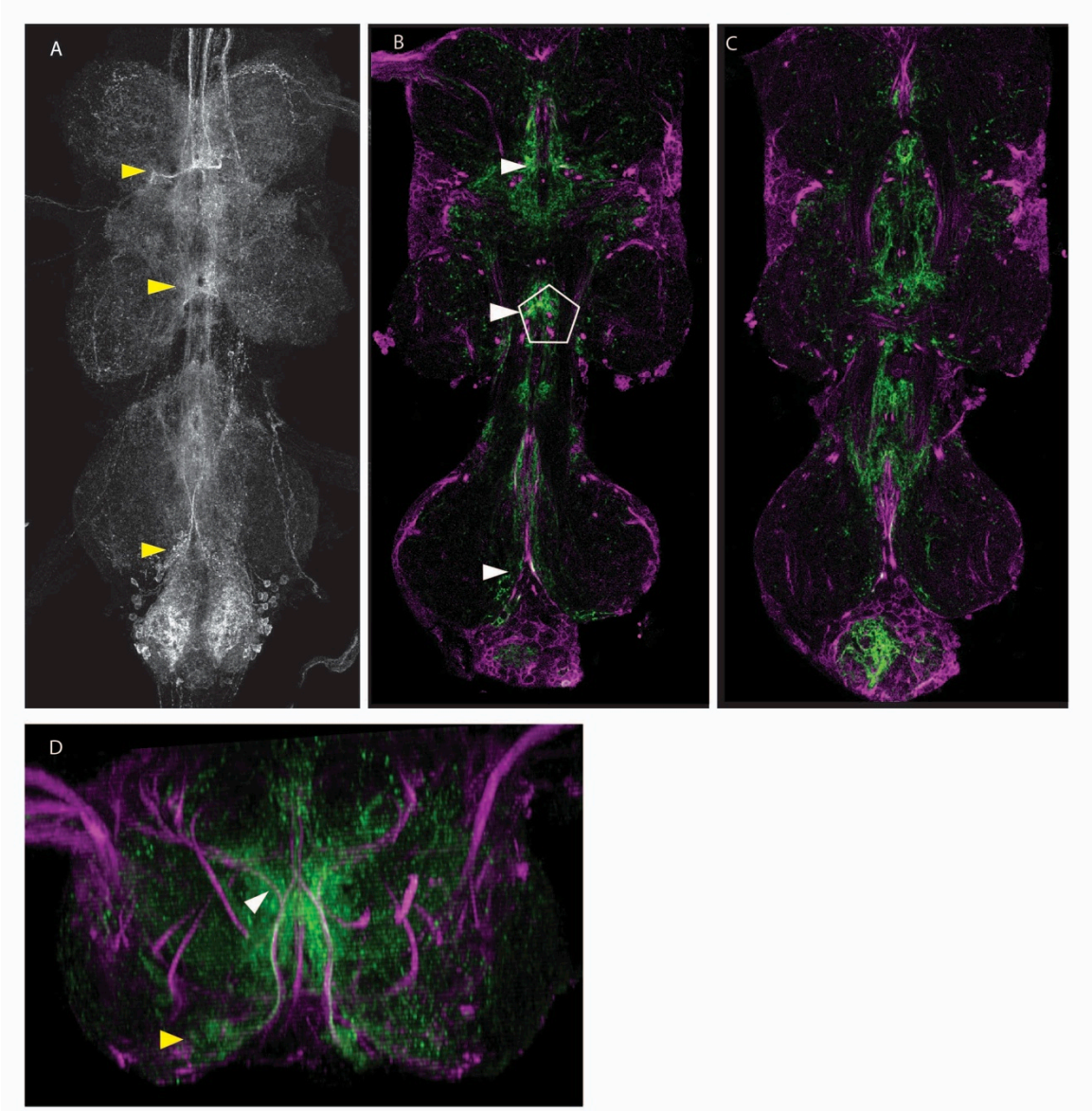

Figure 3.6. The adult anatomy of lineage 5. Yellow arrowheads, cell body clusters. Hemilineage 5A undergoes programmed cell death. (A) z-projection of the ventral CNS showing the hemilineage 5B clusters in T1 through T3. (B) Optical slice from near the middle of the VNS, showing the hemilineage 5B tract (white arrowheads) in the medial cluster (white pentagon in T2). (C) Optical slice 20µm dorsal to (B), showing the main hemilineage 5B arbor in the medial region of the neuropil. (D) Transverse section of T2 showing the hemilineage 5B arbor. White arrowhead, ipsilateral branch of the 5B arbor. Genotype: nSyb-GAL80 (su(Hw)attP8)/w; UAS-flp (attP40)/+; R86D02-GAL4 (attP2)/nSyb-LexA (attP2), LexAop>STOP>GFP (VK00005).

Figure 3.7. The adult anatomy of lineage 6. Yellow arrowheads indicate cell body clusters. (A-E) Hemilineage 6A. (A) z-projection of the ventral CNS showing the hemilineage 6A clusters from T1 through A1. (B) Sagittal section of the VNS in (A), showing the 6A tract from T3 versus A1. (C) Optical slice from halfway through the VNS, showing the 6A neuroglian tracts (white arrowheads) approaching the medial cluster (outlined in white in T2). (D) Transverse section of T2 showing hemilineage 6A. (E) Transverse section showing that nSyt-GFP (magenta) localizes to the distal contralateral parts of the 6A arbor (arrowhead). (F) Transverse section of a lineage 6 MARCM clone in T2. Open arrowhead, 6A cell cluster; filled arrowhead, 6B cell cluster. (G-J) Hemilineage 6B. (G) z-projection of ventral CNS showing the hemilineage 6B clusters in T1 through T3. (H) Optical slice from halfway through the VNS. The 6B neuroglian tracts (white arrowheads) are part of the medial cluster (outlined in white in T2). (I) z-projection of the ventral CNS showing the lineage 6 MARCM clone from (F). (J) Transverse section of hemilineage 6B in T2. (K) Transverse section through neuromere T2 showing that nSyt-GFP (magenta) localizes to the distal parts of the contralateral 6B arbor. (B, C, E, H, I) Green, anti-GFP; magenta, anti-neuroglian. Genotypes: (A-C) nSyb-GAL80 (su(Hw)attP8)/w; UAS-flp (attP40)/+; R35A03-GAL4 (attP2)/nSyb-LexA (attP2), LexAop>STOP>GFP (VK00005). (D) nSyb-GAL80 (su(Hw)attP8)/LexAop-RFP (su(Hw)attP8); UAS-flp (attP40)/act>STOP>LexA (attP40); R35A03-GAL4 (attP2)/LexAop-nSyt-GFP (su(Hw)attP1). (E,F) tsMARCM clone (see Materials and Methods). (G-I) nSyb-GAL80 (su(Hw)attP8)/w; UAS-flp (attP40)/+; R46C11-GAL4 (attP2)/nSyb-LexA (attP2), LexAop>STOP>GFP (VK00005). (J) nSyb-GAL80 (su(Hw)attP8)/LexAop-RFP (su(Hw)attP8); UAS-flp (attP40)/act>STOP>LexA (attP40); R46C11-GAL4 (attP2)/LexAop-nSyt-GFP (su(Hw)attP1).

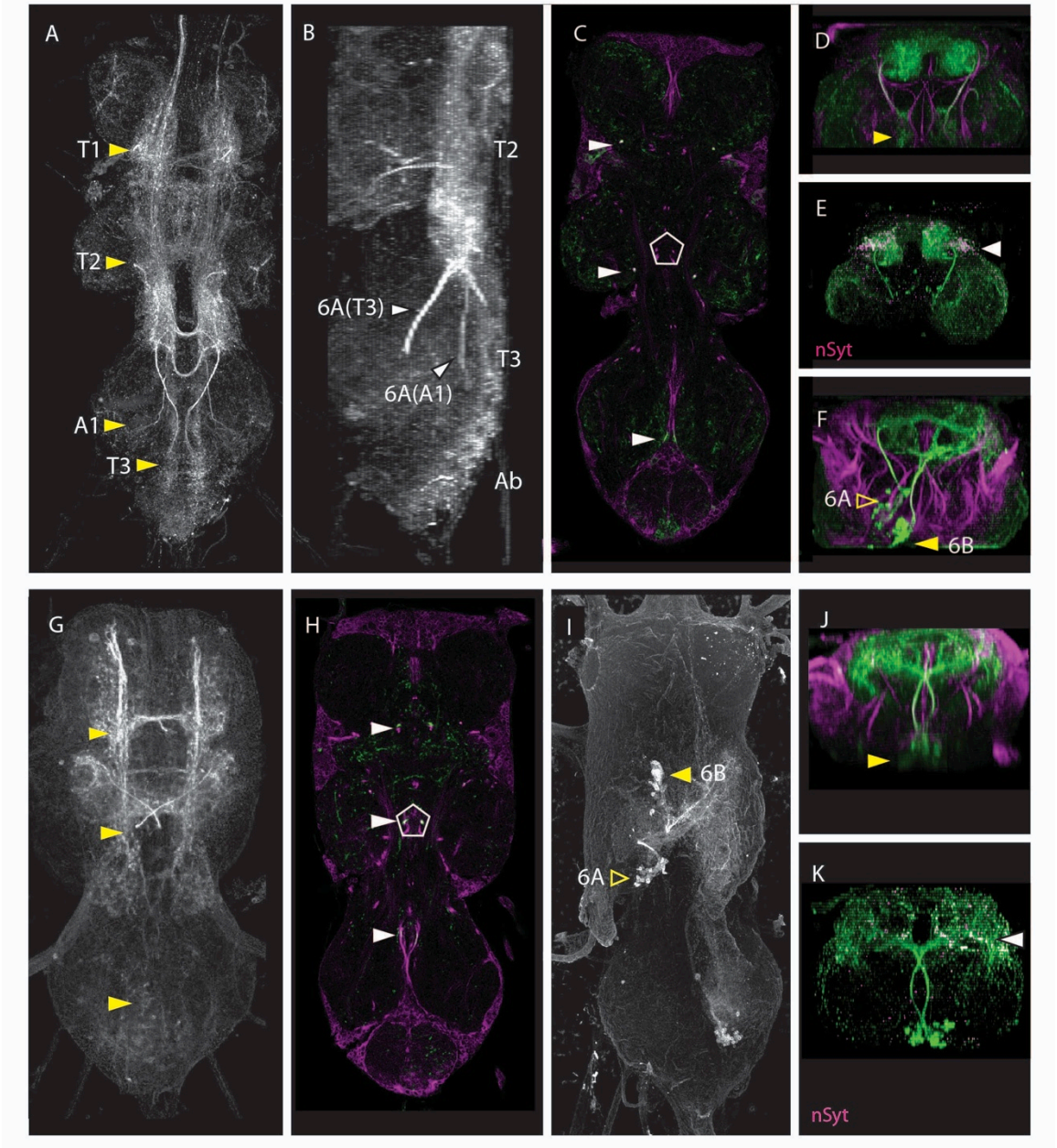
A
T1
T2
A1
T3
B
T2
6A(T3)
T3
6A(A1)
Ab
C
D
E
nSyt
F
6A
6B
G
H
I
6B
6A
J
K
nSyt

Figure 3.8. The adult anatomy of lineage 7. Yellow arrowheads indicate cell body clusters. Hemilineage 7A undergoes programmed cell death. (A) z-projection of the ventral CNS showing hemilineage 7B clusters in T1 through A1. (B) Sagittal section of the posterior segments showing the dorsal translocation of the 7B cluster with the compaction of the abdominal neuromeres. The T3 tract and A1 tract are labeled. (C) Optical slice from the middle of the VNS, showing the ventral arbors in T2 (arrowhead). Inset, boxed region, showing the pairing of the 8B tract (open arrowhead) and the 7B tract (filled arrowhead). (D) Transverse section of T2 showing the major projection of hemilineage 7B arbor into dorsal neuropil. (E, F) Lineage 7 MARCM clone in T3. (E) Transverse section of the clone, showing the ipsilateral dorsal arbor (i) and the ascending and ventral contralateral projections (c-asc and cv, respectively). (F) z-projection of the clone, showing the extent of the ipsilateral arbor (i) and the ascending and ventral contralateral projections (c-asc/cv, respectively). (B-E) Green, anti-GFP; magenta, anti-neuroglian. Gentoypes: (A-D) act>STOP>GAL4/w; UAS-flp (attP40)/R65A12-SplitGAL4-AD (attP40); pJFRC2-UAS-GFP (attP2)/R41E01-SplitGAL4-DBD (attP2). (E-F) tsMARCM clone (see Materials and Methods).

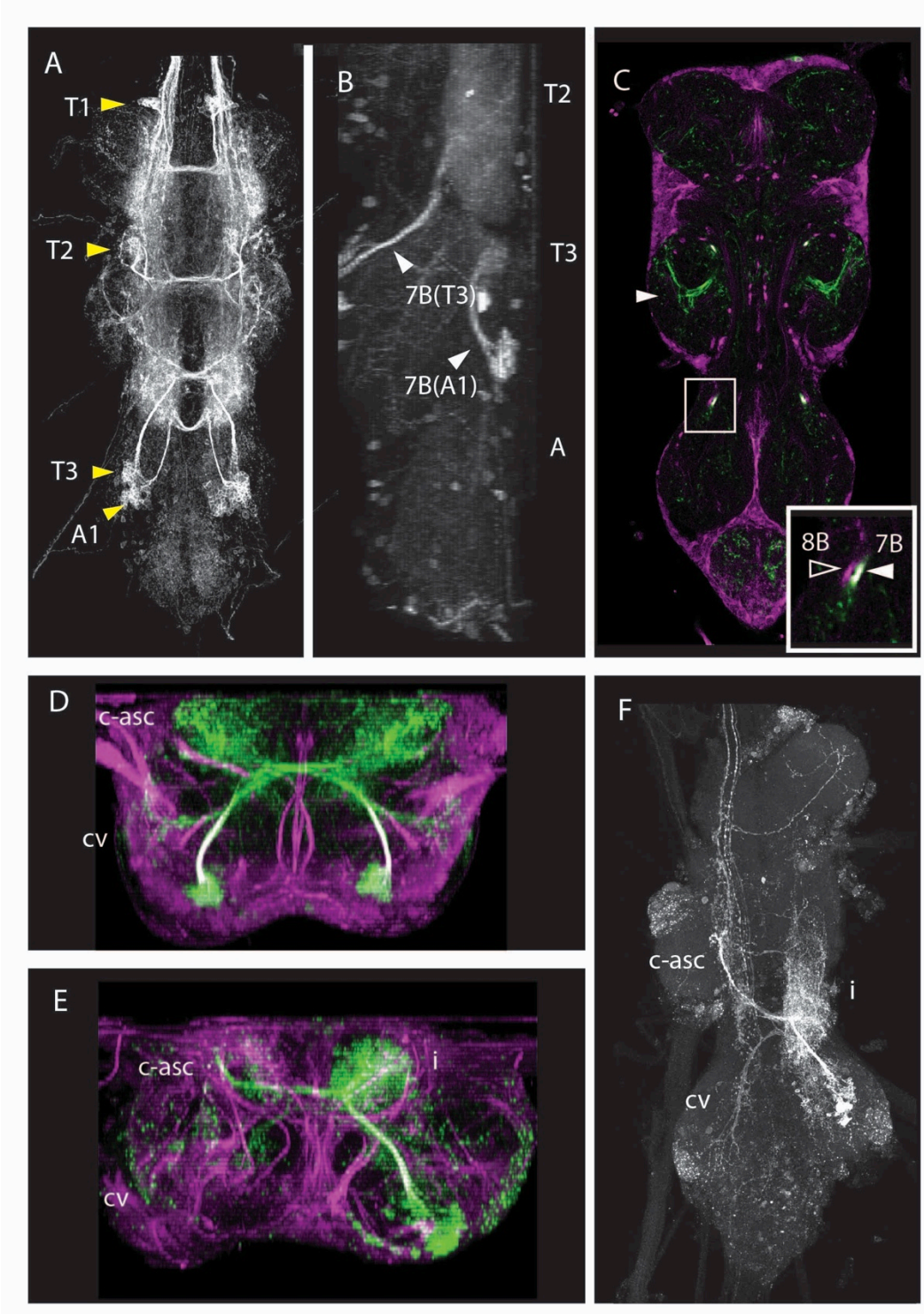
A
T1
T2
T3
A1
B
T2
T3
7B(T3)
7B(A1)
A
C
8B
7B
D
c-asc
cv
E
c-asc
i
cv
F
c-asc
i
cv

Figure 3.9. The adult anatomy of lineage 8. Yellow arrowheads indicate cell body clusters. (A,B) Hemilineage 8A. (A) z-projection of ventral CNS showing the hemilineage 8A clusters in T1 through T3. (B) Transverse section of the T2 neuromere showing the arborization of hemilineage 8A neurons in the lateral leg neuropil. (C,D) MARCM clone of lineage 8 in segment T2. (C) Transverse section of clone at T1-T2 boundary showing the 8A and 8B cell clusters (open arrowhead and filled arrowhead, respectively). The dorsal arbor is from the 8A hemilineage. (D) z-projection of clone showing the close proximity of the 8A (open arrowhead) and 8B (filled arrowhead) cell body clusters. *: Unrelated clone. (E-H) Hemilineage 8B. (E) z-projection of the ventral CNS showing the hemilineage 8B clusters in T1 through T3. Boxed region, the "bowtie" arbor of the cHINs (see text). (F) Dorsal closeups of transverse sections of lineage 8B. The upper arbor (u) and lower arbor (l) are indicated. (F') Hemilineage 8B in T1. The upper arbor (u) is extended, while the lower arbor (l) is less pronounced. *: Ascending projection from hemilineage 8B in T2/T3. (F'') Hemilineage 8B in T2. The upper and lower arbors are present. Asterisk, ascending projection from hemilineage 8B in T3. (F'') Hemilineage 8B in T3. The upper (u) and lower (l) arbors are present. The "bowtie" arbor corresponds to the lower arbor in T3. (B,C,F) Green, anti-GFP; magenta, anti-neuroglian. Genotypes: (A,B) w; +; R69H11-GAL4 (attP2)/pJFRC2-UAS-GFP (attP2). (C,D,F) tsMARCM clone (see Materials and Methods). (E,H) nSyb-GAL80 (su(Hw)attP8)/w; UAS-flp (attP40)/+; R09D08-GAL4 (attP2)/nSyb-LexA (attP2), LexAop>STOP>GFP (VK00005). (G) nSyb-GAL80 (su(Hw)attP8)/LexAop-RFP (su(Hw)attP8); UAS-flp (attP40)/act>STOP>LexA (attP40); R09D08-GAL4 (attP2)/LexAop-nSyt-GFP (su(Hw)attP1).

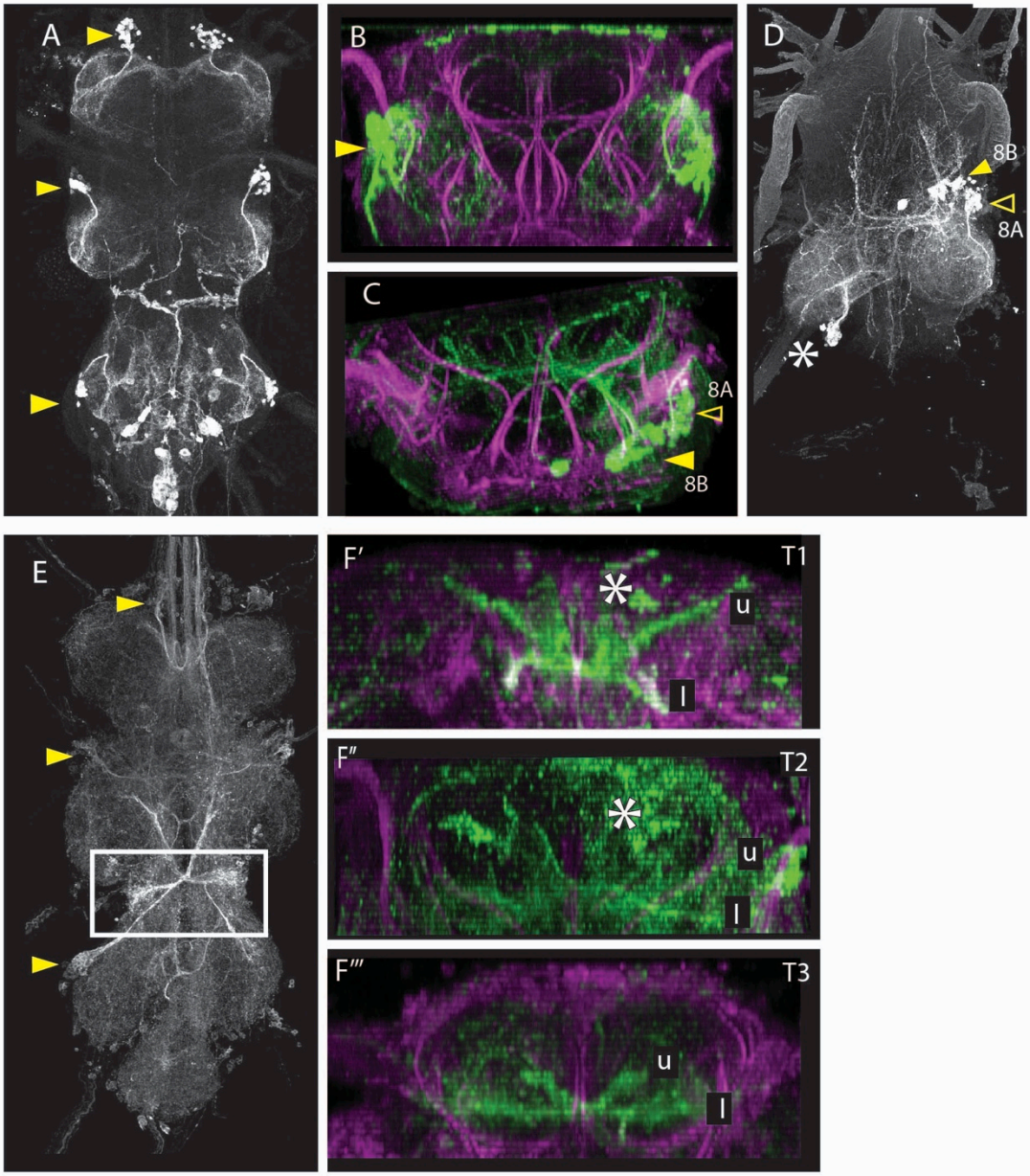
A
B
C
8A
8B
D
8B
8A
E
F′
T1
u
l
F″
T2
u
l
F‴
T3
u
l

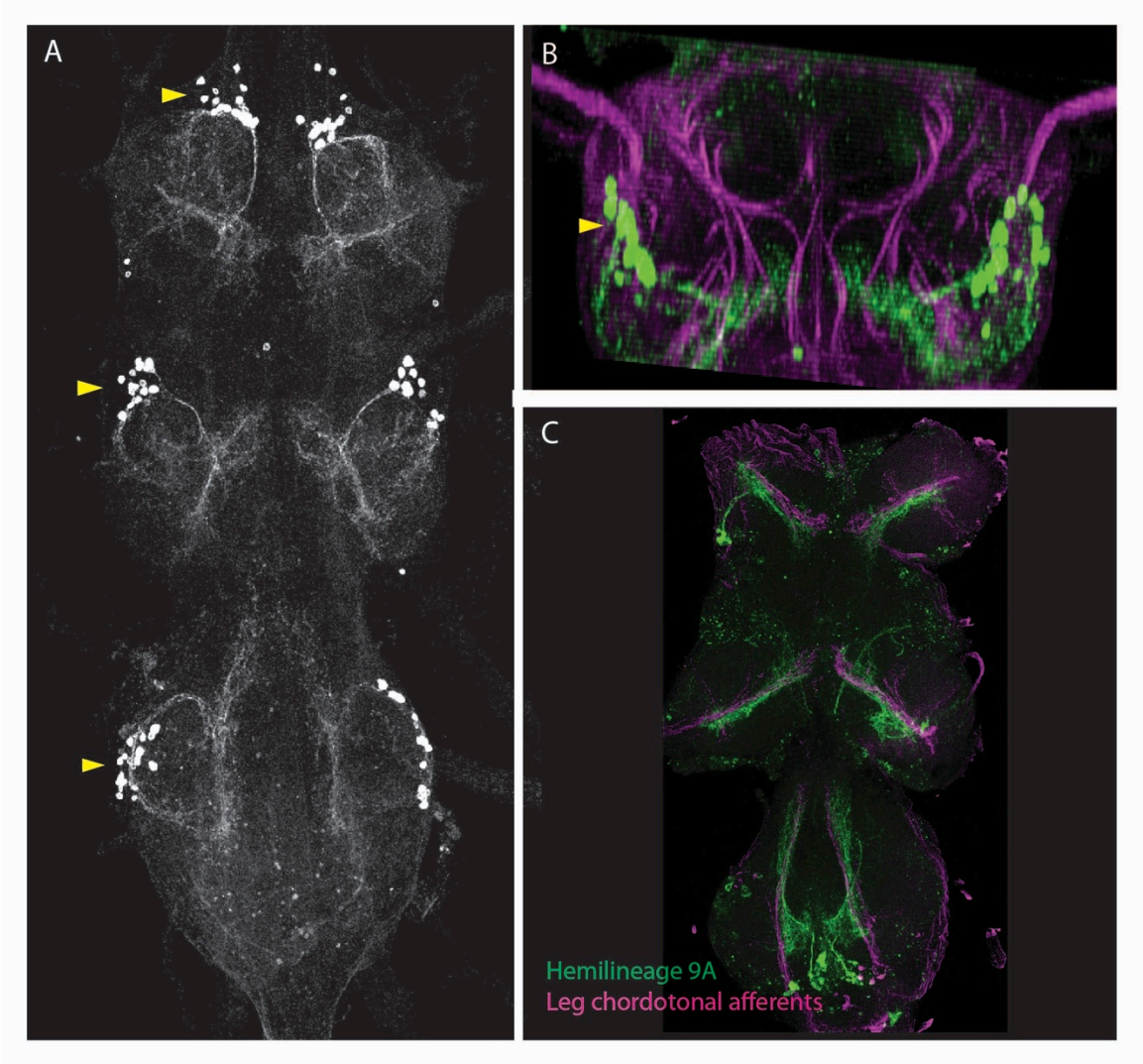

Figure 3.10. The adult anatomy of the neurons of lineage 9. Yellow arrowheads indicate cell body clusters. Hemilineage 9B undergoes programmed cell death. (A) z-projection the ventral CNS showing the hemilineage 9A clusters in T1 through T3. The cells project to a narrow band in the medial portion of the leg neuropil (B) Transverse section of T2 showing the medial projection of the hemilineage 9A cells. (C) Thick section (20µm) showing overlap between the hemilineage 9A arbor (green) and leg chordotonal sensory neurons (magenta). Genotypes: (A,B) w; +; R52E12-GAL4 (attP2)/pJFRC2-UAS-GFP (attP2). (C) LexAop-GFP (su(Hw)attP8), UAS-RFP (attP18)/w; R46G11-LexA (attP40)/+; R52E12-GAL4 (attP2)/+.

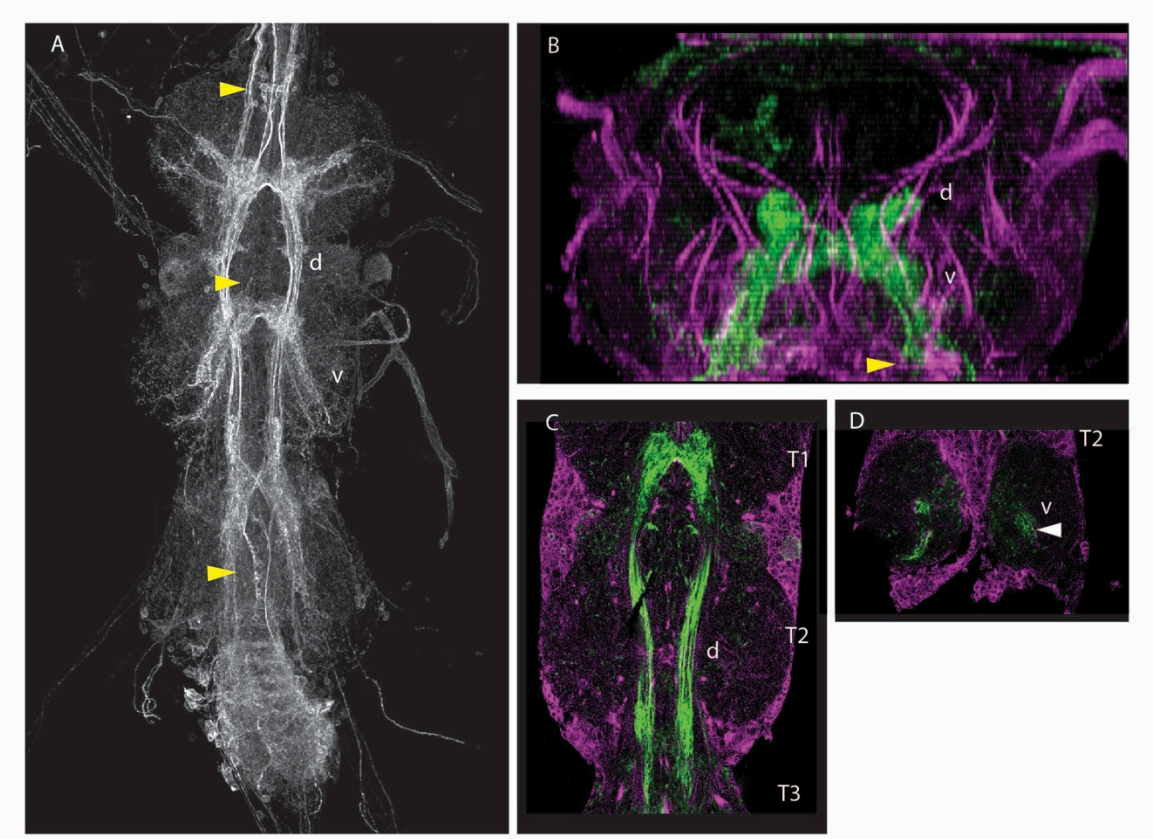

Figure 3.11. The adult anatomy of lineage 10. Yellow arrowheads indicate cell body clusters. Hemilineage 10A undergoes programmed cell death. (A) z-projection of the ventral CNS showing hemilineage 10B clusters in T1 through T3 . The abdominal cells are unrelated to this lineage. (B) Transverse section of T2 showing the dorsal (d) and ventral (v) projections of hemilineage 10B (C, D) Optical slices. (C) Slice through the middle of the VNS, showing the dorsal arbor that projects intersegmentally. (D) Slice through the lower third of the VNS, showing the ventral arbors projecting into the center of the leg neuropil. Genotype: nSyb-GAL80 (su(Hw)attP8)/w; UAS-flp (attP40)/+; R13B08-GAL4 (attP2)/nSyb-LexA (attP2), LexAop>STOP>GFP (VK00005).

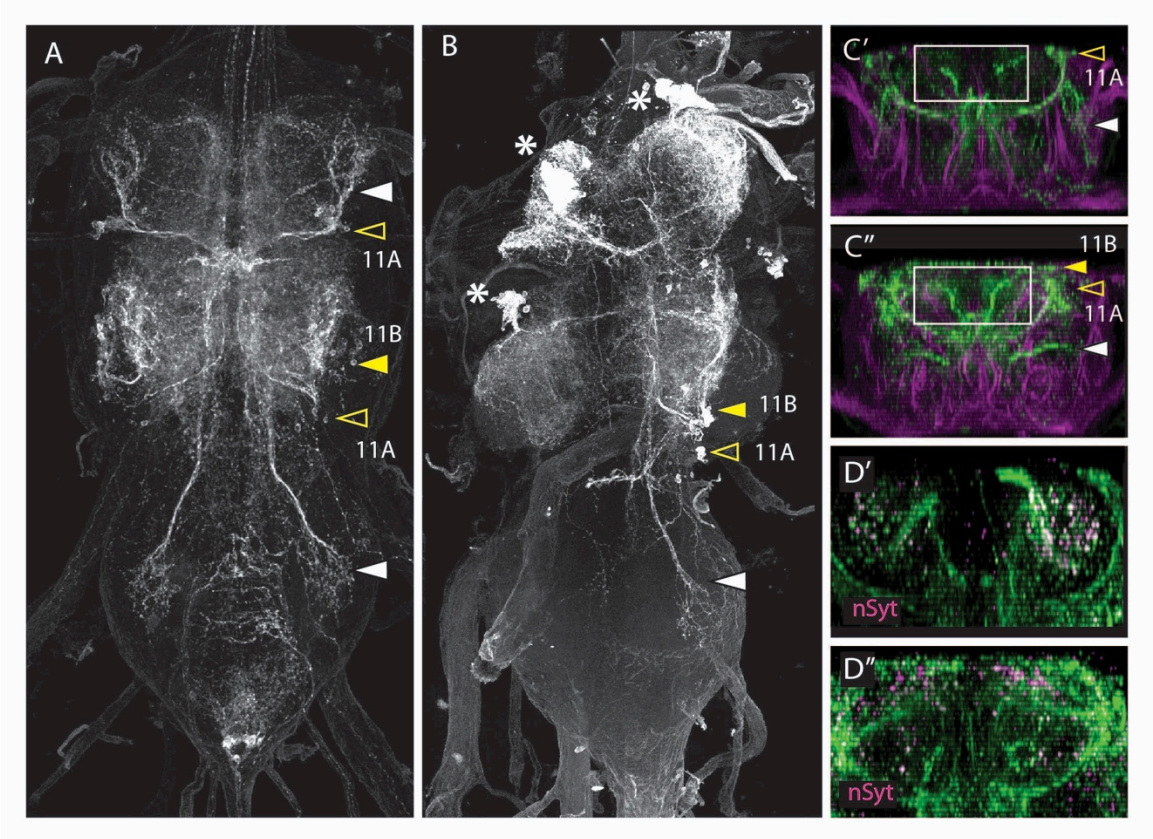

Figure 3.12. The adult anatomy of lineage 11. Yellow arrowheads indicate cell body clusters. (A) z-projection of the ventral CNS showing the lineage 11 clusters in T1 and T2. 11A is present in T1 and T2 (open arrowheads); 11B is only present in T2 (filled arrowhead). White arrowheads: ventral projections, as indicated in (C). (B) z-projection of the ventral CNS showing a T2 MARCM clone of lineage 11. Open arrowhead, 11A cell body cluster; filled arrowhead, 11B cell body cluster. *: Unrelated clones in other hemisegments. (C) Transverse sections of lineage 11 in T1 (C') and T2 (C''). White arrowheads, ventral projections. (D) Transverse sections of the regions boxed in (C), showing presynaptic sites labeled with nSyt-GFP (magenta). Genotypes: (A,C,E) nSyb-GAL80 (su(Hw)attP8)/w; UAS-flp (attP40)/+; R26B05-GAL4 (attP2)/nSyb-LexA (attP2), LexAop>STOP>GFP (VK00005). (B,F) tsMARCM clones (see Materials and Methods). (D,G) nSyb-GAL80 (su(Hw)attP8)/LexAop-RFP (su(Hw)attP8); UAS-flp (attP40)/act>STOP>LexA (attP40); R46C11-GAL4 (attP2)/LexAop-nSyt-GFP (su(Hw)attP1).

Figure 3.13. The adult anatomy of lineage 12. Yellow arrowheads indicate cell body clusters. (A-C) Hemilineage 12A. (A) z-projection of the adult ventral CNS showing the hemilineage 12A clusters in T1 and T2. *: Descending tracts from the subesophageal 12A hemilineages. (B) Transverse sections of hemilineage 12A in T1 (B') and T2 (B''). (C) Transverse sections of the 12A arbor, as indicated in boxes in (B), demonstrating that nSyt-GFP (magenta) localizes to the dorsal part of the 12A arbor in T1 (C') and T2 (C''). (D-G) Hemilineage 12B. (D) z-projection of ventral CNS showing hemilineage 12B clusters in T1 through T3. (E) Transverse section of hemilineage 12B in T1 showing the major projection into the contralateral leg neuropil. *: Dorsal arbor from unrelated neurons. (F,G) MARCM clone of lineage 12 in T3. In this segment the 12A cells die and only the hemilineage 12B cells are present. A major contralateral arbor (c) and a weak ipsilateral arbor (i) are present. (F) Transverse section of clone . *, glia expression. (G) z-projection of the clone showing extensive arbor in leg neuropil. The midline is indicated with a dashed line. Genotypes: (A,B) act>STOP>GAL4 (attP18)/w; UAS-flp (attP40)/+; R24B02-GeneSwitch (attP2)/pJFRC2-UAS-GFP (attP2). (C) nSyb-GAL80 (su(Hw)attP8)/act>STOP>LexA (attP18); LexAop-RFP (attP40)/UAS-flp (attP40); LexAop-nSyt-GFP (su(Hw)attP1)/R24B02-GAL4 (attP2). (D,E) nSyb-GAL80 (su(Hw)attP8)/w; UAS-flp (attP40)/+; R15D11-GAL4 (attP2)/nSyb-LexA (attP2), LexAop>STOP>GFP (VK00005). (F,G) tsMARCM (see Materials and Methods).

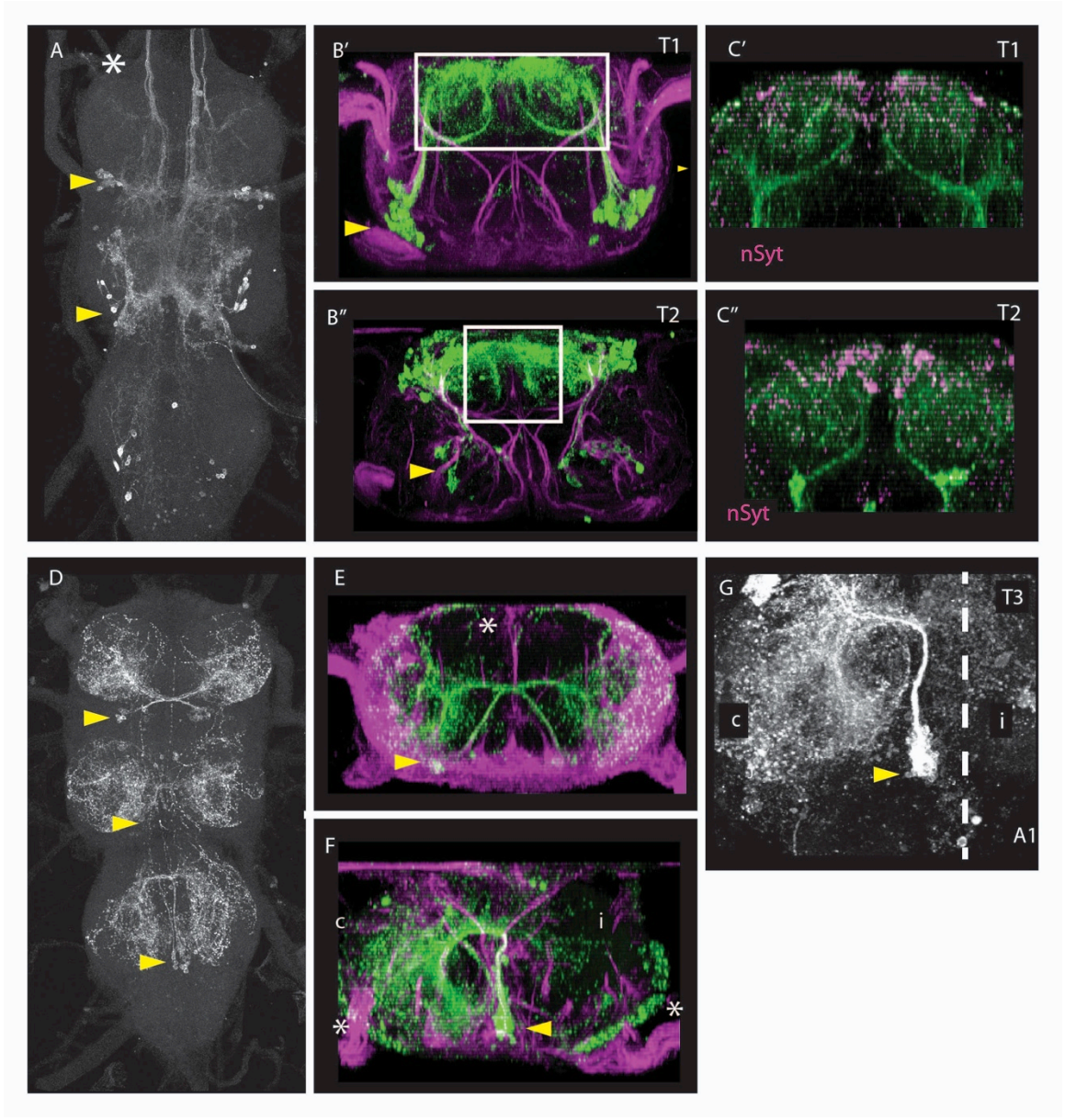
A
B′
T1
C′
T1
nSyt
B″
T2
C″
T2
nSyt
D
E
F
c
i
G
T3
c
i
A1

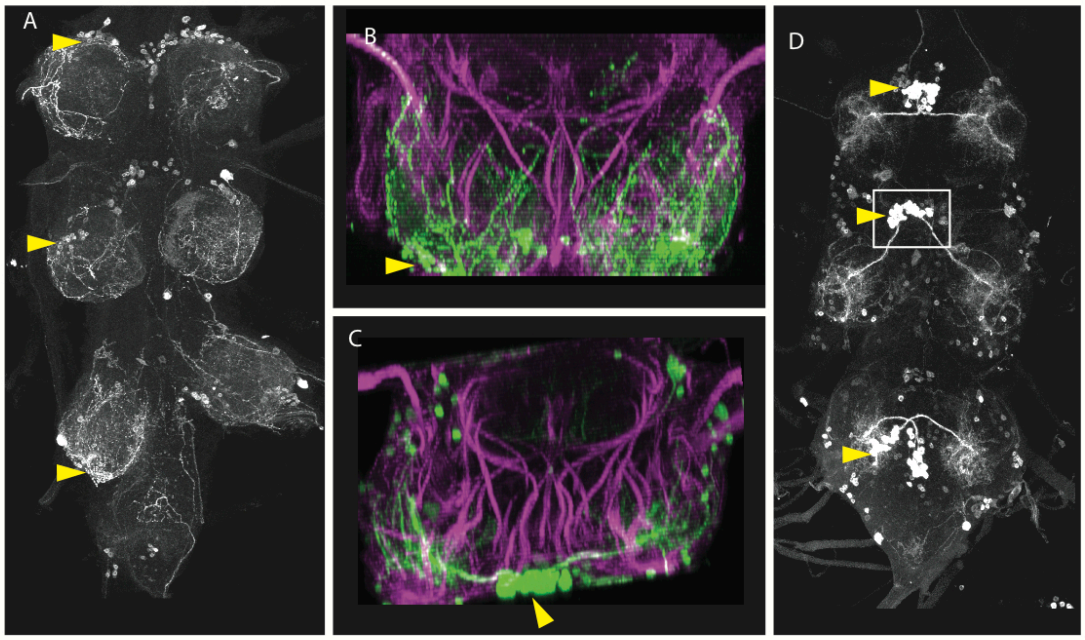

Figure 3.14. The adult anatomy of lineage 13. Yellow arrowheads indicate cell body clusters. (A,B) Hemilineage 13A. (A) z-projection of of the ventral CNS showing the hemilineage 13A clusters in T1 through T3. (B) Transverse section of the T2 neuromere showing the hemilineage 13A cells projecting into ventral leg neuropil. (C,D) Hemilineage 13B. (C) Transverse section of T2 showing the hemilineage 13B cells projecting to the contralateral leg neuropil. (D) z-projection of the ventral CNS showing hemilineage 13B clusters in T1 through T3. In T2 the cell clusters have been pulled across the midline, so they appear to project ipsilaterally (box). Genotypes: (A,B) act>STOP>GAL4 (attP18)/w; UAS-flp (attP40)/+; R81C12-GeneSwitch/pJFRC2-UAS-GFP. (C,D) w; +; R41G09-GAL4/pJFRC2-UAS-GFP.

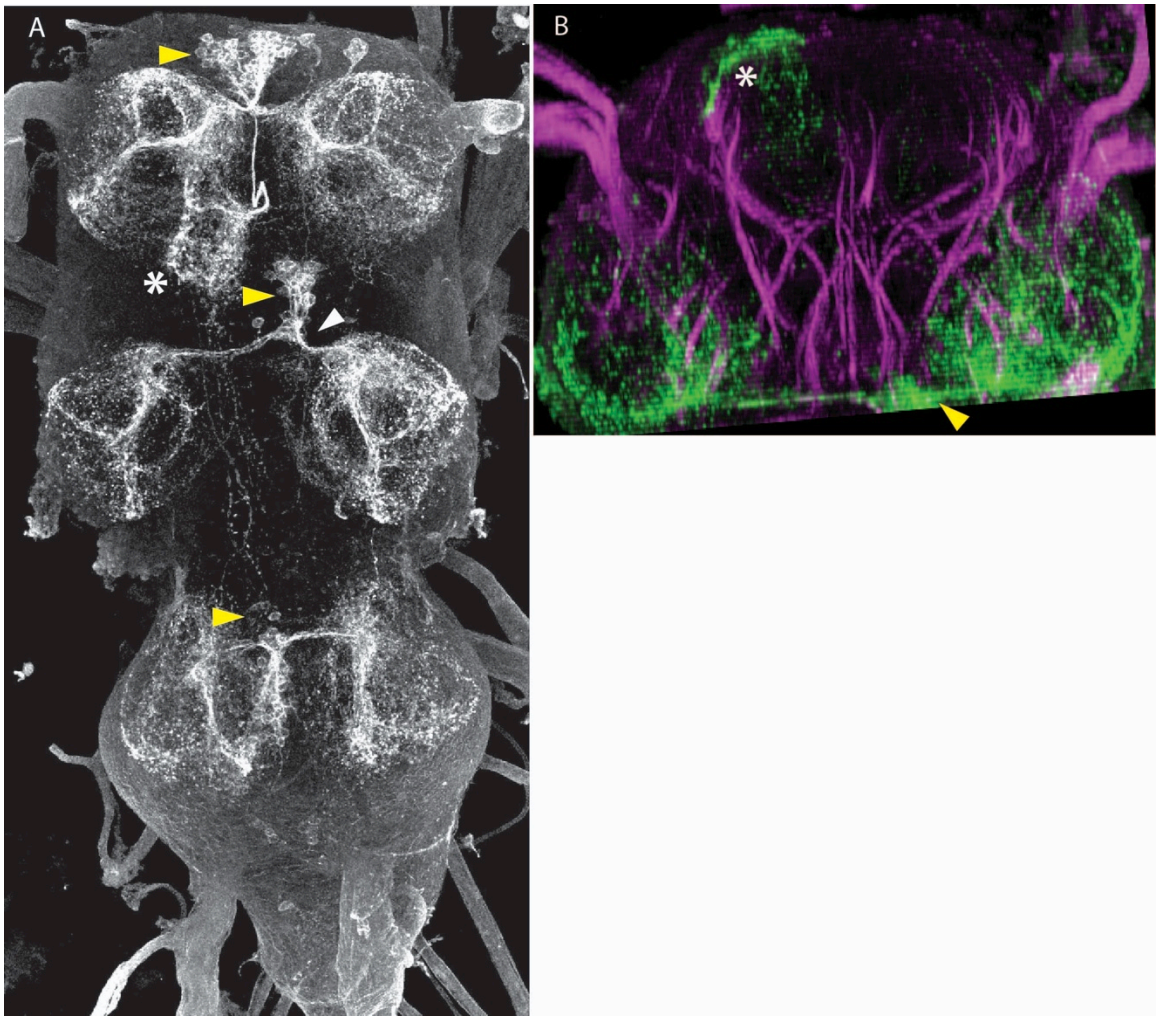

Figure 3.15. The adult anatomy of lineage 14. Yellow arrowheads indicate cell body clusters. Hemilineage 14B undergoes programmed cell death. (A) z-projection of the ventral CNS showing hemilineage 14A clusters in T1 through T3. *: unrelated cell cluster. In T2, one of the cell body clusters has been pulled across the midline, and appears to project ipsilaterally (white arrowhead). (B) Transverse section of the T2 neuromere showing hemilineage 14A projecting into ventral leg neuropil. *: arbor from unrelated neurons. Genotype: nSyb-GAL80 (su(Hw)attP8)/w; act>STOP>Lex (attP40), LexAop-GFP (su(Hw)attP5)/+; R80G10-GAL4 (attP2)/UAS-hPR-flp (VK00005).

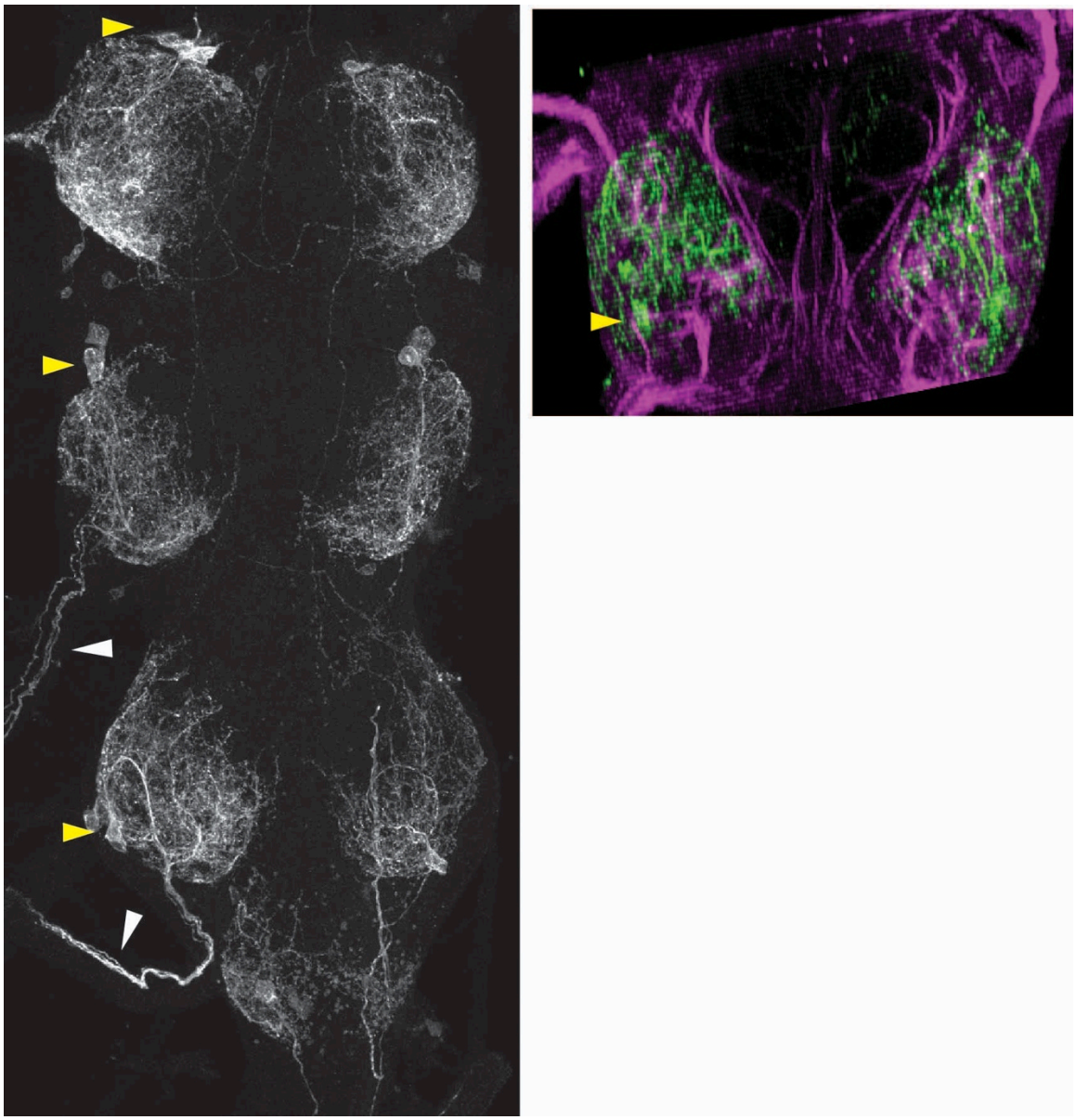

Figure 3.16. The adult anatomy of lineage 15. Yellow arrowheads indicate cell body clusters. Hemilineage 15A undergoes programmed cell death. (A) z-projection of the ventral CNS showing the hemilineage 15B clusters in T1 through T3. The cells arborize primarily through dorsal leg neuropil and their axons exit through the leg nerve (white arrowheads). (B) Transverse section of segment T2 showing the dendritic arbor of hemilineage 15B. Genotype: nSyb-GAL80 (su(Hw)attP8)/w; act>STOP>Lex (attP40), LexAop-GFP (su(Hw)attP5)/+; R19H09-GAL4 (attP2)/UAS-hPR-flp (VK00005).

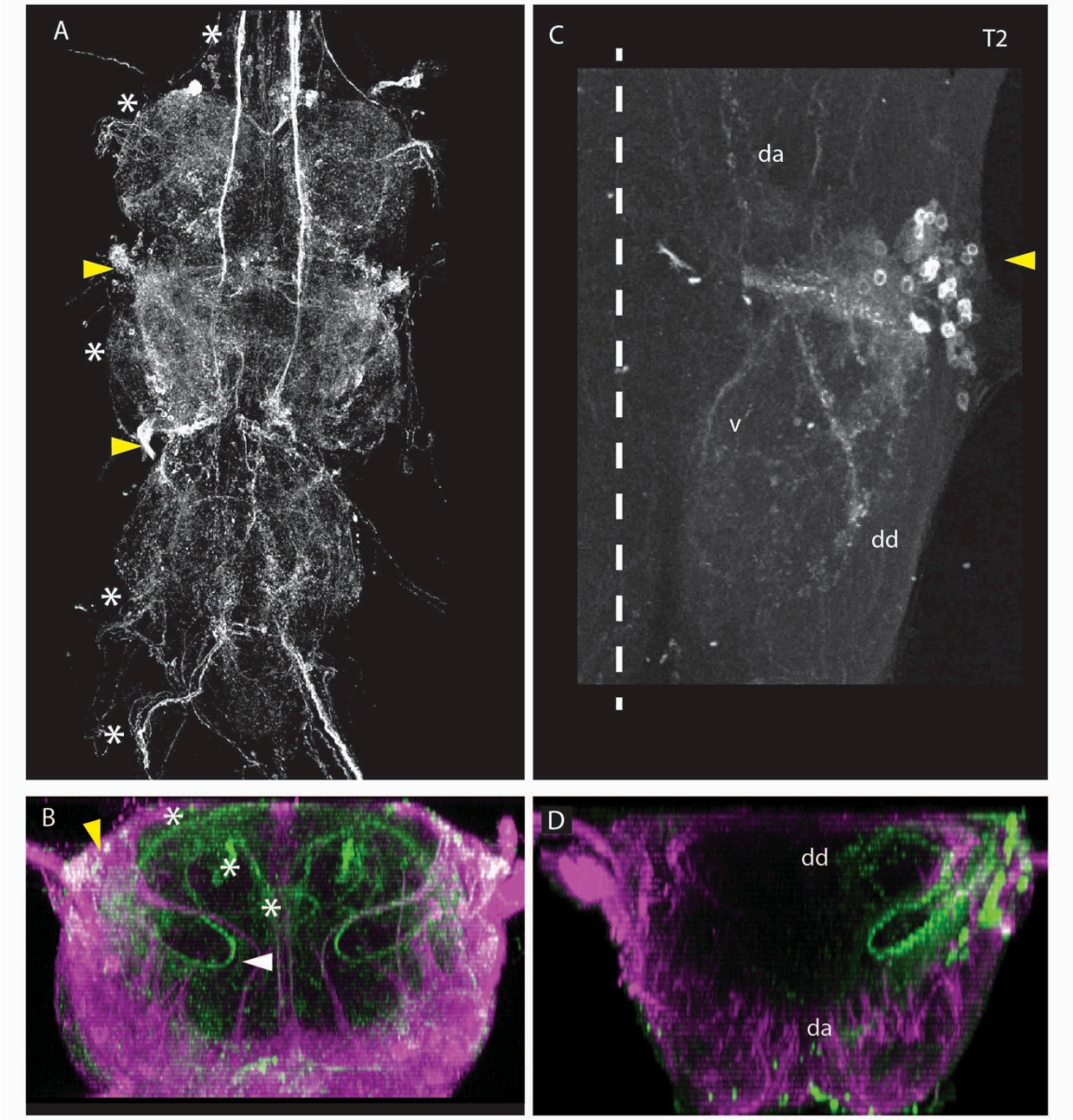

Figure 3.17. The adult anatomy of lineage 17. Yellow arrowheads indicate cell body clusters. Hemilineage 17B undergoes programmed cell death. (A) z-projection of the ventral CNS showing hemilineage 17A clusters in T2 and T3. Multiple other lineages are also visible. (B) Transverse section of T2 showing hemilineage 17A with the distinctive dorsoventral loop formed by the 17A neuroglian tract (white arrowhead). *: projections from unrelated neurons. (C-D) MARCM clone of lineage 17 in segment T2. (C) z-projection of clone showing the dorsal ascending (da) and descending (dd) projections and the ventral (v) projection. (D) Transverse section of clone showing dorsal (d) and ventral (v) arbors. Genotypes: (A,B) nSyb-GAL80 (su(Hw)attP8)/w; UAS-flp (attP40)/+; R78A08-GAL4 (attP2)/nSyb-LexA (attP2), LexAop>STOP>GFP (VK00005). (C,D) tsMARCM clones (see Materials and Methods).

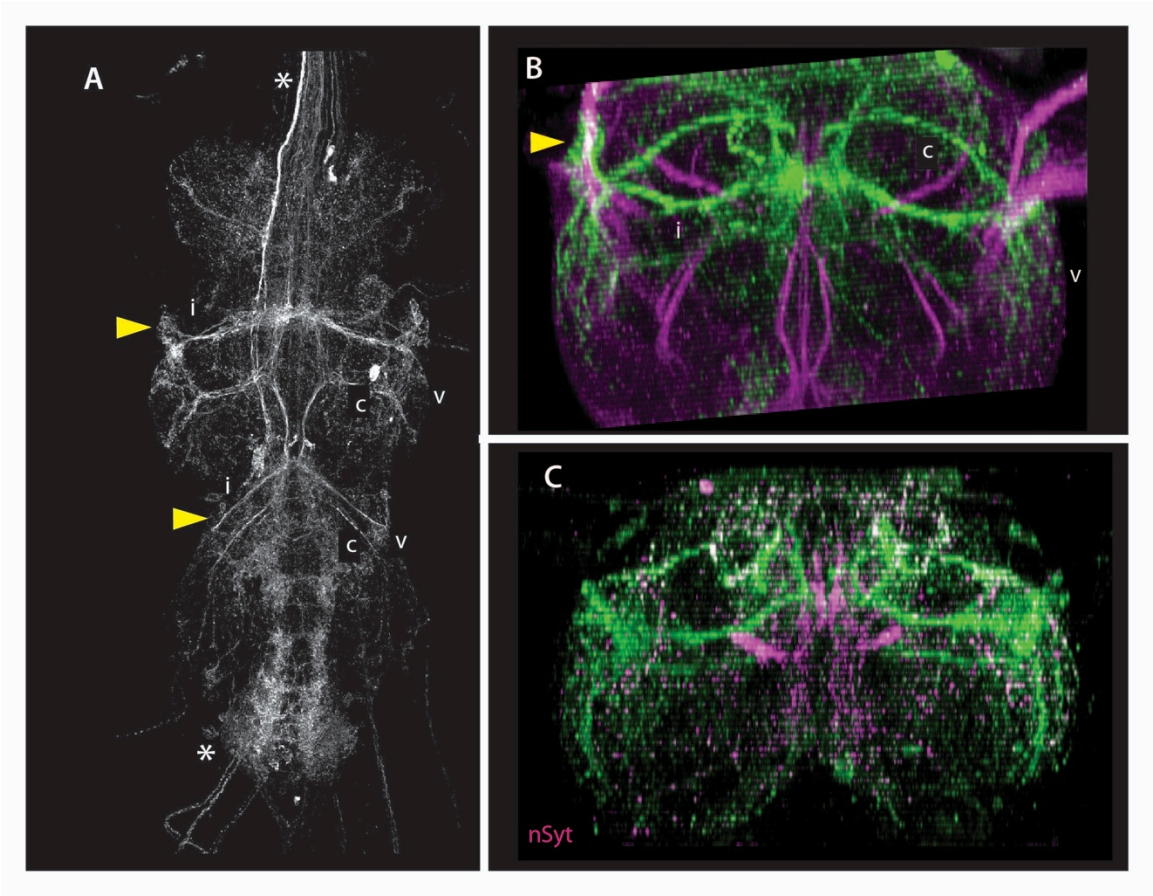

Figure 3.18. The adult anatomy of lineage 18. Yellow arrowheads indicate cell bodies. Hemilineage 18A undergoes programmed cell death. (A) z-projection of ventral CNS showing the hemilineage 18B clusters in T2 and T3. Projections and arborizations are labeled as follows: Anterior, ipsilateral dorsal projection: i. Posterior, presumed contralateral dorsal projection: c. Ventral arbor, v. *: unrelated expression in a descending bundle (top) and in the abdominal ganglia (bottom). (B) Transverse section of T2 showing hemilineage 18B with its associated projections. Labels are as in (A). (C) Transverse section showing that nSyt-GFP (magenta) localizes to the dorsomedial parts of the hemilineage 18B arbor. Genotypes: (A,B) nSyb-GAL80 (su(Hw)attP8)/w; UAS-flp (attP40)/+; R27A09-GAL4 (attP2)/nSyb-LexA (attP2), LexAop>STOP>GFP (VK00005). (C) act>STOP>LexA(attP18)/nSyb-GAL80 (su(Hw)attP8); LexAop-RFP (attP40)/UAS-flp (attP40); LexAop-nSyt-GFP (su(Hw)attP1)/R27A09-GAL4 (attP2).

Figure 3.19. The adult anatomy of lineage 19. Yellow arrowheads indicate cell body clusters. (A-D) Hemilineage 19A. (A) z-projection of the ventral CNS showing the hemilineage 19A clusters in T1 through T3. Boxed region is shown in C and D. (B) Transverse section of T2 showing the 19A neurons and their projection into ventral and medial regions of the leg neuropil. (C) Closeup of an optical slice (20μm) from the middle of the VNS, showing that the arbors of 19A (green) overlap with afferents from leg chordotonal neurons (magenta). (D) Closeup of an optical slice from the middle of the VNS, showing that nSyt-GFP (magenta) localizes to the medial parts of the 19A arbor. (E-G) A lineage 19 MARCM clone in T2. (E) z-projection of the clone showing the cell body clusters for the 19A and 19B hemilineages. (F) Transverse section of clone showing the ipsilateral ventral projections from 19A (v) and the bilaterally symmetric major (maj) and minor (min) bundles from the 19B hemilineage. (G) Dorsal view of thick slices from the clone. (G') Slice near the middle of the VNS, showing the 19A arbor. Note that it stays ipsilateral. (G'') Slice from the dorsal third of the VNS, showing the asymmetric lateral projection of 19B (lat) and the major (maj) and minor (min) symmetric medial projections. (H-J) Hemilineage 19B. (H) z-projection of VNS showing hemilineage 19B clusters in T2 and T3. *, ascending sensory neurons. (I) Transverse section of T2 showing hemilineage 19B with its arbor confined to the dorsocentral neuropil. *, ascending sensory neurons. (J) Optical slice from the dorsal third of the VNS, showing that nSyt-GFP (magenta) localizes primarily to the major ascending projections. Genotypes: (A,B) w; +; R32E04-GAL4 (attP2)/pJfRC2-UAS-GFP (attP2). (C) LexAop-GFP (su(Hw)attP8), UAS-RFP (attP18)/w; R54E06-LexA (attP40)/+; R77C10-GAL4 (attP2)/+. (D) UAS-nSyt-GFP (attP18)/w; UAS-RFP (attP40)/+; R32E04-GAL4 (attP2). (E-G) tsMARCM clone (see Materials and Methods). (H,I) nSyb-GAL80 (su(Hw)attP8)/w; UAS-flp (attP40)/+; R84E06-GAL4 (attP2)/nSyb-LexA (attP2), LexAop>STOP>GFP (VK00005). (J) act>STOP>LexA(attP18)/nSyb-GAL80 (su(Hw)attP8); LexAop-RFP (attP40)/UAS-flp (attP40); LexAop-nSyt-GFP (su(Hw)attP1)/R84E06-GAL4 (attP2).

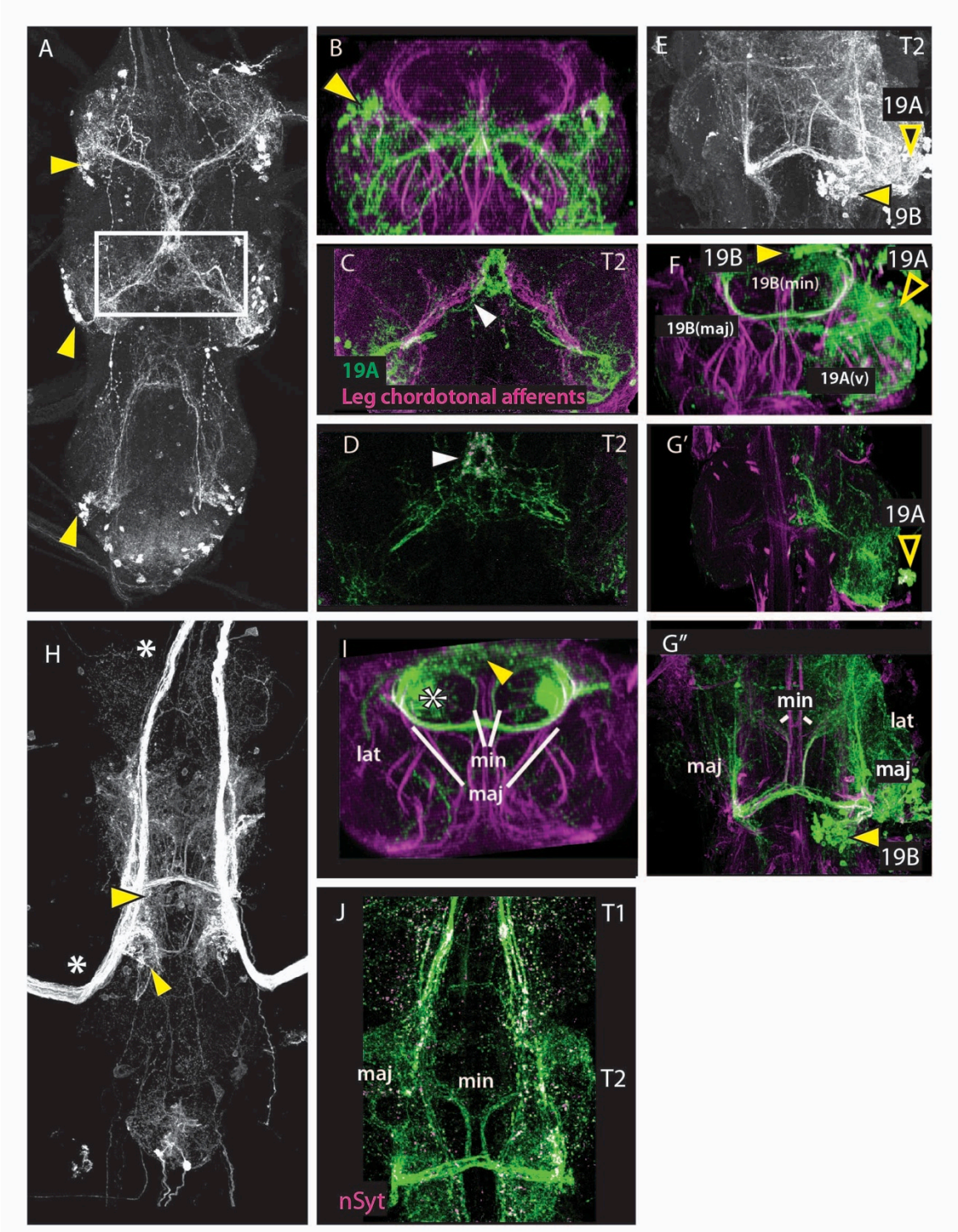
A
B
C
T2
19A
Leg chordotonal afferents
D
T2
E
T2
19A
19B
F
19B
19A
19B(min)
19B(maj)
19A(v)
G′
19A
G″
min
lat
maj
maj
19B
H
I
lat
min
maj
J
T1
maj
min
T2
nSyt

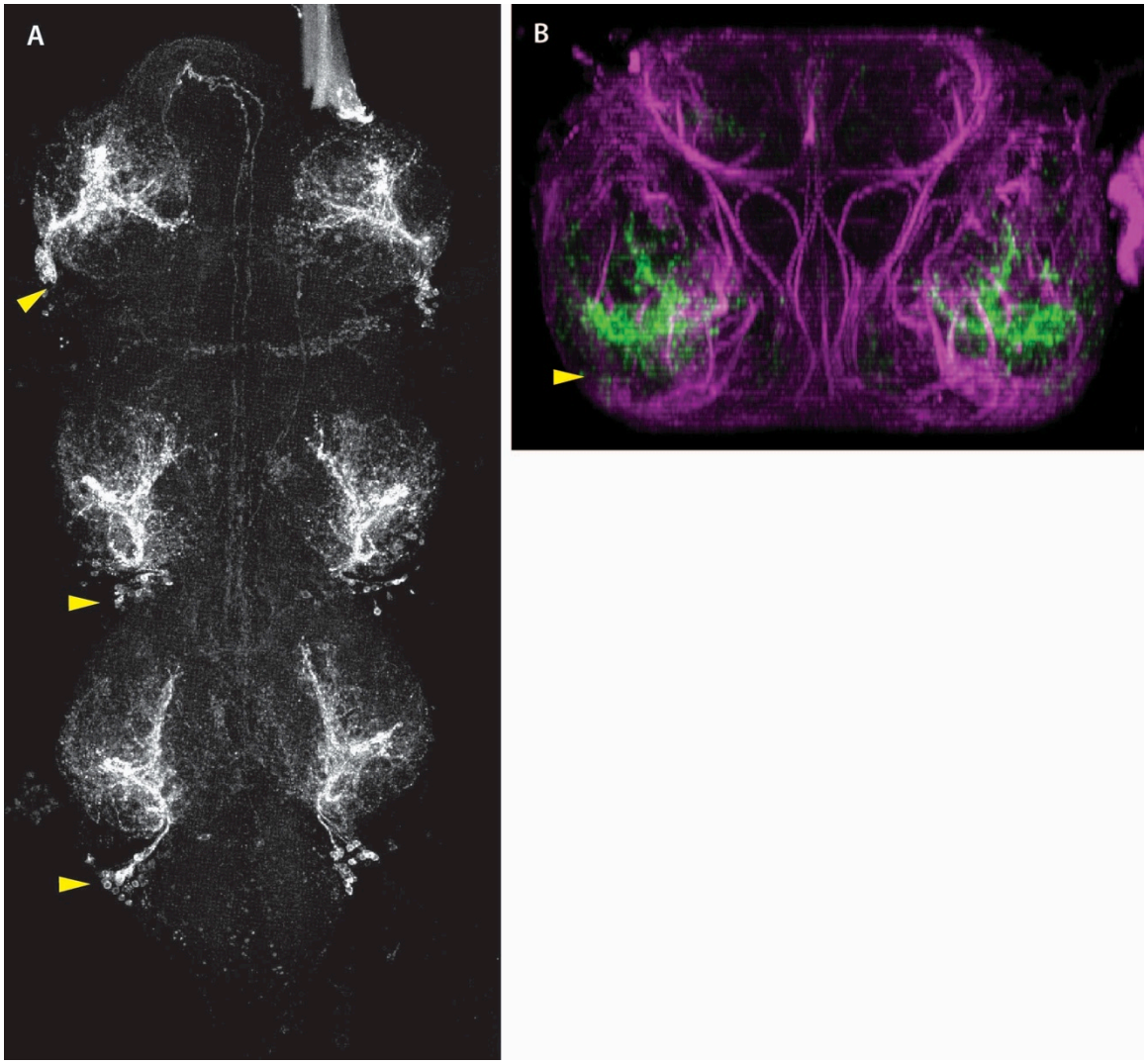

Figure 3.20. The adult anatomy of lineage 20/22. Yellow arrowheads indicate cell body clusters. Hemilineage 20B/22B undergoes programmed cell death. (A) z-projection of ventral CNS showing hemilineage 20A/22A clusters in T1 through T3. (B) Transverse section of hemilineage 20A/22A showing arbor on the midregions of the leg neuropil. Genotype: w; +; R19H10-GAL4 (attP2)/pJFRC2-UAS-GFP (attP2).

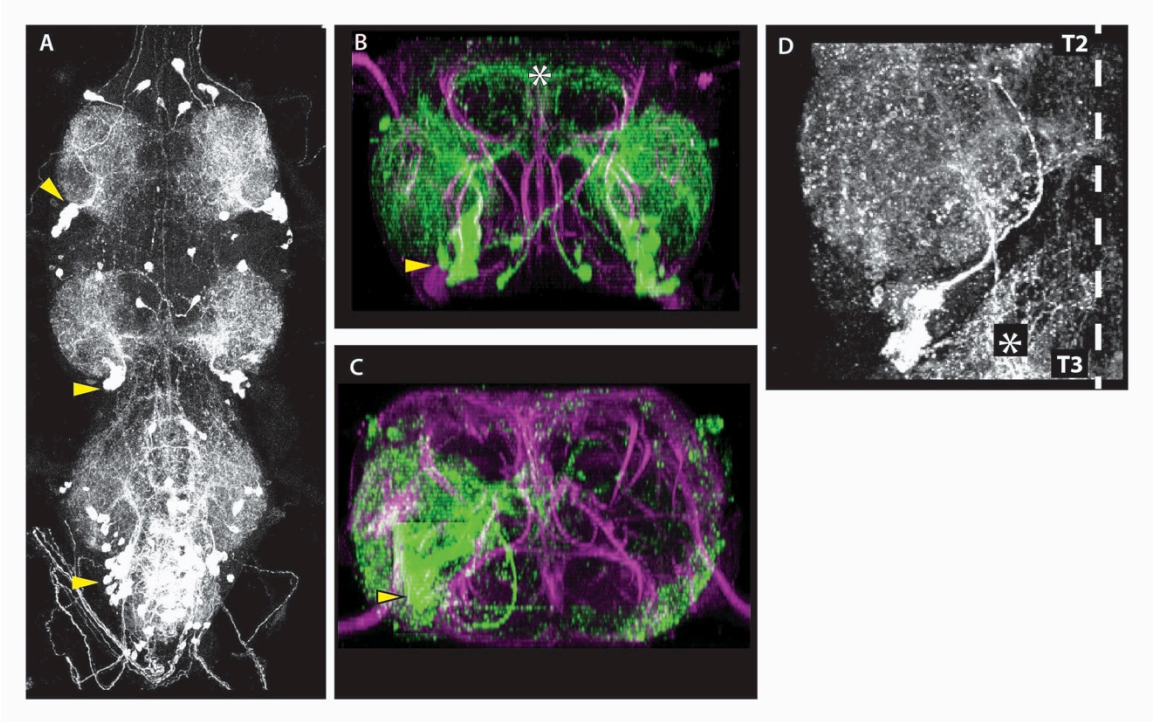

Figure 3.21. The adult anatomy of lineage 21. Yellow arrowheads indicate cell body clusters. Hemilineage 21B undergoes programmed cell death. (A) z-projection of the adult VNS showing hemilineage 21B clusters in T1 through T3. A few neurons not related to the lineage are evident in the thorax, and many are present in the abdomen. (B) Transverse section T2 showing hemilineage 21B and their projection into dorsolateral leg neuropil. *: dorsal arbor from unrelated cells. (C-D) MARCM clone of hemilineage 21B from T2. (C) Transverse view of clone. (D) z-projection of clone showing that the initial processes project medially and then curve anterolaterally, to spread over the ipsilateral neuropil. *: arbor from an unrelated clone in T3. Dotted line, midline. Genotypes: (A,B) nSyb-GAL80 (su(Hw)attP8)/w; act>STOP>Lex (attP40), LexAop-GFP (su(Hw)attP5)/+; R51H05-GAL4 (attP2)/UAS-hPR-flp (VK00005). (C,D) tsMARCM (see Materials and Methods).

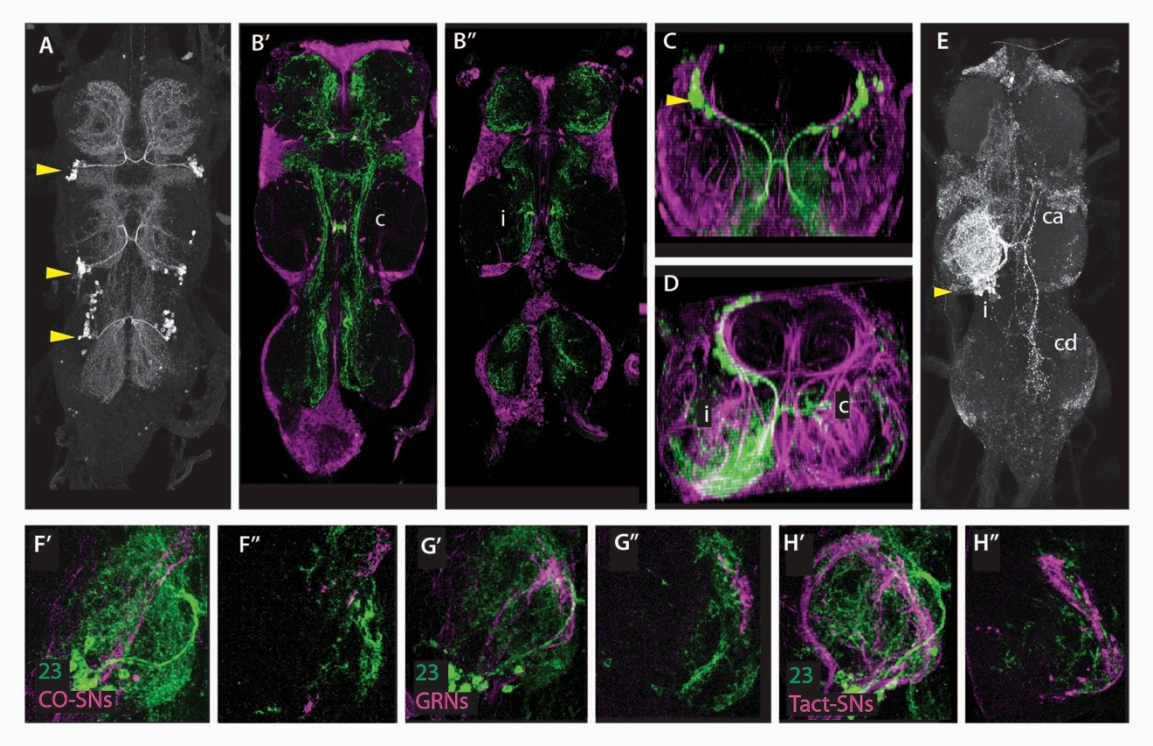

Figure 3.22. The adult anatomy of lineage 23. Yellow arrowheads indicate cell body clusters. Hemilineage 23A undergoes programmed cell death. (A) z-projection of the adult VNS showing the hemilineage 23B clusters in T1 through T3. (B) Thick sections showing different parts of the hemilineage 23B arbor. (B') Section from the middle of the VNS, showing the dorsal, intersegmental part of the arbor. (B'') Section from the ventral third of the VNS, showing the ventral arbors in the medial leg neuropil. (C) Transverse projection of T2 showing the hemilineage 23B clusters projecting across the midline and with ipsilateral (i) and contralateral (c) arbors. (D,E) MARCM clone of lineage 23 in T2. (D) transverse view showing that the ventral arbor is ipsilateral (i) while the intersegmental arbor is contralateral (c). (E) z-projection of the clone showing that the contralateral arbor projects to both T1 (ascending, ca) and T3 (descending, cd). (F-H) Hemilineage 23B appears to overlap multiple classes of leg sensory neuron. Left panels, z-projection of hemilineage 23B in T2 (green) overlapping the sensory projection (magenta); right panels, single optical slice showing arbor proximity. (F) Hemilineage 23B and leg chordotonal afferents (CO-SNs). (G) Hemilineage 23B and gustatory receptor neurons (GRNs). (H) Hemilineage 23B and leg tactile bristle afferents (Tact-SNs). Genotypes: (A-C) w; +; R77C10-GAL4 (attP2)/pJFRC2-UAS-GFP. (D, E) tsMARCM (see Materials and Methods). (F) LexAop-GFP (su(Hw)attP8), UAS-RFP (attP18)/w; R54E06-LexA (attP40)/+; R77C10-GAL4 (attP2)/+. (G) LexAop-GFP (su(Hw)attP8), UAS-RFP (attP18)/w; R13F12-LexA (attP40)/+; R77C10-GAL4 (attP2)/+. (H) LexAop-GFP (su(Hw)attP8), UAS-RFP (attP18)/w; R49C06-LexA (attP40)/+; R77C10-GAL4 (attP2)/+.

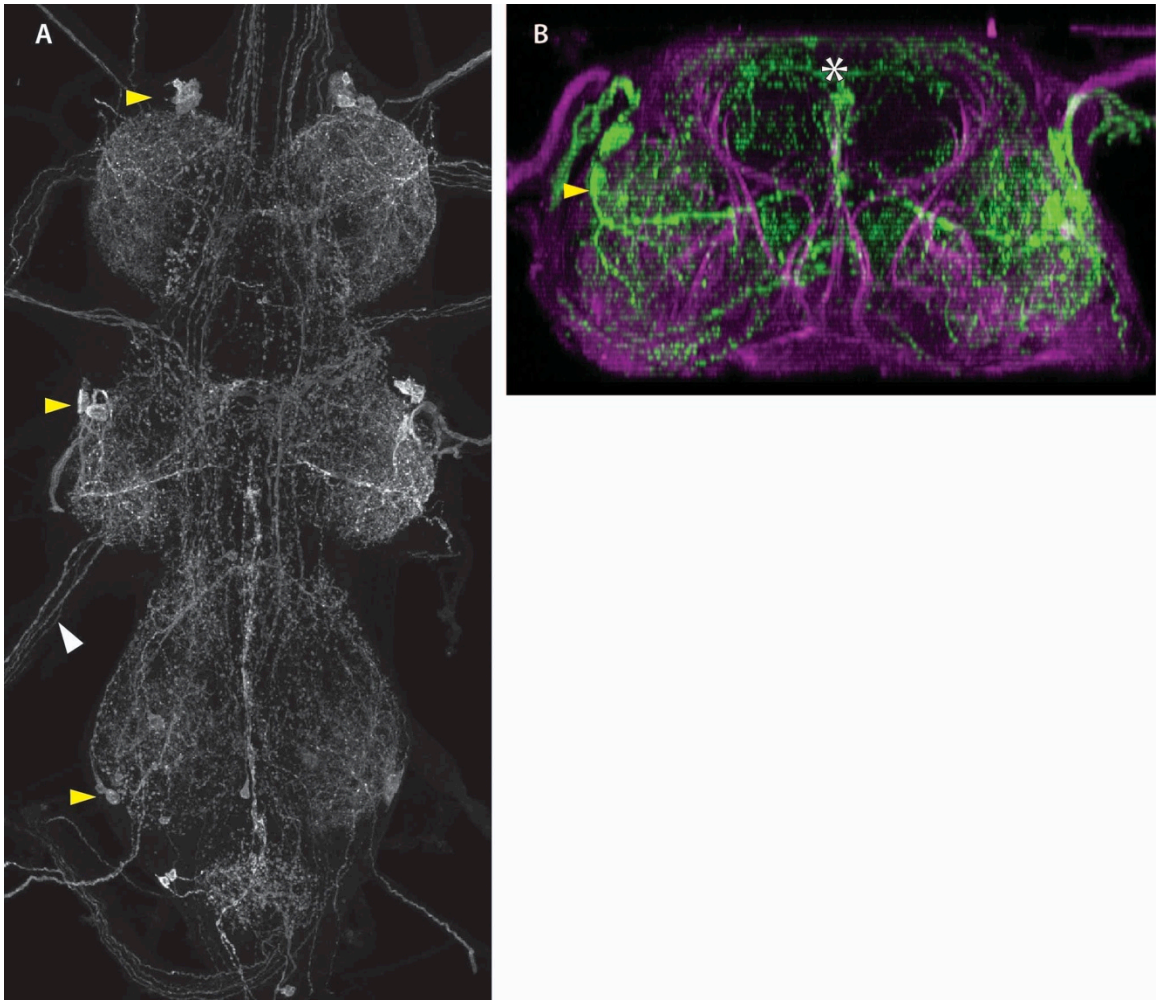

Figure 3.23. The adult anatomy of lineage 24. Yellow arrowheads indicate cell body clusters. Hemilineage 24A undergoes programmed cell death. (A) z-projection of ventral CNS showing the hemilineage 24B clusters in T1 through T3. These are motor neurons whose dendrites cover the area of the leg neuropil and whose axons exit in the leg nerve (e.g., white arrowhead). (B) Transverse section T2 showing the hemilineage 24B motor neurons with their dendrites in the intermediate lag neuropil. *, dorsal arbor from unrelated neurons. Genotype: nSyb-GAL80 (su(Hw)attP8)/w; UAS-flp (attP40)/+; R15A03-GAL4 (attP2)/nSyb-LexA (attP2), LexAop>STOP>GFP (VK00005).

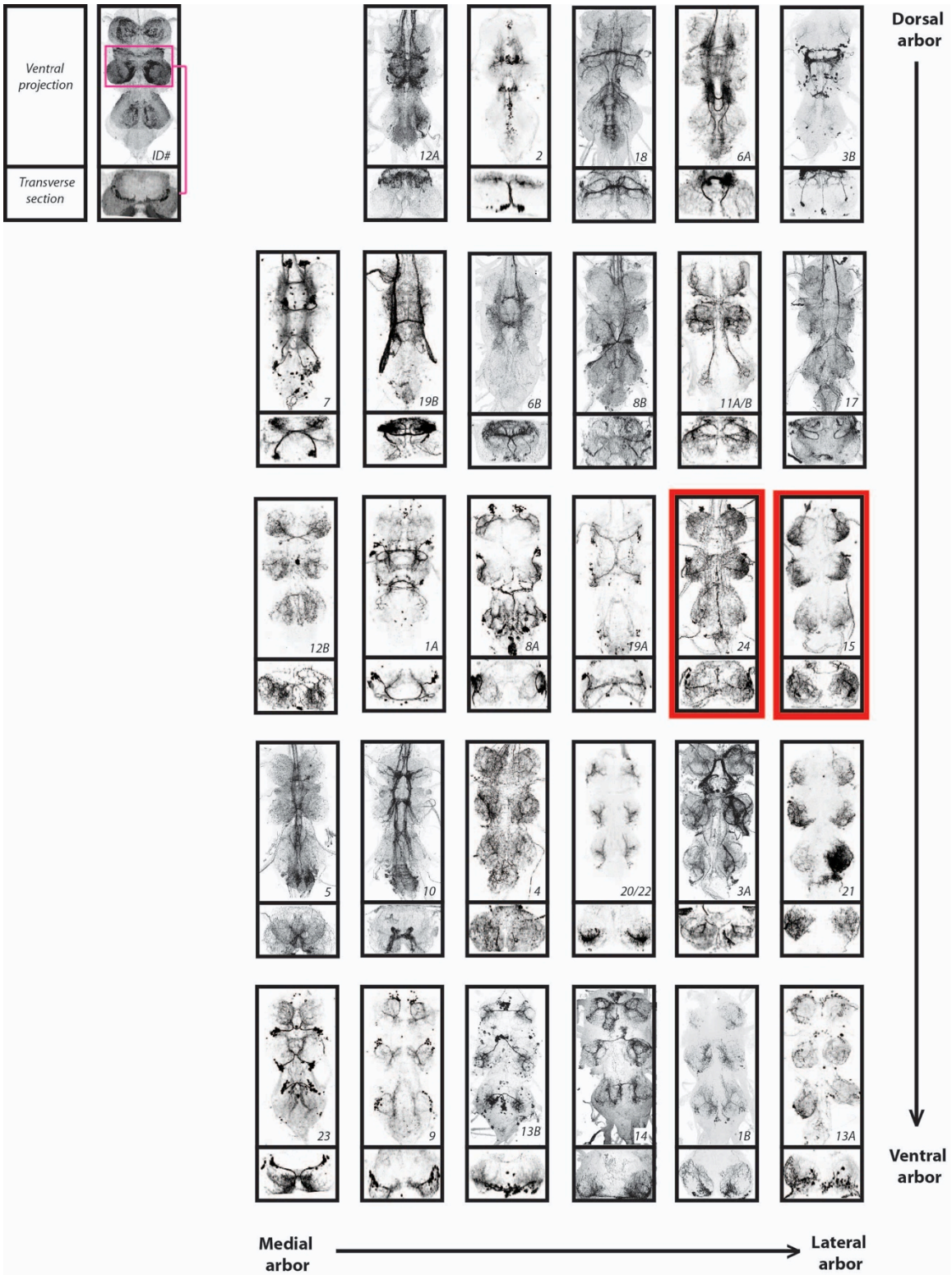

Figure 3.24. Dorsal and transverse views of the adult ventral CNS showing the unique projection pattern for each of the secondary hemilineages. Most hemilineages produce interneurons, except for 15B and 24B (red boxes), which are motor lineages Hemilineages 0A and 16B are not represented.

Figure 3.25. GABA-immunoreactive clusters correspond to eight lineages in Drosophila. (A,B) Witten and Truman (1998) show the GABAergic clusters found in *Calliphora*. (A) anti-GABA staining in the *Calliphora* VNS. Arrowheads, division between T1 and T2. Arrows, the lateral and medial portions of the K cluster. (B) Camera lucida drawing of (A). On the left side, cluster groups are outlined; on the right, the white somata are ventral, and the black ones dorsal. (C) anti-GABA staining in the Drosophila VNS. A similar pattern of GABA clusters can be identified. Red box, T2, shown in (D). (D) GABA-immunoreactive clusters in the Drosophila VNS are produced by eight lineages. Clockwise from top left: Cluster "E" is produced by lineage 9; cluster "K" is produced by lineage 13 (K_L 13A; K_M, 13B); cluster "M" is produced by lineage 5B and/or 6B; cluster "X" is produced by lineage 0A; cluster "N" is produced by lineage 12B; a previously uncharacterized cluster is produced by lineage 11B; cluster "T" is produced by lineage 19A. Center, z-projection of GABA staining in T2; surround, optical slices of GFP expression and anti-GABA staining in lines driving expression in the corresponding lineages. Green, anti-GFP; magenta, anti-GABA. Arrowheads, colocalization of GFP and GABA.

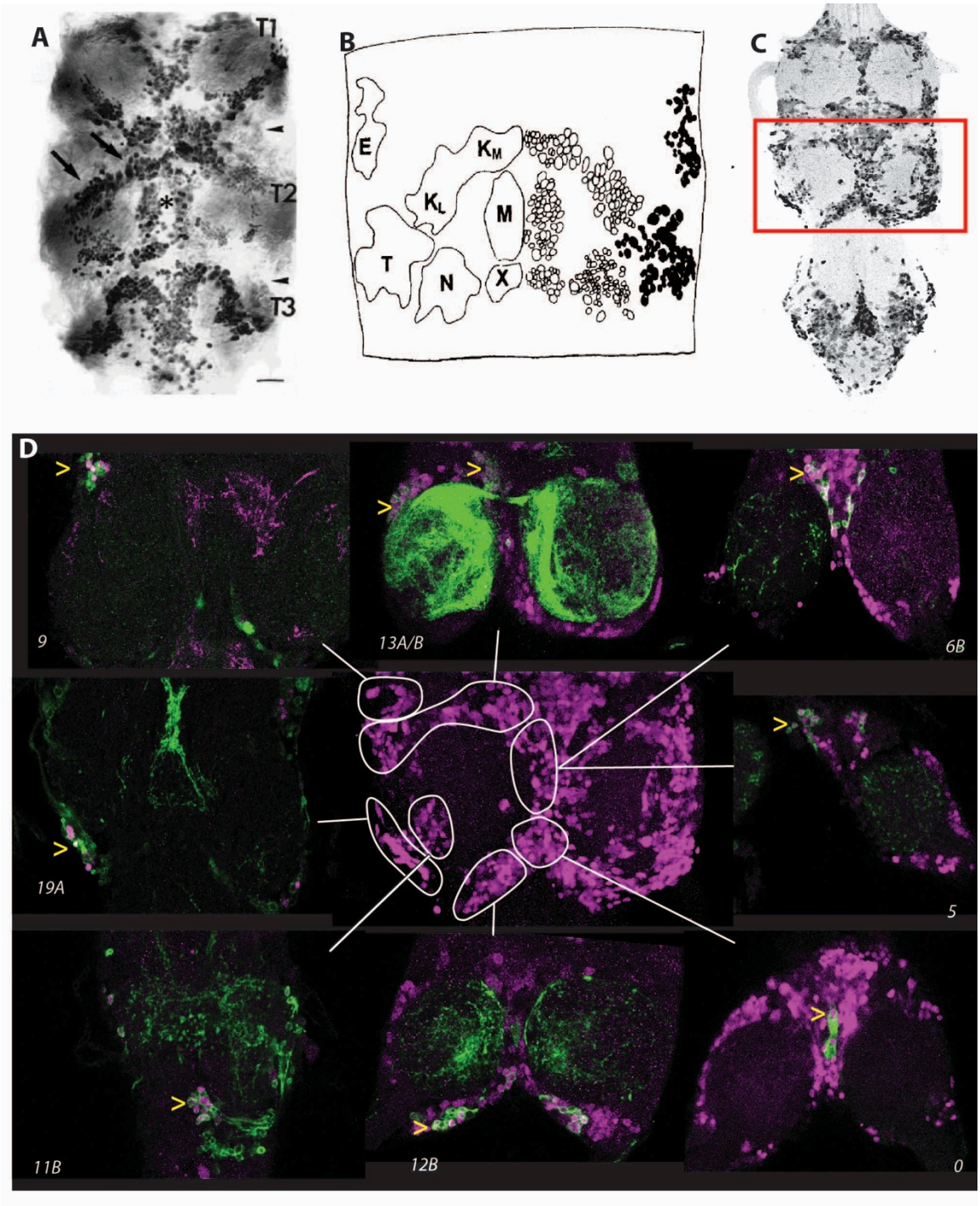
A
T1
T2
T3
B
E
K_M
K_L
M
T
N
X
C
D
9
13A/B
6B
19A
5
11B
12B
0

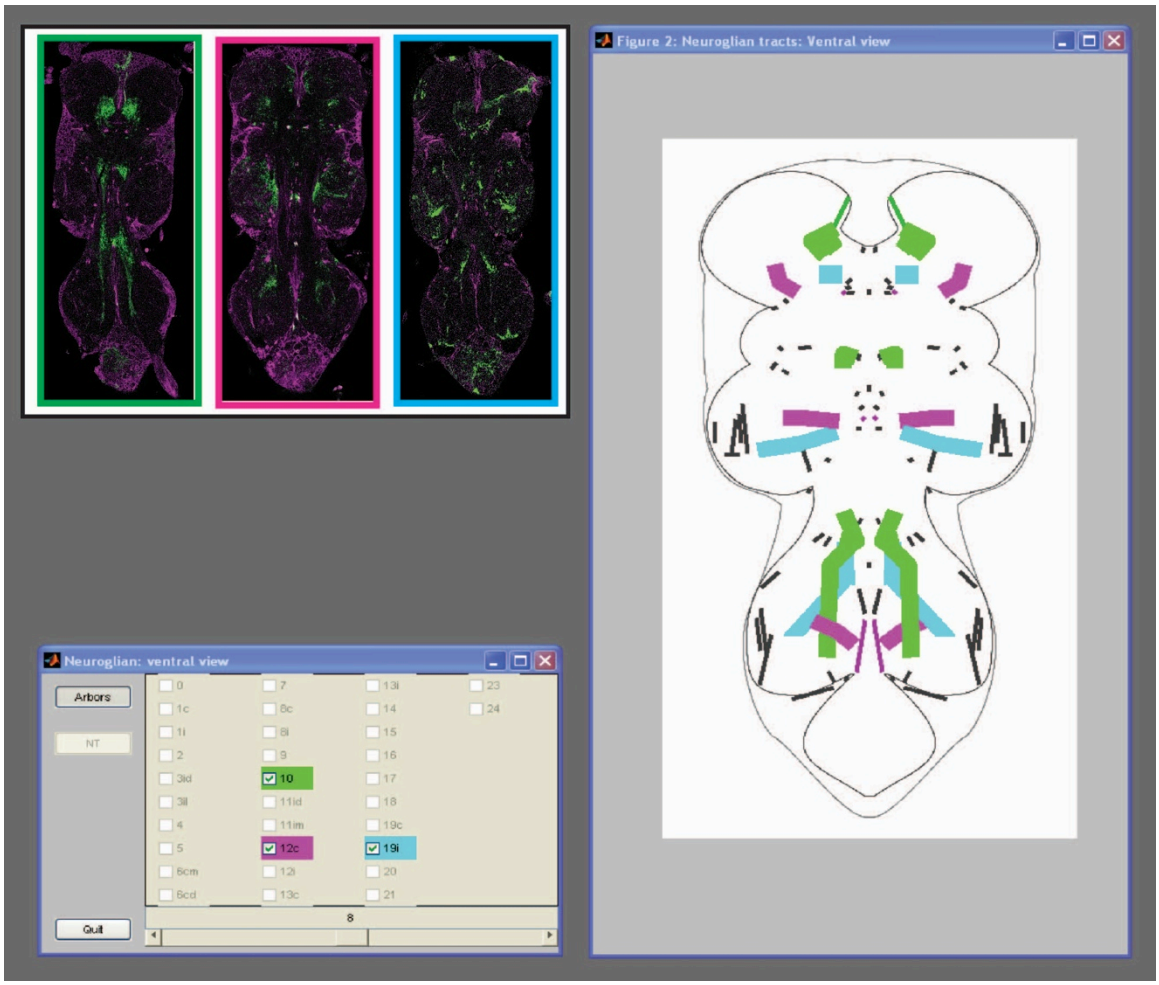

Figure 3.26. A MATLAB graphical user interface (GUI) for visualizing the overlap of up to three lineages in a given optical slice. An example showing overlap in the arbors of the three hemilineages selected in the control panel (left) in an optical slice from the middle of the VNS (right). Inset, optical slices showing the arbors of those lineages at the selected level.

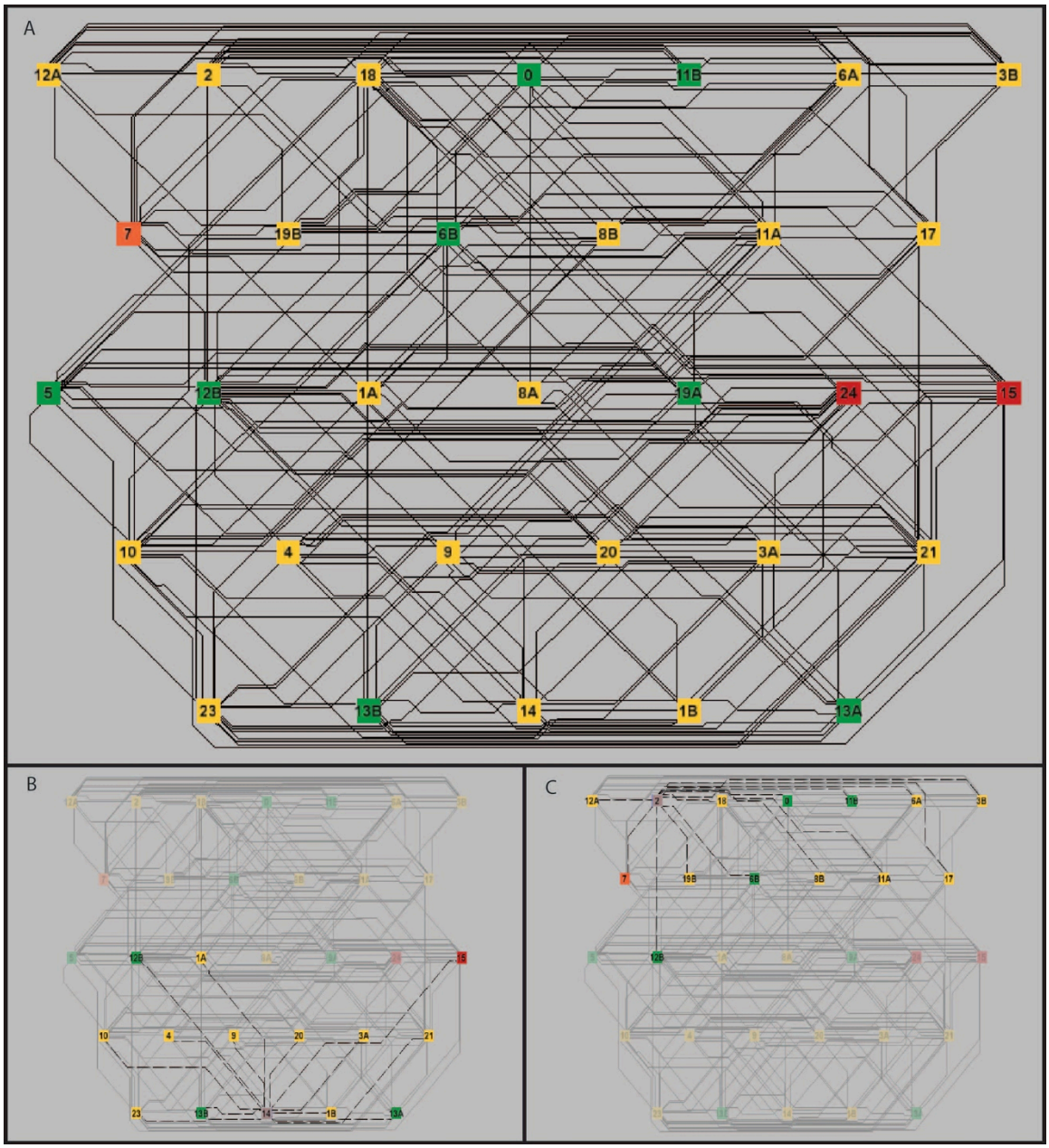

Figure 3.27. Projection overlap between the secondary lineages of the thoracic VNS. (A) Map of putative connectivity based on arbor overlap, made in Neuroptikon. (B,C) Screenshots visualizing the putative potential partners of lineage 14A (B) and lineage 2A (C) using Neuroptikon. Selected lineage is highlighted in blue. Red: motor neurons. Green: GABAergic interneurons. Yellow: Unidentified neurotransmitter, presumed excitatory.

Chapter 4

ACTIVATION SCREEN OF THE SECONDARY HEMILINEAGES

Summary

Unlike the embryonic-born primary neurons, secondary neurons within a hemilineage are relatively homogeneous, all projecting within a limited volume of the thoracic neuropil and therefore positioned to synapse with a limited number of other hemilineages. This suggests that these neurons might share functional properties. To test this hypothesis, I used the transgenic lines described in Chapter 2 to drive the temperature-dependent neural activator TRPA1 in each hemilineage, then analyzed the behavioral phenotypes resulting from hemilineage activation in decapitated flies. In most cases, hemilineage activation results in a repeatable, characteristic behavioral phenotype. Hemilineages that arborize in the ventral two-thirds of the VNS produce leg postural defects, whereas hemilineages that arborize in the dorsal third tend to produce unique, dynamic phenotypes such as walking and/or wing movements.

Introduction

One of the major obstacles to understanding how neurons produce behaviors is the overwhelming number of components (neurons and synapses) comprising even the simplest nervous systems. For example, *C. elegans* has only 302 neurons, but contains some 5000 chemical synapses (White et al. 1986). Thus, it is not simply the number of neurons involved, but the complexity of their interactions, that makes it difficult to model the circuits of a nervous system.

The *Drosophila* ventral nervous system (VNS) contains on the order of ten to fifteen thousand neurons and is capable of producing a variety of complex behaviors. In the absence of the brain, a decapitated fly grooms spontaneously and in response to targeted application of dirt (Phillis et al. 1993). If overturned, it will quickly right itself with a series of coordinated leg and wing motions. Treatment with octopamine (OA) causes sustained walking (Yellman et al. 1997), and repeated disturbance can invoke flight. Because decapitated flies can perform these behaviors, we know the VNS contains the circuitry sufficient to implement them. Since ~90% of the neurons in the VNS are secondary neurons that are born during larval growth, my reagents to target the secondary hemilineages (Chapter 2) must cover most of the neurons underlying those circuits.

In Chapter 3, I detailed the adult morphology of 30 of the 32 secondary hemilineages of the *Drosophila* VNS, and showed that based on arbor proximity, each hemilineage seems poised to form synaptic connections with a maximum of 10-20 other hemilineages. While complex, this is a manageable network size. If hemilineages generally correspond to functional neural classes, then the dataset from Chapter 3 provides the first step towards a broad-scale circuit map of the VNS. In that case, one would like to begin to assign functions to the individual components, with the hope of eventually being able to model VNS function.

For the limited number of cases that have been investigated, NB lineages do encompass established neural classes. Two physiologically and anatomically distinctive populations

of interneurons in the locust, the midline spiking interneurons (Siegler and Burrows 1983) and the anteromedial spiking interneurons (Nagayama 1989), are produced by NB4-1 and NB3-1, respectively (Shepherd and Laurent 1992). These interneurons are not the only neurons produced by those NBs, but in both cases the entire population of interneurons is from a single clone. Also, the locust median NB produces a class of sound-responsive local interneurons and a class of intersegmental interneurons that respond to mechanosensory stimuli (Thompson and Siegler 1991). Thus, at least in these cases, NB lineages are associated with a limited number of discrete functions.

To relate *Drosophila* hemilineages with behavioral functions, I performed an activation screen of the secondary hemilineages in decapitated flies. I used the lines described in Chapter 2 to express the heat-activated cation channel TRPA1 (Hamada et al. 2008) in each hemilineage, then decapitated the flies and heated them to activate those neurons. In most cases, this treatment induced a strong, reproducible, and often unique behavioral phenotype. In general, activation of neurons in hemilineages that arborize ventrally gave rise to postural or uncoordinated leg movements, whereas hemilineages that arborize more dorsally produced wing-related movements and/or intersegmentally coordinated behaviors like walking.

Materials and Methods

Fly stocks

Flies were reared on standard cornmeal and molasses food at either 21°C or 25°C. TRPA1 is slightly active at 25°C, so rearing temperature affected subsequent treatment (see below.) Transgenic constructs and hormone feeding of hormone-inducible reagents were as described in Chapter 2.

Decapitation, neural activation, and video recordings

Three to four days after eclosion, adult females were lightly CO_2 anesthetized, sorted, and returned to food vials, where they were allowed to recover for two days. (CO_2 may affect behavior for at least 24h following anesthesia.) Females were then chilled in an iced vial, transferred to a cold plate (Teca) at 2°C, and quickly decapitated using microscissors in batches of 5-20. Flies were on the cold plate for less than 3 minutes. Decapitated flies were brushed back into a food vial and allowed to recover for at least 1h.

The heat-activated cation channel TRPA1 shows some activity at 25°C, and is fully active in the range of 27°C-32°C (Hamada et al. 2008). For TRPA1 activation, batches of 5-10 decapitated flies were tapped onto a sheet of paper, and any flies that were unable to right themselves were discarded. The paper was then placed on a hot plate (Teca) and ramped from 24°C to maximum activation temperature. For flies reared at 21°C, the maximum activation temperature was 32°C and the ramp took 45s. For flies reared at 25°C, the maximum activation temperature was 37°C and the ramp took 55s. Reference temperatures taken from the hot plate's internal sensor were manually marked in the videos.

For all lineages, low-speed (60fps) videos were taken using a Dragonfly Express digital camera (Point Grey Research) controlled by the MATLAB Image Acquisition (ImAq) tool in the Image Acquisition Toolbox. Videos were taken from above, with a field of view diameter of approximately 50mm. Recordings lasted 60s, encompassing the entire temperature ramp and a period of time at maximum activation temperature.

For lineages that induced flight-related phenotypes, high-speed (1000-6000fps) videos were taken with a Phantom v9 high-speed digital camera (Vision Research) using the Phantom software. Flies were filmed individually or in groups of <5, with a field of view approximately 5mm in diameter. Recordings were saved from the camera's memory buffer from the period preceding a predetermined behavioral trigger-point, such as takeoff.

Data analysis

Low-speed footage was annotated manually using VirtualDub (http://virtualdub.org/) and/or ImageJ (http://rsbweb.nih.gov/ij/). High-speed footage was annotated manually using Phantom software. Behaviors were scored throughout the temperature ramp. Each lineage was assigned "hit" or "no hit" for five behavior categories, based on whether the behavior was part of the "steady-state" phenotype reached at the peak of the activation ramp.

For data analysis, each behavior was treated as a dummy variable (0 for a no-hit, 1 for a hit). The data was organized as a 32-by-5, hemilineage-vs-behavior matrix and grouped

using *k*-means clustering (Hartigan and Wong 1979) in MATLAB. For comparison to the anatomy data from Chapter 3, arbor overlap data was represented as a 32-by-32, hemilineage-vs-hemilineage matrix, in which overlap was treated as a dummy variable (0 for no overlap, 1 for potential overlap) for each pair of hemilineages. Anatomy data was also sorted using *k*-means clustering. I then calculated the Rand index (Rand 1971) of the lineage groups generated by the two datasets. As a control, I compared the resultant index to the Rand indices of *k*-means clusters generated from scrambled versions of the datasets, using a T-test.

Results

TRPA1 activation of VNS lineages induces behavior in decapitated flies

I expressed the heat-activated cation channel UAS-dTRPA1 (Hamada et al. 2008) in each hemilineage using the genotypes described in Chapter 2, then decapitated the flies and recorded their behavioral responses to the depolarization of their target neurons during the heat-ramp. I used decapitated flies for a number of reasons (see Discussion), but this incurs one potential complication: if any descending neurons expressed TRPA1, it is possible that their severed axons would be sufficiently depolarized by the elevated temperature to synaptically drive downstream cells in the thorax, as has been seen for the larval motor axons (S. Pulver, pers. comm.). Thus, in some cases, activation of descending neurons might contribute to the observed behavioral responses. It seemed possible that after decapitation, cut axons would rapidly degenerate, obviating the problem. However, I found that if flies expressing GFP in descending neurons were

decapitated, the GFP was still visible in the severed axons in the VNSs of those flies 24h later, so I have no evidence that aging the flies after decapitation would eliminate the potential activation of severed descending neurons.

To test whether descending neurons were contributing to observed phenotypes, I used the VNS-specific *teashirt-GAL80 (tsh-GAL80)* to suppress GAL4 throughout the VNS in a line with a very reliable phenotype, the lineage 11 line. Activation of the neurons in the lineage 11 line induces a robust jumping response. This driver construction causes expression in lineage 11, but also a few descending interneurons and leg sensory neurons (Fig. 4.1A). When *tsh-GAL80* was added to the lineage 11 genotype, GFP expression in lineage 11 was suppressed while brain and sensory neuron expression remained (Fig. 4.1B). Whereas 35 of 37 flies driving TRPA1 using the lineage 11 line show a jumping phenotype, only 2 of 21 flies driving TRPA1 from the same line but with *tsh-GAL80* showed that phenotype. Thus, for this line, the observed behavioral phenotype is mediated through the targeted lineage, rather than through the descending interneurons or the leg sensory neurons.

I took video recordings of batches of 5 to 10 decapitated flies exposed to a temperature ramp to activate TRPA1. The activation temperature for dTRPA1 is typically cited as 27^{o}C for behavioral studies, although temperatures as high as 37^{o}C are sometimes required to induce behavior, depending on the driver used and the target neurons (e.g. von Philipsborn 2011). I used two TRPA1 temperature regimes, depending on rearing temperature. Most flies were reared at 25^{o}C; for these, the activating temperature ramp

was from 24°C to 37°C. I sometimes saw a stereotyped series of behaviors appear between 27°C and 32°C, but the behaviors nearly always reached a steady state and remained constant by ~33°C (with the exception of jumping, which terminated scoring because flies left the field of view). Because of concerns that TRPA1 might be slightly active at 25°C, and thus might exert a developmental effect on flies reared at 25°C, I also reared several batches of flies at 21°C for comparison. For these flies, the activating temperature ramp was from 24°C to 32°C. The behavioral phenotypes of flies reared at 21°C were indistinguishable from those of the same genotype reared at 25°C under my scoring system. Consequently, I did not distinguish the two datasets in subsequent analysis.

Videos were scored by hand for the presence of five behavior categories: altered leg posture, uncoordinated leg movements, walking, jumping, and wing movements. For each genotype, I calculated the percentage of flies performing each behavior. A behavior was counted as a hit for a lineage if it was performed by the majority of the flies (>50%) of every scored genotype for that lineage.

Behavior categories were scored as follows:

Altered leg posture: Flies were counted as leg posture hits if they showed a deviation from their initial standing posture over the course of heating. The initial standing posture for decapitated flies was quite consistent, so this trait could be scored reliably between lines.

Uncoordinated leg movements: Flies were counted as hits if they demonstrated repetitive leg movements with no intersegmental coordination.

Jumping: The "jumping" phenotype refers specifically to the simultaneous extension of both mesothoracic legs, as in an escape response (Card and Dickinson 2008), and typically had to be confirmed using high-speed video. Jumps were always accompanied by flapping of the wings.

Walking: To qualify as a "walking" hit, a fly had to demonstrate regular leg movements in which the legs on each side were advanced in the order [T3, T2, T1] at least once (Strauss and Heisenberg 1990) and led to translocation of more than one body length during the 60s recording period.

Wing movements: This phenotype encompassed wing postures (e.g., raised wings), non-flight movements (e.g., wing-scissoring), and flapping.

The results are summarized in Table 4.1 and described in detail below.

Hemilineages that only altered leg posture

These lineages all resulted in flies with strong steady-state leg postural defects, and no other behaviors. At low activation temperatures, these flies often seemed to be "fighting" the effect, moving the affected legs back to a normal standing posture. As the temperature ramp continued, the flies lost control of their legs.

Lineage 15B includes only motor neurons that innervate muscles of the distal leg segments. When this population of motoneurons was activated with TRPA1, the legs

eventually went into a tonic contracture, showing a prominent flexion at the femorotibial joint. This typically caused the flies to topple over (Fig. 4.2A).

In contrast, hemilineages 1B, 5B, 8A, 9A, 13A, 13B, and 20A/22A all caused lateral extension of the legs when activated, and hemilineage 12B and lineage 14A induced lateral or ventral extension of the legs. Examples of these postures are shown in Fig. 4.2B-C.

In some cases, such as lineage 20A/22A, one could still detect attempted voluntary movements like grooming, whereas in others, such as hemilineage 5B, all leg motion essentially ceased at maximum temperature.

Hemilineages that altered leg posture and drove uncoordinated leg movements

Stimulation of the neurons in these lineages all caused a postural change, but also drove repetitive leg movements beyond the spontaneous grooming commonly observed in decapitated flies. These motions were not coordinated between segments in an obvious way; a common example is the repeated lifting and lowering of a single leg.

Hemilineages 6B, 8B, 19A, 21A and 24B caused mild to severe lateral extension of the legs and small, repetitive, usually vertical leg movements. Hemilineages 3A and 10B also caused lateral extension of the legs, and tended to produce anteroposteriorly directed leg movements. Lineages 4B and 23B caused large-amplitude leg movements accompanied by severe postural defects: lineage 4B caused ventral extension of the legs, while lineage

23B generally caused flexion. Activation of lineage 4B or 23B caused flies to fall, and they could not right themselves. In many cases, this triggered wing movements that are part of the righting reflex, but these were not scored as part of the phenotype because they were not caused directly by lineage activation.

Hemilineages that only drove walking

When activated with TRPA1, hemilineage 1A caused walking, as defined above, in 14 of 16 flies (Fig. 4.3). That definition is conservative: the behavior displayed by these flies is similar to that described as locomotion for decapitated flies exposed to biogenic amines in Yellman et al. (1997). The legs are not organized in the tripod gait typical of walking in intact flies (Strauss and Heisenberg 1990), but the phenotype is highly distinct from the uncoordinated leg movements described in the previous section. The net movement is always forwards, although the trajectory turns due to uneven step sizes, as observed by Yellman et al. (1997).

Two other hemilineages drove walking: 12A and 18B. The walking demonstrated by these lines is similar to that described for 1A. These hemilineages displayed additional behaviors, so their phenotypes are discussed in more detail below.

Hemilineages that only drove wing movements

Lineages 2A and 3B are the only lineages to cause wing movements with no concomitant leg movement. Lineage 2A caused sustained, sudden-onset flapping in 18 of 31 flies (Fig. 4.4B). Flapping was observed in other lines, but it was usually preceded by either wing-

scissoring or a jump. These phenotypes are described below. Hemilineage 3B caused a unique side-to-side "wing waggle," observed nowhere else, in 4 of 8 tested flies (Fig. 4.4C).

Hemilineages that drove disorganized wing and leg movements and altered posture

Hemilineages 6A, 17A and 19B induced a variety of wing movements and disorganized leg movements. Activation of hemilineage 6A caused raised wings (Fig. 4.4A), while activation of 17A or 19B caused small lateral wing movements. All three lineages caused mild lateral leg extension. They also caused leg movements that resembled walking, in that the movements had both vertical and anteroposterior components and sometimes caused the fly to move backwards or sideways, but the movements did not consistently meet the criteria of at least one (T3-T2-T1) wave and at least one body length's translocation.

Hemilineages that drove organized wing and leg movements

The four remaining hemilineages drove both leg and wing movements when activated with TRPA1. Hemilineage 7B drove jumping and flapping; lineage 11 (A+B) drove lateral wing movements, jumping and flapping; hemilineage 12A drove walking, lateral wing movements, and/or flapping; and hemilineage 18B drove walking, jumping and flapping. In the case of hemilineages 7B, 11A/B and 18B, the combination of jumping and flapping led to takeoff, in which the decapitated flies became airborne and left the hot plate. (Anecdotally, if the flies happened to land back on the hot plate, they repeated the same lineage-specific behaviors as before, ultimately taking flight again.) In intact flies,

voluntary takeoff involves an invariant behavioral sequence: first, the fly raises its wings, then it jumps (extension of the mesothoracic legs), followed closely by wing depression and flapping (Card and Dickinson 2008). High-speed video analysis revealed that hemilineage 7B activation evoked this same sequence (Fig. 4.5A). In contrast, when hemilineages 11A/B and 18B were activated, the wing-raising step was eliminated; rather, wingbeat-frequency wing movements were usually initiated before the jump, often while the wings were still folded, resulting in jerky lateral movements (Fig. 4.5C). After a latent period (varying on the order of milliseconds to seconds), the fly would jump and the wing movements would transition into flapping, but not consistently in that order (Fig. 4.5B-CS).

Correlating behavior and anatomy

I wanted to know whether these behavioral phenotypes correlated with mature hemilineage anatomy. I treated the behavior scores for each lineage as a series of dummy variables ('0' for a no-hit, '1' for a hit) and used these to group the lineages using *k*-means clustering (Hartigan and Wong 1979). In *k*-means clustering, data points (here, lineages) that differ according to *n* variables (here, behaviors) are plotted in *n*-dimensional Euclidian space, then assigned to the closest of several randomly seeded centroids. Centroid assignments and locations are iteratively updated until the net distance from all points to their assigned centroid is minimized. The data sorted well into two clusters, shown in Fig. 4.6A. These clusters correspond to lineages that show only leg posture changes and/or uncoordinated leg movements, versus lineages that show other phenotypes.

I then took the arbor overlap dataset from Chapter 3 and organized it as another set of dummy variables for each lineage, giving the lineage of interest a score of '1' for arbor overlap and '0' if there was none, and again grouped the lineages using *k*-means clustering. Again, the data sorted into two clusters, shown in Fig. 4.6B. The clusters correspond roughly to lineages that arborize primarily in the ventral two-thirds of the thoracic neuropil, versus lineages that arborize primarily in the dorsal third.

I then compared the behavior-based clusters to the anatomy-based clusters (Fig. 4.6C). To quantify this, I calculated their Rand index, which measures the similarity between two data clusterings (Rand 1971). The Rand index takes every pair of points in the dataset (in this case every pair of hemilineages) and asks whether they are grouped together under the first versus the second clustering criteria. The index decreases when a pair of points is put in the same cluster under one set of criteria, but segregated into different clusters under the other. The maximum value the Rand index can take is 1, indicating perfect alignment of the two clusterings. The Rand index of my behavior and anatomy-based clusters was 0.71.

I compared my result to the Rand indices of 1000 randomized versions of the anatomy dataset, subjected to *k*-means clustering and compared to the same behavior clusters. This provided a sense of the degree to which these clusters would overlap by chance. None of the randomized clusterings overlapped as well as the real clusterings; most had a Rand

index near 0.5 (Fig. 4.6D). This difference was highly statistically significant ($p << 0.001$).

Discussion

Supporting the hypothesis that hemilineages represent functional neural classes, each hemilineage is associated with specific, often modular activation phenotypes. I used hemilineage-specific driver lines (Chapter 2) to express the heat-activated cation channel UAS-dTRPA1 (Hamada et al. 2008) in specific classes of neurons and then depolarized the neurons by heating the flies. These studies were performed on decapitated flies because I am interested in circuits wholly contained within the thoracic ganglia and wished to exclude descending influences. Decapitating flies also has three practical advantages: first, the genotypes in Chapter 2 do not address expression in the brain; some lines are restricted to the VNS, while some are not. Second, intact flies show much more variability in their response to TRPA1 activation in the VNS, and the responses tend to be attenuated. This is likely due to descending inhibition that can override thoracic activation. Third, decapitated flies are much easier to film, since in the absence of stimuli they typically do not move except to groom.

TRPA1 activation in decapitated flies resulted in strong, repeatable, and sometimes unique behavioral responses for each studied hemilineage. I analyzed videos of TRPA1 activation of each hemilineage, using multiple genotypes where possible, and categorized the induced responses. For the sake of simplicity, I coded the responses as combinations

of 5 behaviors: leg posture changes, uncoordinated leg movements, jumping, walking, and wing movements.

Two behavior combinations, "leg posture" and "leg posture plus leg movements," encompassed 19 of 30 scored hemilineages, mostly the local leg lineages (see below). The other 10 hemilineages produced behavior combinations that were either unique or shared with only one other hemilineage. When I compared the anatomy of the 19 leg posture/leg movement hemilineages versus the 10 specialized hemilineages, one striking principle emerged: 17 of the 19 lineages that expressed only the two major leg phenotypes formed their major arbors in the lower two-thirds of the neuropil. In contrast, all 11 hemilineages that expressed wing phenotypes and/or walking arborized in the dorsal third of the neuropil. Comparison of clustering analysis based on behavior versus anatomy supported this correlation as statistically significant.

The thoracic neuropil has long been considered to show dorsoventral functional organization. For example, within its lower third, leg sensory neurons arborize ventrally, while leg motor neurons arborize dorsally. On a broader scale, the ventral third of the neuropil is informally considered to be the “leg neuropil,” because leg sensory neurons and motor neurons arborize there, while the dorsal third is referred to as the “wing neuropil” because most wing and haltere sensory and motor neurons arborize there.

However, contrary to such a "leg versus wing" classification, the behavioral phenotypes associated with the dorsal anatomy cluster were not wing-specific. Rather, wing

movements, jumping and walking were all equally associated with dorsal projections. This also seen in hemilineages 12A and 18B, which induced both walking and wing movements.

The neural substrates of flight evolved from the CNS of a flightless ancestor, and it seems reasonable to speculate that they integrated into and expanded upon existing circuits for the production of rhythmic movements. Perhaps the ancestral neuropil was organized hierarchically from ventral to dorsal, with "command neurons" that coordinated intersegmental movements in the dorsal third of the neuropil; with the evolution of flight, this dorsal region was invaded by (and expanded to produce) flight circuits. This could explain the observed comingling of lineages that cause wing movements and/or walking.

It is plausible that walking and jumping are associated with more dorsal lineages because they require bilateral and/or intersegmental coordination, whereas the ventralmost lineages are all local leg interneurons. However, there are a number of hemilineages that form intersegmental arbors in the middle third of the neuropil, such as 10B, 12B, and 23B, but none of these induces walking or jumping. Thus, there appears to be some sort of dorsoventral computational stratification in the thoracic neuropil independent of obvious constraints like the locations of intersegmental tracts and leg versus wing sensory inputs.

This is certainly not to say that lineages such as 10B and 23B cannot be involved in walking. For example, most models of insect walking rely on the existence of

intersegmental inhibitory signals that prevent a load-bearing leg from lifting until the legs adjacent to it are on the ground. If one were to activate neurons mediating such a signal in all segments simultaneously, the resultant phenotype would simply be a fly that could not lift any of its legs. Some of the ventral intersegmental lineages may play roles in dynamic behaviors that are not revealed by the type of activation screen I performed. However, it is interesting that a number of lineages are, in fact, able to produce an intersegmentally coordinated gait when activated in all segments simultaneously, and that these all have dorsal arbors.

There were two exceptions to the ventral-static/dorsal-dynamic trend: hemilineages 6B and 8B. These lineages arborize in the dorsal third of the VNS, but neither produces a strong behavioral phenotype when activated. Hemilineage 6B is GABAergic (Chapter 3), which might explain the lack of a strong activating phenotype. However, hemilineage 8B produces the contralateral haltere interneurons (cHINs) (Strausfeld and Seyan 1985), which are known to receive sensory inputs from the halteres, so it is unclear why activation of this lineage caused a leg-posture phentoype, rather than a wing/haltere-related phenotype. It is possible that these lineages play a role in coordinated behaviors such as walking and flying, but only in the appropriate context (e.g., during flight).

It may be possible to infer putative circuit organization by comparing lineages that induce similar behaviors. For example, three hemilineages cause takeoff when activated: 7B, 11A/B, and 18B. All three of these lineages induce both a flight-initiation jump (simultaneous extension of both mesothoracic legs) and flight-frequency (~200Hz) wing

movements. Interestingly, the lineages vary in the precision with which they coordinate the jump and the wing movements. When hemilineage 7B is activated with TRPA1, decapitated flies first raise both wings, followed by mesothoracic leg extension, followed by the initiation of flapping. This is precisely the behavioral sequence of voluntary takeoff in intact flies (Card and Dickinson 2008). In contrast, high-speed video analysis reveals that when hemilineages 11A/B or hemilineage 18B is activated, flight-frequency wing movements can be initiated substantially before the jump. Moreover, these flies frequently do not raise their wings before initiating high-frequency movements, so they display jerky lateral wing movements for a variable amount of time before transitioning into smooth flapping.

The anatomy data from Chapter 3 suggest that the arbors of hemilineage 7B overlap strictly with other dorsal lineages, including all of the "flight lineages" (except 17A) and 0A, 6B, 8B, 12B, and 1A. In contrast, the arbors of 11A/B and 18B overlap with all of those lineages, plus multiple "leg lineages"; for example, both overlap with 10B, 21A, and motor hemilineage 15B, among others. One could speculate that 11A/B and 18B are downstream of inhibitory lineages that would ordinarily prevent the premature initiation of wing movements prior to the jump, while 7B is upstream of those influences; thus, activation of hemilineage 7B elicits the correct sequence, whereas activation of hemilineage 11A/B or 18B bypasses that inhibition, resulting in simultaneous or misordered activation of wing-raising versus jumping versus flapping. It will be interesting to perform epistasis and/or loss-of-function experiments on these lineages to

probe such hypotheses. I attempted these experiments, but many of the genotypes were lethal, for as yet unknown reasons.

The prevalence of lineage-specific phenotypes supports the hypothesis that the neurons that comprise hemilineages form distinctive neural classes. There are unquestionably subclasses within each hemilineage, but it appears that inter-lineage differences are larger than intra-lineage differences. That is, if neurons performing a given function could be produced by any lineage, one would expect many lineages to have similar activation phenotypes, but this is clearly not the case. Moreover, hemilineage anatomy appears to correlate strongly with function, and suggests a dorsoventral hierarchical organization in the thoracic neuropil. With the tools described in Chapter 2, the anatomical data from Chapter 3, and the preliminary behavioral studies outlined here, I hope that the hemilineages of the VNS will provide a powerful and worthwhile system in which to study neural circuits.

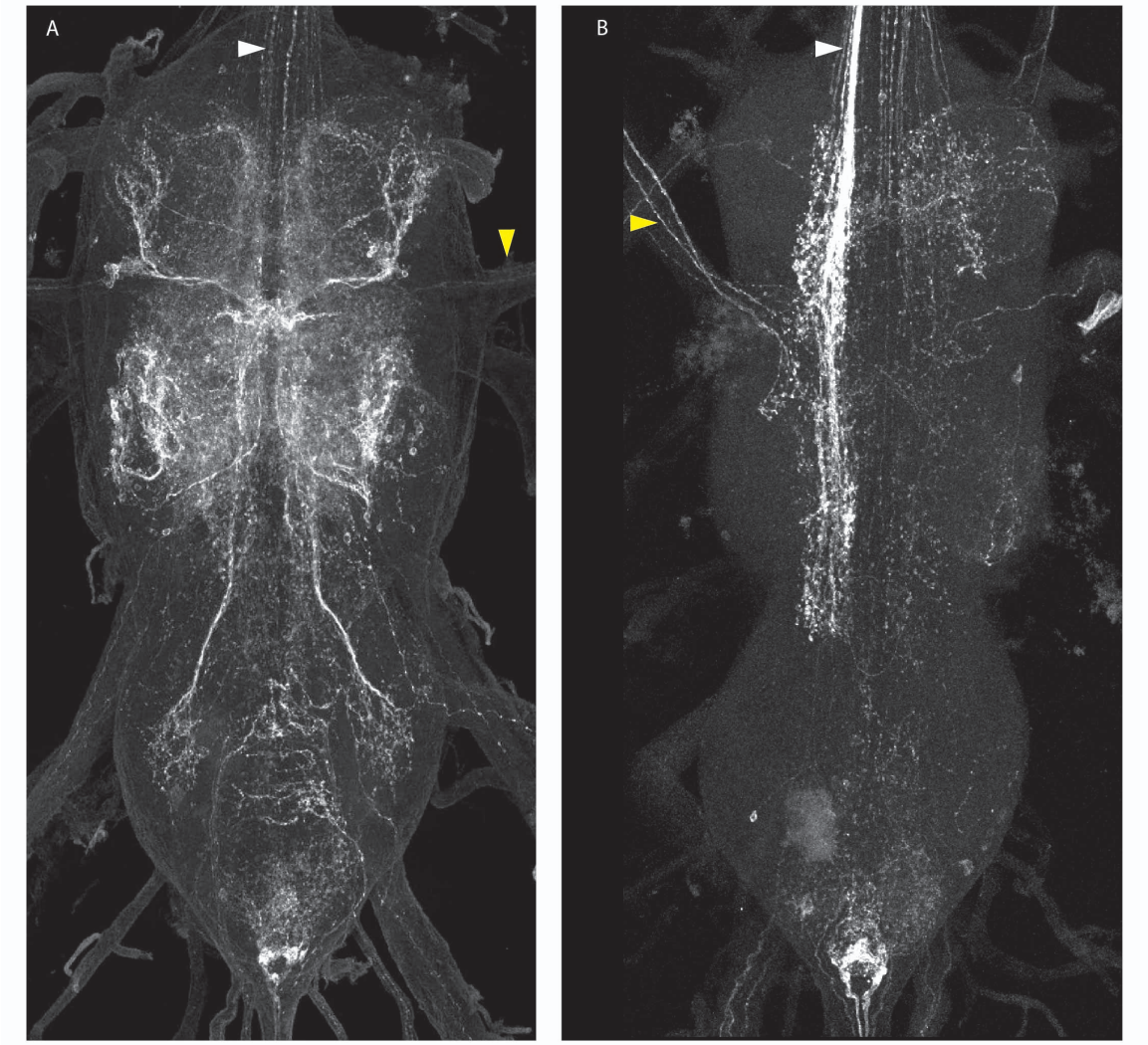

Figure 4.1. tsh-GAL80 eliminates expression specifically in the VNS. (A) The lineage 11 genotype drives GFP expression in the VNC in lineage 11, descending axons (white arrowheads), and leg sensory neurons (yellow arrowheads). (B) The same genotype as in (A), but with the addition of tsh-GAL80. Expression is eliminated in lineage 11, but remains in descending neurons (e.g. white arrowhead) and leg sensory neurons (e.g. yellow arrowhead).
Genotypes: (A) nSyb-GAL80 (su(Hw)attP8)/w; UAS-flp(attP40)/+; R26B05-GAL4 (attP2)/nSyb-LexA (attP2), LexAop>STOP>GFP (VK00005). (B) nSyb-GAL80 (su(Hw)attP8)/w; UAS-flp(attP40)/tsh-GAL80; R26B05-GAL4 (attP2)/nSyb-LexA (attP2), LexAop>STOP>GFP (VK00005).

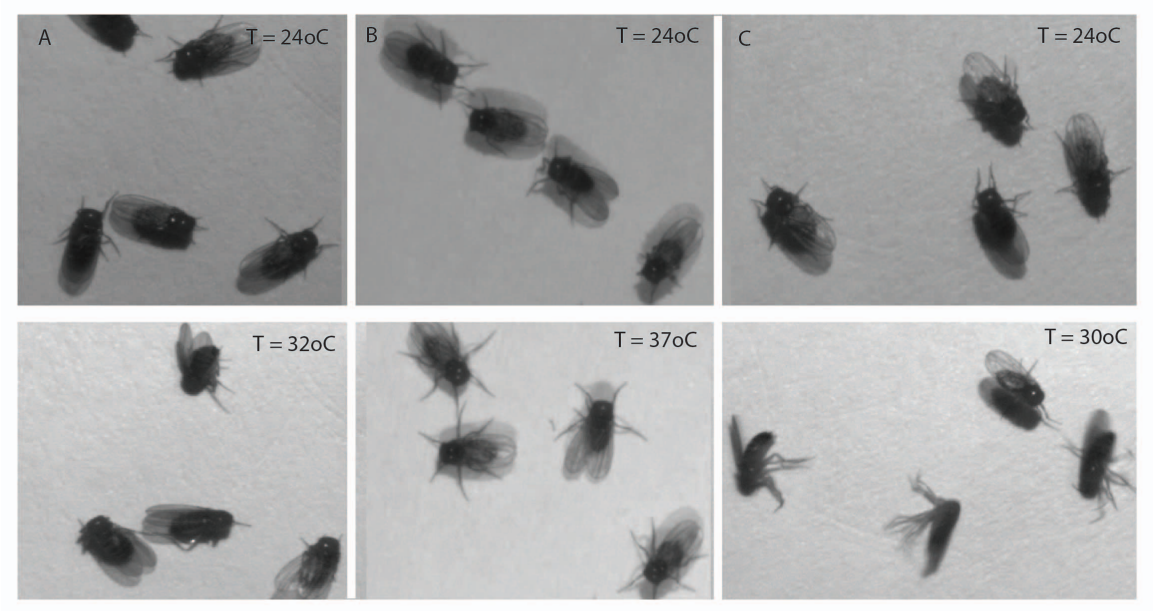

Figure 4.2. Examples of phenotypes scored as "altered leg posture." Still frames from video taken during a temperature ramp from 24oC to 37oC. Upper row, stills at 24oC demonstrating that normal posture is observed before the ramp. Lower row, stills at the activation temperature indicated in the upper right. (A) Activation of lineage 15 causes tonic leg contracture with a prominent flexion at the femorotibial joint. (B) Activation of lineage 13B causes lateral extension of the legs. (C) Activation of lineage 4 causes ventral extension of the legs, as well as leg movements.
Genotypes: (A) nSyb-GAL80 (su(Hw)attP8)/w; UAS-flp(attP40)/+; R19H09-GAL4 (attP2)/nSyb-LexA (attP2), LexAop>STOP>TRPA1 (VK00005). (B) nSyb-GAL80 (su(Hw)attP8)/w; UAS-flp(attP40)/+; R41G09-GAL4 (attP2)/nSyb-LexA (attP2), LexAop>STOP>TRPA1 (VK00005). (C) nSyb-GAL80 (su(Hw)attP8)/w; UAS-flp(attP40)/+; R51D02-GAL4 (attP2)/nSyb-LexA (attP2), LexAop>STOP>TRPA1 (VK00005).

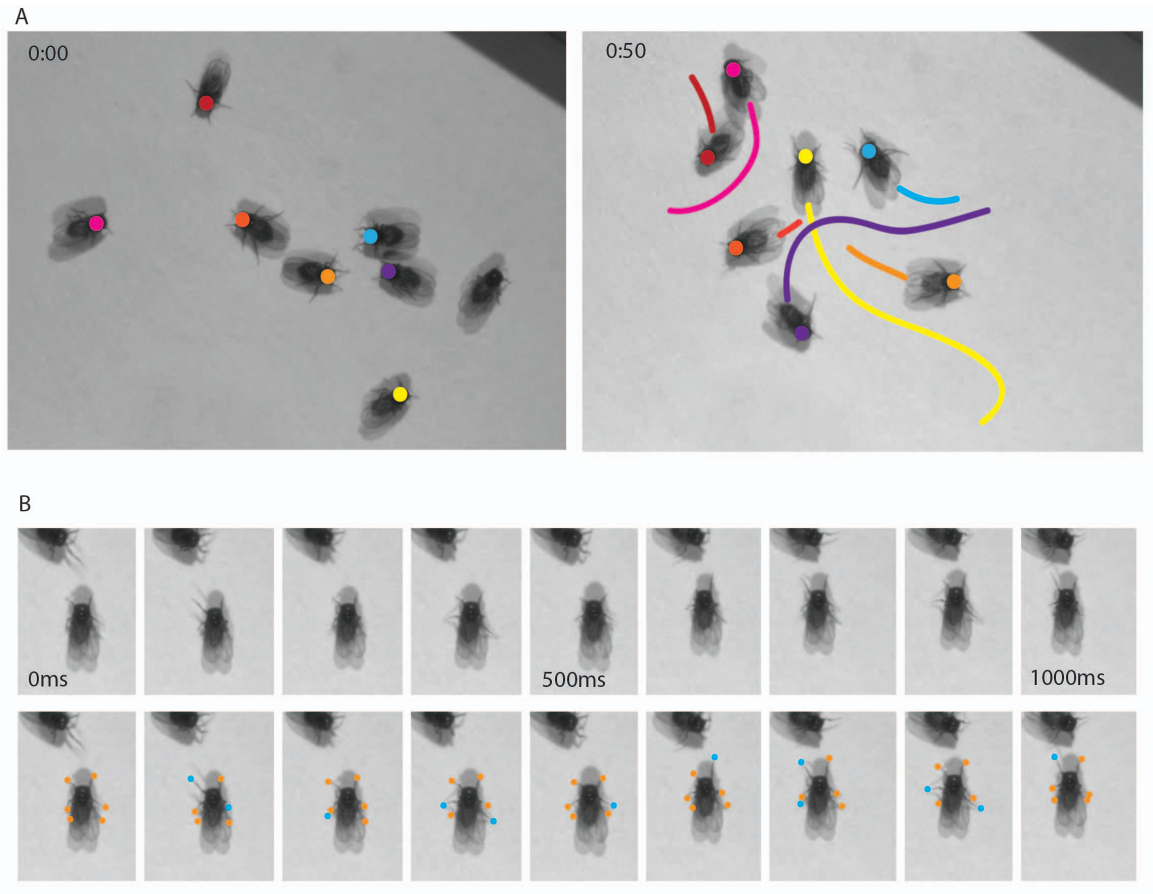

Figure 4.3. Example of hemilineage activation that causes walking behavior. Frames from a video of hemilineage 1A activation: flies translocate more than one body length due to leg movements that occur in the order (T3, T2, T1) on each side. Flies were filmed at 60fps. (A) Trajectories of flies during a heat ramp from 24oC to 37oC. Left, initial positions; right, final positions. The unmarked fly jumped out of the field of view. Time stamp, seconds. (B) Close-up of the fly marked in yellow in (A). Upper row: cropped still frames. Lower row: The same images, with each leg marked. Legs in contact with the ground are marked in orange; lifted legs are marked in blue. Note that the legs are lifted in the order (T3, T2, T1) on each side, and contralateral legs alternate (although the classic "tripod" organization is not observed). Stills were taken at approximately 125ms intervals, adjusted to capture frames where legs were lifted. Genotype: w; R22G11-LexA (attP40)/+; LexAop-TRPA1 (attP2)/+.

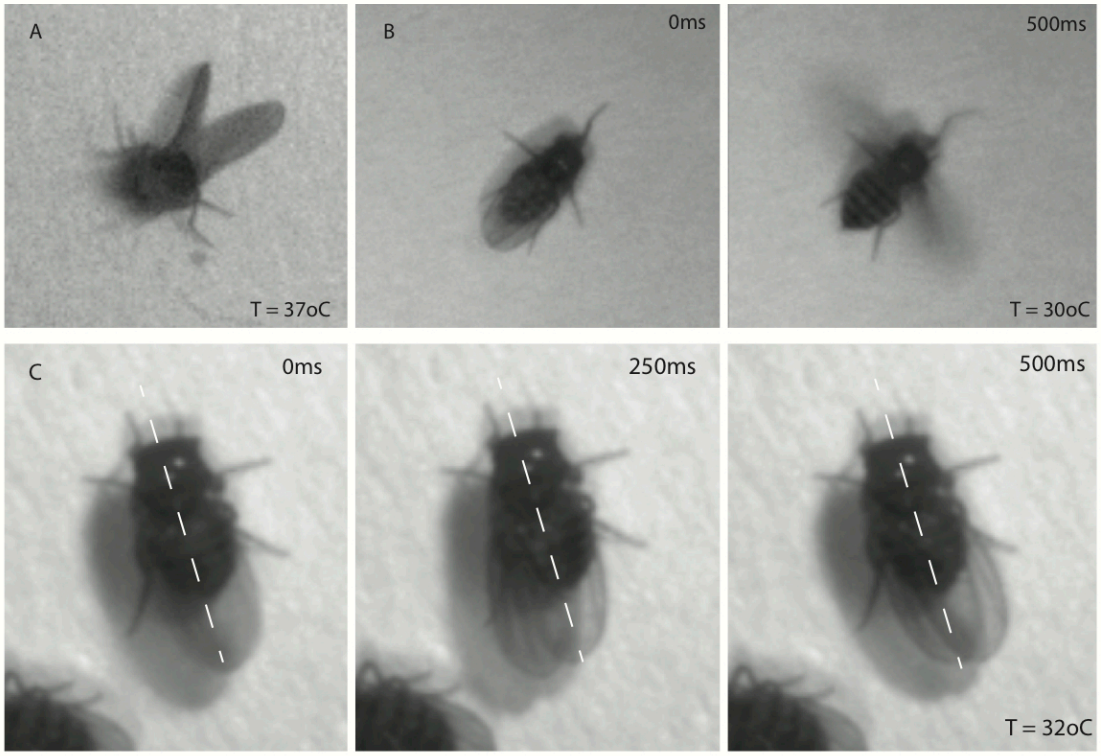

Figure 4.4. Examples wing movement evoked by hemilineage activation. Still frames from videos of flies during a temperature ramp from 24oC to 37oC, taken at 60fps. (A) Lineage 6A causes raised wings and altered leg posture. The fly's neck connective is towards the camera. (B) Lineage 2 causes flapping. Left, a fly expressing TRPA1 in lineage 2 displays no phenotype just prior to the onset of flapping; right, 500ms later, the wings (blurred) are fully extended and beating at wingbeat frequency. (C) Lineage 3B causes synchronized left-right wing movements. Note the movement of both wingtips relative to the body axis (dashed line).
Gentoypes: (A) nSyb-GAL80 (su(Hw)attP8)/w; UAS-flp(attP40)/+; R35A03-GAL4 (attP2)/nSyb-LexA (attP2), LexAop>STOP>TRPA1 (VK00005).(B) w; UAS-TRPA1/+; R50G08-GAL4 (attP2)/+. (C) w; R23B05-LexA (attP40)/+; LexAop-TRPA1 (attP2)/+.

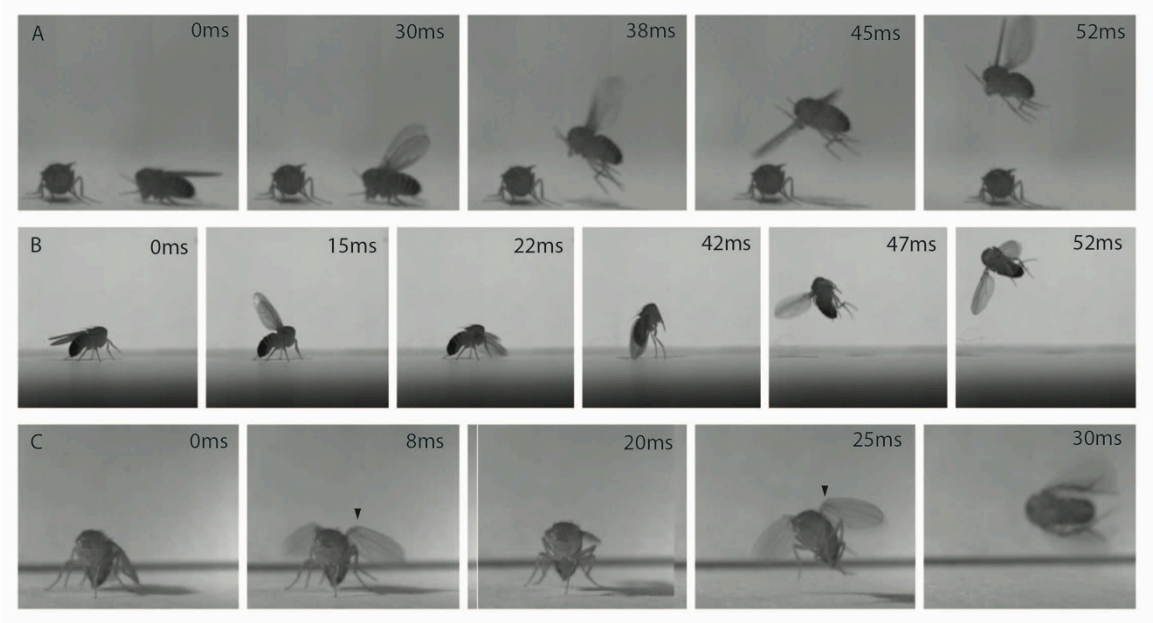

Figure 4.5. Examples of different takeoff sequences evoked by the activation of specific lineages. Still frames from 2000fps videos of TRPA1-induced takeoff. Upper right of each panel, time elapsed relative to leftmost image. (A) Activation of lineage 7 evokes a normal takeoff sequence in which the fly raises its wings (30 ms), extends both mesothoracic legs (38 ms), and then begins to flap (45 ms). (B) Activation of lineage 11 can evoke flapping (22 ms) before leg extension (42 ms). Abnormal wing movements are also sometimes observed (not shown). (C) Activation of lineage 18 can evoke flapping (not shown) or abnormal wing movements (8 ms) before leg extension (25 ms). Note the crease in the wings (e.g., arrowheads): this happens when the wings are not raised before flapping begins. Also, leg extension is markedly reduced (fourth panel).
Genotypes: (A) nSyb-GAL80 (su(Hw)attP8)/w; UAS-flp(attP40)/+; R65A12-GAL4 (attP2)/nSyb-LexA (attP2), LexAop>STOP>TRPA1 (VK00005). (B) nSyb-GAL80 (su(Hw)attP8)/w; UAS-flp(attP40)/+; R26B05-GAL4 (attP2)/nSyb-LexA (attP2), LexAop>STOP>TRPA1 (VK00005). (C) nSyb-GAL80 (su(Hw)attP8)/w; UAS-flp(attP40)/+; R27A09-GAL4 (attP2)/nSyb-LexA (attP2), LexAop>STOP>TRPA1 (VK00005).

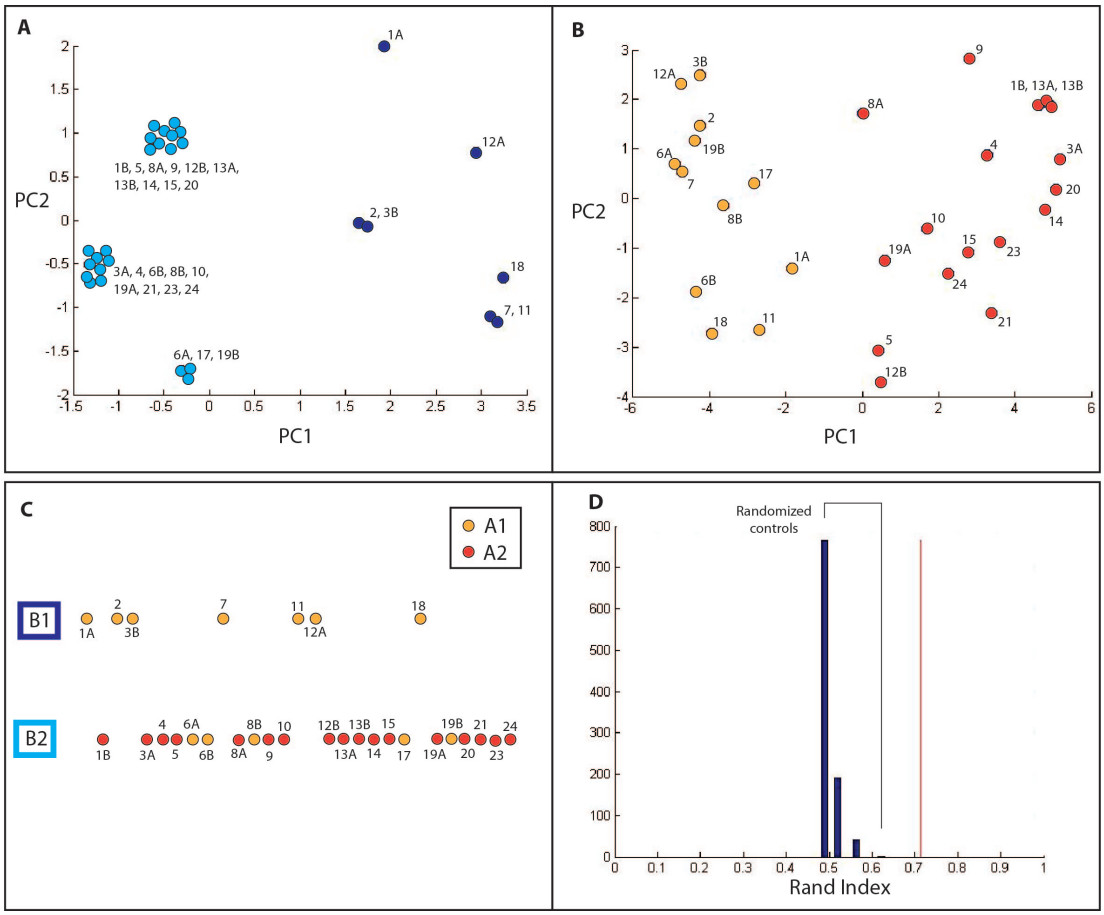

Figure 4.6. Lineage anatomy correlates with behavior. (A) Principal component analysis (PCA) of the behavior data. The first principal component (PC1) corresponds roughly to wing movements versus uncoordinated leg movements, and explains 47% of the observed variance. PC2 corresponds roughly to altered posture, walking or jumping, and explains another 19% of the observed variance. (B) PCA of connectivity data. PC1 corresponds roughly to dorsoventral location, and explains 46% of the observed variance. PC2 corresponds with the number of overlap partners, and explains another 11% of the variance. (C) Comparison of k-means clustering of hemilineages based on behavior (rows) versus anatomy (colors). Note that only five points are in disagreement (hemilineages 6A, 6B, 8B, 17, and 19B: see text). (D) The Rand index, a measure of similarity between two clustering systems, calculated for the data in (C) (red line) versus 1000 random permutations of the anatomy data, shown as a histogram in blue. The index for the real data is significantly higher than expected by chance ($p<<0.001$). The maximum value the Rand index can take is 1.

Table 4.1. TRPA1-induced activation phenotypes. For each lineage, genotypes are indicated as Rubin collection CRM IDs; for full genotypes, see Chapter 2 (Table 2.1). *n* indicates the number of flies analyzed for that genotype. The number in each cell is the percentage of flies performing the indicated behavior. Scores that were counted as hits (>50% of flies perform the behavior for all tested genotypes) are indicated in bold.

	Genotype(s)	*n*	Posture	Leg mvt	Walk	Jump	Wing mvt
1A	*R22G11*	14	0.14	0	**0.85**	0	0
1B	*R13G06*	18	**1.00**	1.00	0	0.61	0.67
	R58F02	26	**1.00**	0.15	0	0	0
2A	*R50G08*	31	0.16	0	0	0.20	**0.58**
3A	*R31H10*	13	**0.92**	**0.92**	0	0	0.15
3B	*R23B05*	8	0	0.13	0.13	0	**0.50**
4B	*R49E04*	5	**1.00**	**1.00**	0	0.20	0.20
	R51D02	18	**1.00**	**1.00**	0	0.11	0.17
5B	*R86D02*	30	**0.90**	0.30	0	0	0.10
6A	*R35A03*	20	**1.00**	**1.00**	0	0	**0.60**
6B	*R09A12*	35	**1.00**	**0.94**	0	0	0.51
	R46C11	19	**1.00**	**1.00**	0.11	0.05	0.11
7B	*R65A12*	7	0	0	0.29	**0.86**	**0.86**
	R75H06	13	0	0	0	**1.00**	**1.00**
8A	*R69H11*	16	**0.81**	0.06	0	0	0
8B	*R09D08*	33	**1.00**	**0.97**	0	0.09	0.33
9A	*R48H02*	2	**1.00**	0.50	0.50	0	0
	R52E12	21	**0.62**	0.05	0	0	0.04
10B	*R13B08*	29	**1.00**	**1.00**	0	0.10	0.35
11	*R26B05*	37	0.03	0	0	**0.95**	**0.95**
12A	*R24B02*	16	0.44	0.25	**0.69**	0	**1.00**
12B	*R15D11*	19	**1.00**	0.26	0	0.11	0.26
13A	*R49C05*	24	**1.00**	0	0	0.13	0.46
13B	*R41G09*	22	**0.95**	0	0	0	0.05
14A	*R73H04*	2	**1.00**	0	0	0	0.50
15B	*R12F11*	5	**0.80**	0.40	0	0	0
	R19H09	22	**1.00**	0.14	0	0.27	0.23
17A	*R78A08*	27	**1.00**	**1.00**	0.07	0.15	**0.70**
18B	*R27A09*	16	0.375	0	**0.81**	**0.94**	**0.94**
19A	*R32E04*	23	**1.00**	**1.00**	0	0	0
	R50C03	7	**1.00**	**0.86**	0	0	0.43
19B	*R84E06*	23	**1.00**	**1.00**	0.13	0	**0.52**
20A	*R19H10*	16	**1.00**	0	0.88	0	0.19
	R24G06	19	**1.00**	0.05	0	0	0.21
21A	*R51H05*	32	**1.00**	**1.00**	0	0.13	0.25

Table 4.1, continued

23B	*R67A11*	4	**1.00**	**1.00**	0	0.50	0
	R77C10	24	**1.00**	**1.00**	0	0.04	0.17
	R81C12	1	**1.00**	**1.00**	0	1.00	1.00
24BS	*R15A03*	31	**1.00**	**0.97**	0.06	0	0.23
	R73B01	1	**0.50**	**0.50**	0	0	0

REFERENCES

Bachmann, A., and Knust, E. (2008). The use of p-element transposons to generate transgenic flies. *Meth Molec Biol* 420: 61-77.

Baek, M., and Mann, R.S. (2009). Lineage and birth date specify motor neuron targeting and dendritic architecture in adult Drosophila. *J Neurosci* 29(21): 6904-6916.

Bello, B.C., Izergina, N., Caussinus, E., and Reichert, H. (2008). Amplification of neural stem cell proliferation by intermediate progenitor cells in Drosophial brain development. *Neural Dev* 3: 5.

Benzer, S. (1967). Behavioral mutants of Drosophila isolated by countercurrent distribution. *Proc Natl Acad Sci USA* 58(3): 1112-9.

Boll, W., and Noll, M. (2002). The Drosophila Pox neuro gene: control of male courtship behavior and fertility as revealed by a complete dissection of all enhancers. *Development* 129(24): 5667-81.

Booker, R., and Truman, J.W. (1987). Postembryonic neurogenesis in the CNS of the tobacco hornworm, *Manduca sexta. J Comp Neurol* 255: 548-59.

Boone, J.Q., and Doe, C.Q. (2008). Identification of Drosophila type II neuroblast lineages containing transit amplifying ganglion mother cells. *Dev Neurobiol* 68(9): 1185-95.

Bowman, S.K., Rolland, V., Betschinger, J., Kinsey, K.A., Emery, G., and Knoblich, J.A. (2008). The tumor suppressors Brat and Numb regulate transit-amplifying neuroblast lineages in Drosophila. *Dev Cell* 14(4): 535-46.

Brand, A., and Perrimon, N. (1993). Targeted gene expression as a means of altering cell fates and generating dominant phenotypes. *Development* 118: 401-15.

Brent, R., and Ptashne, M. (1985). A eukaryotic transcriptional activator bearing the DNA specificity of a prokaryotic repressor. *Cell* 43(3): 729-36.

Brierley, D.J., Rathore, K., Rhagavan, K.V., and Williams, D.W. (2012). Developmental origins and architecture of Drosophila leg motoneurons. *J Comp Neurol* 520: 1629-49.

Broach, J.R., Guarascio, V.R., and Jayaram, M. (1982). Recombination within the yeast plasmid 2mu circle is site-specific. *Cell* 29(1): 227-34.

Brown, H.L., and Truman, J.W. (2009). Fine-tuning of secondary arbor development: the effects of the ecdysone receptor on the adult neuronal lineages of the Drosophila thoracic CNS. *Development* 136: 3247-56.

Burrows, M. (1996). *The neurobiology of an insect brain*. Oxford: Oxford University Press.

Card, G., and Dickinson, M. (2008). Performance trade-offs in the flight initiation of Drosophila. *J Exp Biol* 211(3): 341-53.

Certel, S.J., Leung, A., Lin, C.Y., Perez, P., Chiang, A.S., and Kravitz, E.A. (2010). Octopamine neuromodulatory effects on a social behavior decision-making network in Drosophila males. *PLoS ONE* 5(10): e13248.

Cruse, H. (1990). What mechanisms coordinate leg movement in walking arthropods? *Trends Neurosci* 13: 15-21.

Cuccati, J. (1888). Uber die organziation des gehirns der Somomya erythrocephala. *Z f wiss Zool* 46: 240-269.

de la Escalera, S., Bockamp, E.O., Moya, F., Piovant, M., and Jimenez, F. (1990). Characterization and gene cloning of neurotactin, a Drosophila transmembrane protein related to cholinesterases. *EMBO J* 9: 3593-3601.

DiAntonio, A., Burgess, R.W., Chin, A.C., Deitcher, D.L., Scheller, R.H., Schwarz, T.L. (1993). Identification and characterization of Drosophila genes for synaptic vesicle proteins. *J Neurosci* 13(11): 4924-35.

Duffy, J.B. (2002). GAL4 system in Drosophila: a fly geneticist's Swiss army knife. *Genesis* 34: 1-15.

Fire, A., Xu, S., Montgomery, M.K., Kostas, S.A., Driver, S.E., and Mello, C.C. (1998). Potent and specific genetic interference by double-stranded RNA in Caenorhabditis elegans. *Nature* 391: 806-11.

Graham, D. (1977). The effect of amputation and leg restraing on the free walking coordination of the stick insect Carausius morosus. *J Comp Physiol* 116A: 91-116.

Groth, A.C., Fish, M., Nusse, R., and Calos, M.P. (2004). Construction of transgenic Drosophila by using the site-specific integrase from phage phiC31. *Genetics* 166(4): 1775-82.

Hamada, F.N., Rosenzweig, M., Kang, K., Pulver, S.R., Ghezzi, A., Jegla, T.J., and Garrity, P.A. An internal thermal sensor controlling temperature preference in Drosophila. *Nature* 454: 217-20.

Han, D.D., Stein, D., and Stevens, L.M. (2000). Investigating the function of follicular subpopulations during Drosophila oogenesis through hormone-dependent enhancer-targeted cell ablation. *Development* 127(3): 573-83.

Hartenstein, V., Spindler, S., Pereanu, W., and Fung, S. (2008). The development of the Drosophila brain. *Adv Exp Med Biol* 628: 1-31.

Hartigan, J.A., and Wong, M.A. (1979). Algorithm AS 136: a k-means clustering algorithm. *Appl Stat* 28(1): 100-08.

Herculano-Houzel, S. (2009). The human brain in numbers: a linearly scaled-up primate brain. *Front Hum Neurosci* 3: 31.

Hotta, Y., and Benzer, S. (1976). Courtship in Drosophila mosaics: sex-specific foci for sequential action patterns. *Proc Natl Acad Sci USA* 73(11): 4154-8.

Huang, M.T., and Gorman, C.M. (199). Interveneing sequences increase efficiency of RNA 3' processing and accumulation of cytoplasmic RNA. *Nucleic Acids Res* 18(4): 937-47.

Isshiki, T., Pearson, B., Holbrook, S., and Doe, C.Q. (2001). Drosophila neuroblasts sequentially express transcription factors which specify the temporal identity of their neuronal progeny. *Cell* 106(4): 511-21.

Ito, K., Awano, W., Suzuki, K., Hiromi, Y., and Yamamoto, D. (1997). The Drosophila mushroom body is a quadruple structure of clonal units each of which contains a virtually identical set of neurones and glial cells. *Development* 124(4): 761-71.

Kamikouchi, A., Wiek, R., Effertz, T., Gopfert, M.C., and Fiala, A. (2010). Transcuticular optical imaging of stimulus-evoked neural activities in the Drosophial peripheral nervous system. *Nature Protoc* 5(7): 1229-35.

Kao, D.F., Yu, H.H., He, Y., Kao, J.G., and Lee, T. (2012). Hierarchical deployment of factors regulating temporal fate in a diverse neuronal lineage of the Drosophila central brain. *Neuron* 74(4): 677-84.

Keegan, L., Gill, G., and Ptashne, M. (1986). Separation of DNA binding from the transcription-activating function of a eukaryotic regulatory protein. *Science* 231(4739): 699-704.

Kumar, A., Fung, S., Lichtneckert, R., Reichert, H., and Hartenstein, V. (2009). Arborization patterns of engrailed-positive neural lineages reveal neuromere boundaries in the Drosophila brain neuropil. *J Comp Neurol* 517(1): 87-104.

Kunisch, M., Haenlin, M., and Campos-Ortega, J.A. (1994). Lateral inhibition mediated by the Drosophila neurogenic gene Delta is enhanced by proneural proteins. *Proc Natl Acad Sci USA* 91: 10139-43.

Lai, S. L., and Lee, T. (2006). Genetic mosaic with dual binary transcriptional systems in Drosophila. *Nat Neurosci* 9: 703-9.

Lai, S.L., Awasaki, T., Ito, K., and Lee, T. (2008). Clonal analysis of Drosophila antennal lobe neurons: diverse neuronal architectures in the lateral neuroblast lineage. *Development* 135(17): 2883-93.

Lee, T., and Luo, L. (1999). Mosaic analysis with a repressible cell marker for studies of gene function in neuronal morphogenesis. *Neuron* 22(3): 451-61.

Lee, T., and Luo, L. (2001). Mosaic analysis with a repressible cell marker (MARCM) for Drosophila neural development. *Trends Neurosci* 24(5): 251-4.

Luan, H., Peabody, N.C., Vinson, C.R., and White, B.H. (2006). Refined spatial manipulation of neuronal function by combinatorial restriction of transgene expression. *Neuron* 52(3): 425-36.

Ma, J., and Ptashne, M. (1987). The carboxy-terminal 30 amino acids of GAL4 are recognized by GAL80. *Cell* 50: 137-42.

Marella, S., Mann, K., and Scott, K. (2012). Dopaminergic modulation of sucrose acceptance behavior in Drosophila. *Neuron* 73(5): 941-50.

Mellert, D., Knapp, J.M., Manoli, D.S., Meissner, G.W., and Baker, B.S. (2010). Midline crossing by gustatory receptor neuron axons is regulated by fruitless, doublesex and the Roundabout receptors. *Development* 137(2): 323-32.

Mellert, D., and Truman, J.W. (2012). Transvection is common throughout the Drosophila genome. *Genetics* epub 29 May 2012.

Murphey, R.K., Possidente, D.R., Vandervorst, P., and Ghysen, A. (1989). Compartments and the topography of leg afferent projections in Drosophila. *J Neurosci* 9(9): 3209-17.

Nagayama, T. (1989). Morphology of a new population of spiking local interneurones in the locust metathoracic ganglion. *J Comp Neurol* 198: 101-20.

Nassel, D.R., Helgee, A., and Sivasubramanian, P. (1986). Development of axon paths of motorneurons after removal of target muscles in a holometabolous insect. *Dev Brain Res* 26(2): 211-19.

Nern, A., Pfeiffer, B.D., Svoboda, K., and Rubin, G.M. (2011). Multiple new site-specific recombinases for use in manipulating animal genomes. *Proc Natl Acad Sci USA* 108(34): 14198-203.

Nicolai, L.J., Ramaekers, A., Raemaekers, T., Drozdzecki, A., Mauss, A.S., Yan, J., Landgraf, M., Annaert, W., and Hassan, B.A. (2010). Genetically encoded dendritic marker sheds light on neuronal connectivity in Drosophila.

O'Dell, D.A., and Watkins, B.L. (1988). The development of GABA-like immunoreactivity in the thoracic ganglia of the locust Schistocerca gregaria. *Cell Tissue Res* 254: 635-46.

Osterwalder, T., Yoon, K.S., White, B.H., and Keshishian, H. (2001). A conditional tissue-specific transgene expression system using inducible GAL4. *Proc Natl Acad Sci USA* 98(22): 12596-601.

Pan, Y., Meissner, G.W., and Baker, B.S. (2012). Joint control of Drosophila male courtship behavior by motion cues and activation of male-specific P1 neurons. *Proc Natl Acad Sci USA* 109(25): 10065-70.

Parisky, K.M., Agosto, J., Pulver, S.R., Shang, Y., Kuklin, E., Hodge, J.J., Kang, K., Liu, X., Garrity, P.A., Rosbash, M., and Griffith, L.C. (2008). PDF cells are a GABA-responsive wake-promoting component of the Drosophila sleep circuit. *Neuron* 60:672-82.

Pauli, A., Althoff, F., Oliviera, R.A., Heidmann, S., Schuldiner, O., Lehner, C.F., Dickson, B.J., and Nasmyth, K. (2008). Cell-type-specific TEV protease cleavage reveals cohesin functions in Drosophila neurons. *Dev Cell* 14(2): 239-51.

Pfeiffer, B.D., Jenett, A., Hammonds, A.S., Ngo, T.T., Misra, S., Scully, A., Carlson, J.W., Wan, K.H., Laverty, T.R., Mungall, C., Svirskas, R., Kadonaga, J.T., Doe, C.Q., Eisen, M.B., Celniker, S.E., and Rubin, G.M. (2008). Tools for neuroanatomy and neurogenetics in Drosophila. *Proc Natl Adcad Sci USA* 105(28): 9715-20.

Pfeiffer, B.D., Ngo, T.T., Hibbard, K.L., Murphy, C., Jenett, A., Truman, J.W., and Rubin, G.M. (2010). Refinement of tools for targeted gene expression in Drosophila. *Genetics* 186(2): 735-55.

Phillis, R.W., Bramlage, A.T., Wotus, C., Whittaker, A., Gramates, L.S., Seppala, D., Farahanchi, F., Caruccio, P., and Murphey, R.K. (1993). Isolation of mutations affecting neural circuitry required for grooming behavior in Drosophila melanogaster. *Genetics* 133: 581-592.

Pignoni, F., and Zipursky, S.L. (1997). Induction of Drosophila eye development by decapentaplegic. *Development* 124(2): 271-8.

Power, M. (1943). The brain of Drosophila melanogaster. *J Morphol* 72: 517-59.

Prokop, A., and Technau, G.M. (1991). The origin of postembryonic neuroblasts in the ventral nerve cord of Drosophila melanogaster. *Development* 111: 79-88.

Rand, W.M. (1971). Objective criteria for the evaluation of clustering methods. *J Amer Stat Assoc* 66(336): 846-50.

Roman, G., Endo, K., Zong, L., and Davis, R.L. (2001). P[Switch], a system for spatial and temporal control of gene expression in Drosophila melanogaster. *Proc Natl Acad Sci USA* 98(22): 12602-7.

Rowell, C.H.F. (1989). The taxonomy of invertebrate neurons: a plea for a new field. *Trends Neurosci* 12: 169-174.

Rubinstein, C.D., Rivlin, P., and Hoy, R.R. (2010). Genetic feminization of the thoracic nervous system disrupts courtship song in male Drosophila melanogaster. *J Neurogenetics* 24(4): 234-45.

Ryckebusch, S., and Laurent, G. (1993). Rhythmic patterns evoked in locust leg motor neurons by the muscarine agonist pilocarpine. *J Neurophysiol* 69: 1583-95.

Shang, Y., Griffith, L.C., and Rosbash, M. (2008). Light-arousal and circadian photoreception circuits intersect at the large PDF cells of the Drosophila brain. *Proc Natl Acad Sci USA* 105: 19587-94.

Shepherd, D., and Laurent, G. (1992). Embryonic development of a population of spiking local interneurones in the locust (Schistocerca gregaria). *J Comp Neurol* 219: 438-53.

Shimomura, O., Johnson, F., and Saiga, Y. (1962). Extraction, purification and properties of aequorin, a bioluminescent protein from the luminous hydromedusan, Aequorea. *J Cell Comp Physiol* 59(3): 223-39.

Siegler, M.B., and Burrows, M. (1983). Spiking local interneurons as primary integrators of mechanosensory information in the locust. *J Neurophysiol* 50(6): 1281-95.

Skeath, J.B., and Carroll, S.B. (1994). The achaete-scute complex: generation of cellular pattern and fate within the Drosophila nervous system. *FASEB J* 8(10): 714-21.

Spana, E.P., Kopczynski, C., Goodman, C.S., and Doe, C.Q. (1995). Asymmetric localization of numb autonomously determines sibling neuron identity in the Drosophila CNS. *Development* 121(11): 3489-94.

Spana, E.P., and Doe, C.Q. (1996). Numb antagonizes Notch signaling to specify sibling neuron cell fates. *Neuron* 17(1): 21-6.

Stevenson, P.A., and Kutsch, W. (1987). A reconsideration of the central pattern generator concept for locust flight. *J Comp Physiol* 161A: 115-29.

Strausfeld, N.J., and Seyan, H.S. (1985). Convergence of visual, haltere, and prosternal inputs at neck motor neurons of Calliphora erythrocephala. *Cell Tissue Res* 240: 601-615.

Strauss, R., and Heisenberg, M. (1990). Coordination of legs during straight walking and turning in Drosophila melanogaster. *J Comp Physiol A* 167(3): 403-12.

Struhl, G., and Basler, K. (1993). Organizing activity of wingless protein in Drosophila. *Cell* 72(4): 527-40.

Svoboda, K. (2011). The past, present, and future of single neuron reconstruction. *Neuroinform* 9: 97-98.

Thomas, J.B., Bastiani, M.J., Bate, M. J., and Goodman, C.S. (1984). From grasshopper to Drosophila: a common plan for neuronal development. *Nature* 310: 203-207.

Thompson, K.J., and Siegler, M.B. Anatomy and physiology of spiking local and intersegmental interneurons in the median neuroblast lineage of the grasshopper. *J Comp Neurol* 305(4): 659-75.

Thorpe, H.M., and Smith, M.C. (1998). In vitro site-specific integration of bacteriophage DNA catalyzed by a recombinase of the resolvase/invertase family. *Proc Natl Acad Sci USA* 95(10): 5505-10.

Truman, J.W., and Ball, E.E. (1998). Patterns of embryonic neurogenesis in a primitive wingless insect, the silverfish, Ctenolepisma longicaudata: comparison with those seen in flying insects. *Dev Genes Evol* 208: 357-68.

Truman, J.W., and Bate, M. (1988). Spatial and temporal patterns of neurogenesis in the central nervous system of Drosophila melanogaster. *Dev Biol* 125: 145-57.

Truman, J.W., Schuppe, H., Shepherd, D., and Williams, D.W. (2004). Developmental architecture of adult-specific lineages in the ventral CNS of Drosophila. *Development* 131: 5167-84.

Truman, J.W., Moats, W., Altman, J., Marin, E.C., and Williams, D.W. (2010). Role of Notch signaling in establishing hemilineages of secondary neurons in Drosophila melanogaster. *Development* 137: 53-61.

Vandervorst, P., and Ghysen, A. (1980). Genetic control of sensory connections in Drosophila. *Nature* 286(5768): 65-7.

von Philipsborn, A.C., Liu, T., Yu, J.Y., Masser, C., Bidaye, S.S., and Dickson, B.J. (2011). Neuronal control of Drosophila courtship song. *Neuron* 69(3): 509-22.

Wang, L., and Anderson, D.J. (2010). Identification of an aggression-promoting pheromone and its receptor neurons in Drosophila. *Nature* 463(7278): 227-31.

Wang, S., and Hazelrigg, T. (1994). Implications for bcd mRNA localization from spatial distribution of exu protein in Drosophila oogenesis. *Nature* 369(6479): 400-03.

Wendler, G. (1974). The influence of proprioceptive feedback on locust flight coordination. *J Comp Physiol* 88A: 173-200.

White, J.G., Southgate, E., Thomson, J.N., and Brenner, S. (1986). The structure of the nervous system of the nematode Caenorhabditis elegans. *Phil Trans R Soc Lond B Biol Sci* 314(1165): 1-340.

Witten, J.L., and Truman, J.W. (1991). The regulation of transmitter expression in postembryonic lineages in the moth, Manduca sexta. II. Role of cell lineage and birth order. *J Neurosci* 11: 1990-97.

Witten, J.L., and Truman, J.W. (1998). Distribution of GABA-like immunoreactive neurons in insects suggests lineage homology. *J Comp Neurol* 398(4): 515-28.

Wolf, H., and Lang, D.M. (1994). Origin and clonal relationship of common inhibitory motoneurons CI_1 and CI_3 in the locust CNS. *J Neurobiol* 25: 846-64.

Yellman, C., Tao, H., He, B., and Hirsh, J. (1997). Conserved and sexually dimorphic behavioral responses to biogenic amines in decapitated Drosophila. *Proc Natl Acad Sci USA* 94(8): 4131-6.

Yu, H.H., Chen, C.H., Shi, L., Huang, Y.L., and Lee, T. (2009). Twin-spot MARCM to reveal the developmental origin and identity of neurons. *Nature Neurosci* 12: 947-53.

Yu, J.Y., Kanai, M.I., Demir, E., Jefferis, G.S., and Dickson, B.J. (2010). Cellular organization of the neural circuit that drives Drosophila courtship behavior. *Curr Biol* 20(18): 1602-14.

Zamore, P.D., Tuschi, T., Sharp, P.A., and Bartel, D.P. (2000). RNAi: double-stranded RNA directs the ATP-dependent cleavage of mRNA at 21 to 23 nucleotide intervals. *Cell* 101(1): 25-33.

Zhang, Y.Q., Rodesch, C.K., and Broadie, K. (2002). Living synaptic vesicle marker: synaptotagmin-GFP. *Genesis* 34: 142-145.

Zufferey, R., Donello, J.E., Trono, D., and Hope, T.J. (1999). Woodchuck hepatitis virus posttranscriptional regulatory element enhances expression of transgenes delivered by retroviral vectors. *J Virol* 73: 2886-2892.